RJ676

Numerical Simulation of Wind Driven F1ow Through the Bering Strait

M. Spaulding
T. Isaji
D. Mendelssohn
A.C. Turner

Applied Science Associates, Inc.
70 Dean Knauss Drive"
Narragansett, Rhode Island 02882

List of Figures

List of Tables

Abstract

A two dimensional vertically averaged hydrodynamic model has been applied to predict the wind forced circulation in the Bering and Chukchi Seas. A simulation of the steady state flows induced by a 10^{-6} sea surface slope between the North Pacific and Arctic oceans gives a northward transport of 1.97 Sv with 67% and 33% of the flow passing through the Anad yr and Shpanberg Straits, respectively. A wind field derived from the Fleet Numerical Oceanographic Center (FNOC) and validated with available observations was used as input to perform simulations for February 1982. Comparison of model predictions to current observations in the Shpanberg and Bering Straits collected by Aagaard et al (1985) are generally in good agreement. The model however normally underpredicts the wind driven response. Correlation of model predicted transports with mean current speed and wind speed are in reasonable agreement" with the data and have correlations of 0.90 or higher. The transport wind speed correlation is approximately a factor of two higher than earlier estimates by Aagaard et al (1985). The simulations show that the latitudinal and longitudinal momentum balances are geostrophic and the area between St. Lawrence Island north to Cape Lisburne responds essentially as a unit to wind forcing.

Introduction

The Bering Strait allows exchange of water between the Pacific and Arctic oceans. The mean northward flow through the straits appears to be driven by a sea surface slope on the order of 10-' (Coachman and Aagaard, 1966} and according to Coachman et al (1975) and Stigebrandt (1984) is of steric origin associated with the mean density differences between the Arctic and North Pacific Oceans. The mean transport through the strait has been estimated to be on the order of 1 Sv by Coachman et al (1975) but more recent estimates based on field measurements and a correlation analysis between the wind and transport through the straits give a value of 0.6 Sv with a strong season cycle (Aagaard et al, 1985); summer transport being about 50% greater than in winter,

Aagaard et al (1985) have shown that there is substantial variability y in the flow associated with atmospheric forcing, including reversals of the mean northward transport. These reversals have also been observed in satellite tracked drogues deployed in free drifting ice (Reynolds and Pease, 1984). Coachman and Aagaard (1981) have shown that these reversals may be frequent and intense enough to reduce the annual mean transport.

During the winter season (November - June) the water in the region is generally homogeneous and baroclinic circulation is minimal. (Aagaard et al, 1985) except near polynyas (Scuhmacher et al, 1983). In the summer, baroclinic effects can be significant. For the winter situations Coachman and Aagaard (1966) suggest that the principal force balance in the meridional momentum equation is between the sea surface slope and the frictional and nonlinear terms.

In this paper, we apply a two dimensional vertically *averaged* hydrodynamic and ice model to predict the circulation and ice movement

through the strait in response to atmospheric forcing. Two one month long periods were selected for model application, February and June 1982, because field observations of currents and surface elevation (Aagaard et al, 1985) and ice drift motion (Reynolds and Pease, 1984) are available for comparison to model predictions.

Oceanographic Setting

The northern Bering Sea shelf (Figure 1) is characterized by three major passages. The Bering Straits (8.5 km wide) connects the Bering to the Chukchi Sea. Anad yr Strait (75 km) to the west and Shpanberg Strait (190 km) to the east of St. Lawrence Island connect the northern to the southern Bering Sea. Two major sounds are also present on the northern (Kotezbue Sound) and southern (Norton Sound) sides of the Seward Peninsular. The depths in the three passages range for 20 to 50 meters with the Shpanberg Strait being shallower than the other two. The depths in the sounds are generally 20 m or less.

The mean flows through the straits are northward and vary from 25 cm/s in Bering Strait to 15 cm/s in Anadyr Strait to a low of 5 cm/s in Shpanberg Strait. (Salo et al 1983; Aagaard et al, 1985). The flows are nearly rectilinear and closely aligned to the local bathymetry.

Sea ice is present in the area from November to early June with thickness and concentration depending on time and seasonal conditions. Reynolds and Pease (1984) suggest that the ice is normally in free drift in this region and hence does not modify the momentum transfer between the atmospheric forcing field and the water column.

Aagaard et al (1985) summarizes atmospheric forcing patterns as being formed by a juxtaposition of the Siberian high and an Aleutian low pressure systems, the relative strengths controlling the horizontal scale of forcing and

the magnitude of the geostrophic wind. If the Aleutian low penetrates far to the north the closely spaced isobars align in a north-south direction and generate strong northerly winds. These winds, if of sufficient strength, can cause a reversal of the flow through the Bering Strait (Coachman and Aagaard, 1981).

Data Sets for Model Comparison

Two data sets, collected in 1982, have been selected to provide observations for model-data comparisons.

The first data set was collected by Aagaard et al (1985). Recording current meters (Aanderaa RCM-4) and pressure gauges (Aanderaa TG-3) were deployed from 2 November 1981 to 24 April 1982 in the Bering, Anadyr, and Shpanberg Strait. A pressure gauge was deployed 150 km north of the Bering Strait in the south central Chukchi Sea. Current meters were located at approximately 60% of the local depth (referenced to the surface) in each of the straits.

Data recovery was good with the exception that a speed ambiguity was observed in the Anadyr Strait record and hence that observation could only be used for direction purposes. A complete description of the data set and its analysis is presented in Aagaard et al (1985).

The second data set was collected by Reynolds and Pease (1984). From 26 January to 10 February 1982 an array of six (6) ARGOS drifting ice platforms were deployed in the vicinity of Nome, Alaska in the northeastern Bering Sea. Two of the six platforms had meteorological and oceanographic stations which measured surface winds and currents and telemetered the data to the GOES - West satellite. Meteorological measurements were taken at a height of 3 m above the ice surface and consisted of wind speed, direction and air temperature. Current measurements were made 2 m below the bottom

of the ice water interface by a savonious rotor current meter designed by NOAA/PMEL. Samples were collected hourly and transmitted every 6 hours to GOES-West. The ARGOS platforms were allowed to drift freely and terminated in the ice pack either due to ice deformation or to melt out. The last platform stopped on 30 June 1986. A complete description of this data set and its analysis is presented in Reynolds and Pease (1984).

Hydrodynamic and Ice Models - Equations and Solution Methodology

The numerical hydrodynamic model employed for the present study follows the development originally given in Owen (1980) and reported in our earlier work (Isaji and Spaulding, 1984). Only a brief overview is therefore presented here.

The three dimensional conservation equations for water mass and momentum with the Boussinesq and hydrostatic assumptions invoked form the basis for the model. The three dimensional conservation equations suitable for limited shelf waters in Cartesian cooridnates may be written:

Conservation of water mass

$$\frac{\delta u}{\delta x} + \frac{\delta v}{\delta y} + \frac{\delta w}{\delta z} = 0 \qquad (1)$$

Conservation of momentum

$$\frac{\delta u}{\delta t} + u\frac{\delta u}{\delta x} + v\frac{\delta u}{\delta y} + w\frac{\delta u}{\delta z} - fv = -\frac{1}{\rho}\frac{\delta p}{\delta x} + \frac{\delta}{\delta z}\left(N\frac{\delta u}{\delta z}\right) \qquad (2)$$

$$\frac{\delta v}{\delta t} + u\frac{\delta v}{\delta x} + v\frac{\delta v}{\delta y} + w\frac{\delta v}{\delta z} + fu = -\frac{1}{\rho}\frac{\delta p}{\delta y} + \frac{\delta}{\delta z}\left(N\frac{\delta v}{\delta z}\right) \qquad (3)$$

$$\frac{\delta p}{\delta z} = -\rho g \qquad (4)$$

where the following notation has been used:

x,y,z	Cartesian coordinate system with x and y measured in the horizontal plane, and z measured vertically upward from mean sea level.
u,v,w	components of the current in the x, y, and z, directions, respectively
P	pressure
ρ	density
$\bar{\rho}$	depth-averaged density
N	vertical eddy viscosity
f	Coriolis parameter ($2\Omega\sin\phi$), assumed constant, where Ω is the angular speed of the earth's rotation and ϕ the latitude angle,
g	gravitational acceleration

These equations are solved subject to the following boundary conditions. (a) At land boundaries the normal components of velocity is set to zero. (b) At the open boundaries the sea surface elevation is specified as a series of sine waves each with its own amplitude and phase or appropriate gradients of the local surface elevation. (c) At the sea surface the applied stress due to the wind is matched to the local stress in the water column and the kinematic boundary condition is satisfied. The wind induced stress at the sea surface is related to the wind speed by a quadratic law with the drag coefficient following the formulation of Smith and Banke (1975):

$$C_d = (0.63 + 0.0066\ V_{10}) \times 10^{-3} \qquad (5)$$

where V_{10} is the 10 m wind speed.

This relationship gives similar stress levels to that of Wu (1969, 1980) for the wind speed range of interest here. (d) At the sea floor a quadratic

stress law, based on the local bottom velocity, is used to represent frictional dissipation and a friction coefficient parameterizes the loss rate.

Anticipating the use of a weighted residual method, in which vertical variations are represented in terms of a set of basis functions, a new set of independent variables is introduced that transforms both the surface and the bottom onto coordinate surfaces. This transformation represents a simple nondimensionalization with the local water column depth. A detailed presentation of the transformed equations can be found in Owen (1980).

The numerical solution methodology follows that of Davies (1977a, b) and Owen (1980). The vertical variations in horizontal velocity are described by an expansion of Legendre polynomials. The resulting equations are then solved by a Galerkin weighted residual method in the vertical and by an explicit finite difference algorithm in the horizontal.

A space staggered grid scheme in the horizontal plane is used to define the stud y area. Sea surface elevation and vertical velocity are specified in the center of each ceil while the horizontal velocities are *given* on the cell faces. The u and v velocities are defined on the cell faces normal to the x and y directions, respectively.

To reduce computational costs, a "split-mode" or "two-mode" formulation was used (Owen, 1980; Gordon, 1982). In the split-mode model, the free-surface elevation is treated separately from the internal, three-dimensional flow variables. The free-surface elevation and vertically integrated velocities are calculated using the vertically integrated equations of motion (external mode} for which the Courant-Friedrichs-Lewy (CFL) limit must be met. The vertical structure of the horizontal components of the current then may be calculated such that the effects of surface gravity waves are separated from the three-dimensional equations of motion (internal mode).

Surface gravity waves, therefore, no longer limit the internal mode calculations and much longer time steps are possible.

The external mode equations are approximated by a forward in time, centered in space (FTCS) finite difference scheme. The internal mode is solved using a forward in time technique with vertical diffusive terms centered in time, to ease the vertical time step restriction from the standard FTCS procedure.

Although the model equations presented here are in cartesian coordinates for ease of presentation, the equations used for the present study are in spherical coordinates.

The ice motion is described by the ice momentum equations given as

$$- \frac{\delta v_i}{\delta t} + m \frac{\delta}{\delta x_j} (v_i v_j) + m \varepsilon_{ij} v_j = - mg \frac{\delta \zeta}{\delta x_i} + c (\tau_i^a - \tau_i^w) + F_i \quad (6)$$

The rate of change of the ice mass (m) over a specific area is equal to the net influx of mass to that area plus sources and sinks (Rothrock, 1970). The equation of continuity for the ice mass is given by:

$$\frac{\delta m}{\delta t} + \frac{\delta (m v_j)}{\delta x_i} = \Phi \quad (7)$$

The following notation is used:

i,j Indices, (i,j = 1,2) where 1 stands for east coordinate, and 2 for west coordinate
t - time
Vi components of the ice velocity vector
τ_i^a components of the wind stress vector over the ice
τ_i^w components of water stress
Fi components of the force due to internal ice stress
ε_{ij} Coriolis tensor
ζ variation of the sea level or the ice around the undisturbed level
c ice compactness
m ice concentration or mass per unit area
g - gravity acceleration

ϕ – ice source/sink term

All indexed expressions use the Einstein summation convention.

Assuming that the ice is not spread evenly over the whole sea surface, the mass of ice can be expressed through the ice compactness (c), ice thickness (h), and ice density (p)

$$m = \rho hc \tag{8}$$

The equation of mass balance (Eq. 7) can now be divided into two separate equations: a continuity equation for ice compactness and an equation of thickness balance

$$\frac{\delta c}{\delta t} + \frac{\delta (v_i c)}{\delta x_i} = S_c \tag{9}$$

$$\frac{\delta h}{\delta t} + v_i \frac{\delta h}{\delta x_i} = S_h \tag{10}$$

where S_c and S_h are thermodynamic terms given by Hibler (1979). Because of the short duration of the simulations these terms are set to zero for the present studies.

The Fi term on the right hand side of Eq. (6) represents the internal ice stresses and is normally expressed by the divergence of a stress tensor. The expressions for the stress law range from a simple linear relationship between stress and strain to a nonlinear viscous compressible fluid representation (Hibler 1979; Pritchard, 1980). Based on Reynolds and Pease' (1984) observation that the ice is in free drift, we have ignored the internal stresses in the present application.

Equations (6} - (13) are solved in conjunction with the hydrodynamic

equations described earlier to predict the ice thickness and ice compactness distributions. To complete the description of the ice motion equations, we must specify the shear stresses at the ice-air and ice-water interfaces, For the wind stress over the ice the standard quadratic expression is employed:

$$\tau_i^a = C_{10} \rho_a |W_i| W_i \quad (8)$$

where C_{10} is a drag coefficient, ρ_a is the air density and Wi is the 10 m wind speed. A review of the data gathered during AIDJEX (Pritchard 1980) suggests a value of 0.003.

Interaction of the water and ice is described by two forces - the pressure gradient and the water stress. The pressure gradient is fully specified by the sea level distribution predicted by the hydrodynamic model. The ice-water stress relationship is again specified by the quadratic law

$$\tau_i^w = R_w |v_i - u_i| (v_i - u_i) \quad (11)$$

where R_w is the drag coefficient and ui and vi are the water and ice velocities, respectively. Following McPhee (1980) R_w is set to 0.0055.

Description of Wind Forcing

To describe the temporal and spatial variation of the wind field the Fleet Numerical Oceanographic Center (FNOC) weather model predictions were employed. The model predicts the global winds on a 2.5° degree square grid every six hours. Figure 2 shows a typical plot of the wind field for the study area.

Figure 3 shows a comparison between the FNOC model predictions Bakun winds (Metlib), and observations taken from ice drifting buoys 2320 and 2322B (Reynolds and Pease, 1984). One can visually see that the patterns also compare well. In general, the model correctly predicts the speed and

direction of the wind for most of Feburary 1982.

The FNOC wind speed and direction predictions, scaled to agree with the observations, were used to provide input to the hydrodynamic and ice cover models on a time step of 6 hours. Linear interpolation in time and bilinear interpolation in space were used to match the wind data input to the hydrodynamic grid system.

Model Application

The hydrodynamic model was applied to the study area using one Legendre polynomial to describe the vertical structure and hence resulted in a two dimensional vertically simulation. Two model grid systems were selected for study because of concern over accurately representing the geometry in and near the Bering Strait. The coarse grid (hereafter referred to as CG) model has a 0.25° latitude by 0.60 longitudine resolution. The fine grid (FG) model had exactly twice this resolution and used the same framework as the CG model. Figure 4 shows the FG model representation for the area. The model extends from the shelf break in the southern Bering Sea to 740 N in the Chukchi Sea.

Bathymetric data necessary as input to the hydrodynamic model was derived from a digitized version of the NOAA/National Ocean Survey (NOS) charts for the region. All bathymetric data within a given grid were averaged to determine the depth value at the appropriate location,

Boundary conditions for the wind driven simulations were specified using an inverted barometric pressure specification along the northern and southern boundaries. This boundary approximation is reasonable along the southern boundary as it is applied in deep water where wind induced setups or setdowns are typically small (Beardsley and Haidvogel, 1981; Spaulding and Isaji, 1985). At the northern boundary where water depths are shallower (40

to 60 m) this specification is not as readily justified. Given the distance from the Bering Strait and the time scale of significant wind forcing it appears that the flows through the strait are not greatly affected by this clamped boundary condition. The bottom friction coefficient was kept constant at 0.003 for all simulations.

As a first case the hydrodynamic model was used to simulate the observed mean northward flow from the Bering to the Chukchi Sea. Following previous estimates a sea surface slope of 1×10^{-6} was imposed across the model boundaries. Figure 5 shows the FG model predicted vertically averaged currents and sea surface elevation contours after steady state conditions were achieved.

The flow field is in approximate geostrophic balance with water being transported along the Soviet coast splitting at St. Lawrence Island and recombining before passing through the Bering Strait. Table 1 summarizes the results for the two model grid systems in terms of the transport and mean velocities through the Anad yr, Shpanberg and Bering Straits. The transport is on the order of 1.7-2.0 Sv through the Bering Strait with 67% and 33% of the flow going through the Anadyr and Shpanberg Straits, respectively. The cross sectionally averaged mean vector velocities for the FG model are 54, 13, and 52 cm/s for the Anadyr, Shpanberg and Bering Straits, respectively. The FG simulations show an increase of approximately 10% in transport compared to the CG calculations.

Simulations were next made using the FNOC model to describe the wind forcing field for the month of February 1982. No mean elevation gradient was assumed between the Bering and Chukchi Sea and hence in the absence of wind forcing there is no mean flow. Plots showing the wind forcing fields and the corresponding vertically averaged currents and surface elevation contours

at daily increments for the entire February simulation period are shown in Appendix A (wind) and C (currents).

A comparison of the FG model predictions to observations are shown in Figure 6. The presentation is in three sections; wind, currents (Shpanberg and Bering Straits) and sea level differences (Shpanberg - Anadyr, Anadyr - Chukchi, and Shpanberg - Chukchi). The wind data is derived from Tin City, Alaska, while the remaining data is taken from Aagaard et al (1985) (See Figure 3 of that paper). As seen the model predictions are in reasonable agreement with data showing strong wind driven response. The model in general slightly underestimates the peak velocities for the strongest wind events. The model response is clearly wind driven. However for the northward wind event from 16-20 February the model predicts no velocity in the Bering Strait. The reason for this is unknown and is contrary to the response predicted in the rest of the simulation.

Comparison of the transport through the Bering Straits to the mean velocity (Figure 7) show a high correlation ($r = 0.995$) and give a cross sectional area of approximately 3.9×10^6 m^2. Data collected by Coachman and Aagaard (1981) are shown for comparison. The agreement is in general quite good.

Correlation of Anad yr and Shpanberg transport with that in the Bering Strait are 0.70 or greater with the approximate 67%, 33% partitioning calculated for the composed slope case. To better understand the dynamics the local momentum balances are shown in Figure 8a, b and c for the Bering, Anadyr, and Shpanberg Straits, respectively. Balances are presented in the east - west and north - south directions and include acceleration, sea surface slope, coriolis, surface and bottom stress, atmospheric pressure gradient, and advective terms. Independent of location, the balance is primarily geostrophic.

The bottom stress is a direct response to the surface stress and only becomes important when the surface stress is large. Contrary to Coachman and Aagaard's (1966) analysis, the advective terms are always extremely small.

A review of these figures and the spatial plots shows that the area between St. Lawrence Island and Cape Lisburne acts as a unit in terms of its hydrodynamic response to wind forcing. This is in agreement with Aagaard et al (1985) and Coachman and Aagaard's (1981) observation.

One relationship of particular interest is between the wind forcing and transport through the Bering Strait. Figure 9 shows the FG model predicted transport versus wind speed at the strait for the one month simulation. A regression equation $T = 0.240 + 0.911\ W$ fits the available data with a correlation of 0.91, where T is the transport in Sverdrups and W is the wind speed in m/s. Taking the local wind at the straits or averaging over a larger area (5 or 100) has little effect on the regression formula. If we consider only the wind correlated component of the flow, the present simulation gives approximately twice the flow at a given wind speed as Aagaard's et al (1985) estimate (T a 0.0604 W).

Conclusions

A hydrodynamic modeling study has been performed to investigate the wind driven response of the northern Bering and Chukchi Seas. Primary conclusions from the stud y include:

(1) For an assumed mean sea elevation differential between the North Pacific and the Arctic oceans, slope of 10^{-6}, results in a northward directed transport through the Bering Straits of 1.98 Sv. Sixty-six percent (66%) of this flow passes through the Anadyr Strait and the remaining (33%) passes through the Shpanberg Strait. The cross sectionally averaged vector velocity magnitudes for the FG model are

52, 54, and 11 cm/s for the Bering, Anadyr, and Shpanberg Straits, respectively. Refinement of the model grid has a modest effect and increases the transport by 10%. The flow is primarily in geostrophic balance.

(2) Comparison of the Fleet Numerical Oceanographic Center (FNOC) wind model predictions to available observations show that the wind model accurately reproduces the basic pattern of the wind events during the study period.

(3) A simulation with the hydrodynamic model using FNOC model winds for February 1982 show generally good agreement to current measurements made by Aagaard et al (1985) in the Bering and Shpanberg Straits and confirm the role of the wind *in* driving the circulation. The model tends to underpredict the current magnitudes, but correctly predicts the response to wind forcing.

(4) The simulations show that the flows are in geostrophic balance through each of the three straits and also that the region from St. Lawrence Island to Cape Lisburne responds as a unit to wind forcing. The response is direct with little phase lag.

(5) The correlation between wind speed, W, and transport, T, at the Bering Strait is given by T = 0.240 + 0.117 W and the constant multiplied time the wind speed is approximately twice that observed by Aagaard et al (1985).

References

Aagaard, K., A. Roach and J.D. Schumacher, 1985. On the Wind Driven Variability of the Flow through the Bering Strait, Journal of Geophysical Research, Vol. 90, No. C4, p. 7213-7221.

Aagaard, K., L.K. Coachman and E. C. Carmack, 1981. On the Halocline of the Arctic Ocean. Deep Sea Res., 29, 529-545.

Albright, M., 1980. Geostrophic Wind Calculations for AIDJEX, in Sea Ice Processes and Models, edited by R.S. Pritchard, pp. 402-409, University of Washington Press, Seattle.

Beardsley, R.C. and D.B. Haidvogel, 1981. Model Studies of the Wind Driven Transient Circulation *in* the Middle Atlantic Bight. Part 1: Adiabatic Boundary Conditions. J. Ph ys. Oceanogr. 11: 335-375.

Coachman, L.K, and K. Aagaard, 1966.. On the Water Exchange Through Bering Strait, Limnol. Oceanogr., 11, 44-59.

Coachman, L.K. and K. Aagaard, 1981. Reevaluation of Water Transports *in* the Vicinity of Bering Strait, in: The Eastern Bering Sea Shelf: Oceanography and Resources, Vol. 1, edited by D.W. Hood and J.A. Calder, pp. 95-110, National Oceanic and Atmospheric Administration, Washington, D.C.

Coachman, L.K. and C.A. Barnes, 1961. The Contribution of Bering Sea Water to the Arctic Ocean, Arctic, 14, 147-161.

Coachman, L. K., K. Aagaard, and R. B.Tripp, 1975. Bering Strait: The Regional Physical Oceanogrpahy, 172 pp. University of Washington Press, Seattle.

Davies, A. M., 1977a. The Numerical Solution of the Three-DimensionaI Hydrodynamical Equations Using a B-Spline Representation of the Vertical Current Profile. In: Bottom Turbulence, Proceedings of the 8th Liege Colloquium on Ocean Hydrodynamics, J.C.J. Nihoul, (cd.), Elsevier, New York: 27-48.

Davies, A.M., 1977b. Three-Dimensional Model with Depth-Varying Eddy Viscosity. In: Bottom Turbulence, Proceedings of the 8th Liege Colloquium on Ocean Hydrodynamics, J.C.J. Nihoul (cd.), Elsevier, New York: 27-48.

Hibler, W. D., 1979. A Dynamic Thermodynamic Sea Ice Model, Jour. of Physical Oceanography y, Vol. 9, July, pp. 815-846.

Isaji, T. and M.L. Spaulding, 1984. A Model of the Tidally Induced Residual Circulation in the Gulf of Maine and Georges Bank, J. of Phys. Oceanogr., Vol. 14, No. 6, 1119-1126.

Isaji, T., M.L. Spaulding, J.C. Swanson, 1982. A Three-Dimensional Hydrodynamic Model of Wind and Tidally Induced Flows on Georges Bank. Appendix A in: Interpretation of the Physical Oceanography of Georges Bank, EG&G Environmental Consultants.

Kowalik, Z., 1984. Numerical Modeling of Storm Surges in the Beaufort and Chukchi Seas, Final Report to NOAA/OCSEAP Research Unit 627., 118 p.

Kowalik, Z., 1981. A Study of the M2 Tide in the Ice Covered Arctic Oceans, Modeling, Identification, and Control, Vol. 2, No. 4, 201-223.

Liu, S.K. and J.J. Leenderste, 1981. A 3-D Oil Spill Model with and Without Ice Cover. International Symposium on Mechanics of Oil Slicks, Paris France.

McPhee, M. G., 1980. An Analysis of Pack Ice Drift in Summer. In: Proceedings of the AIDJEX Symposium. University of Washington Press, p. 62-75.

Noble, M., B. Butman, and E. Williams, 1983. On the Longshelf Structure and Dynamics of Subtidal Currents on the Eastern United States Continental Shelf, Wind Forced Currents, Free Topographic Waves, Wind Driven Momentum Balance, and Bottom Stress, J. Phys. Oceanog. 13, pp. 2125-2147.

Owen, A., 1980. A Three Dimensional Model of the Bristol Channel. J. Phys. Oceanogr. 10: 1290-1302.

Pritchard, R. S., (cd.), 1980. Sea Ice Processes and Models. Proceedings of the Arctic Ice Dynamics Joint Experiment International Commission on Snow and Ice Symposium, University of Washington press.

Rothrock, D.A., 1975. The Mechanical Behavior of Pack Ice. Annual Review of Earth and Planetary Sciences, 3, pp. 317-342.

Reynolds, R.M. and C.H. Pease, 1984, Drift Characteristics of Northeastern Bering Sea Ice During 1982, NOAA Tech. Memo ERL-PMEL, 55, 135 pp. (Available as PB 84-213982 from the Natl. Tech. Inf. Serv., Springfield, VA.)

Rothrock, D.A., 1970. The Kinematics and Mechanical Behavior of Pack Ice: The State of Subject. AIDJEX Bulletin, 2, pp. 1-10.

Sale, S.A., J.D. Schumacher, and L.K. Coachman, 1983. Winter Currents on the Eastern Bering Sea Shelf, NOAA Tech. Memo ERL-PMEL, 45 53 pp. (Available as PB 83-248823 from the Natl. Tech. Inf. Serv., Springfield, VA).

Schumacher, J. D., K. Aagaard, C.H. Pease, and R.B. Tripp, 1983. Effects of a Shelf Polynya *on* Flow and Water Properties in the Northern Bering Sea. J. Geophys. Res. 88, 2723-2732.

Smith, S. D., and E.G. Banke, 1975. Variation of the Sea Surface Drag Coefficient with Wind Speed, Q.J.R. Meteorol. Sot., 101 665-673.

Spaulding, M.L. and T. Isaji, 1985. Design Flow Conditions Near Bottom-Phase II: Coupling of a Continental Shelf Hydrodynamics Model to a Bottom Boundary Layer Model, Volume I - Theoretical Development and Application, report to American Gas Association Pipeline Research Committee (PRC), Arlington, Virginia. April.

Spaulding, M. L., T. Isaji, E. Anderson, A.C. Turner, K. Jayko, and M. Reed, 1986. Ocean Circulation and Oil Spill Trajectory Simulations for Alaskan

Waters: Spill Trajectory Simulations for Shumagin Oil and Gas Lease Sale No. 86., prepared for NOAA Ocean Assessment Division, Anchorage, Alaska.

Stigebrandt, A., 1984. The North Pacific: A Global-Scale Estuary, J. Phys. Oceanogr., 14, 464-470.

Wu, J., 1969. Wind Stress and Surface Roughness at Air-Sea Interface. J. Geophys. Res., 74, 444-455.

Wu, J., 1980. Wind-stress coefficients over sea surface near neutral conditions: A Revisit, J. Phys. Oceanogr., 10, 727-740.

Acknowledgements

The research was supported by the Minerals Management Service through an interagency agreement with the National Oceanic and Atmospheric Administration (NOAA) as part of the Outer Continental Shelf Environmental Assessment Program. Mr. David Hale served as the technical contract monitor. The observational data was kindly provided to us by Drs. K. Aagaard and C. Pease of the NOAA, Pacific Marine Environmental Laboratory (PMEL). Their review of the work and helpful suggestions on the analysis of the simulations is gratefully acknowledged.

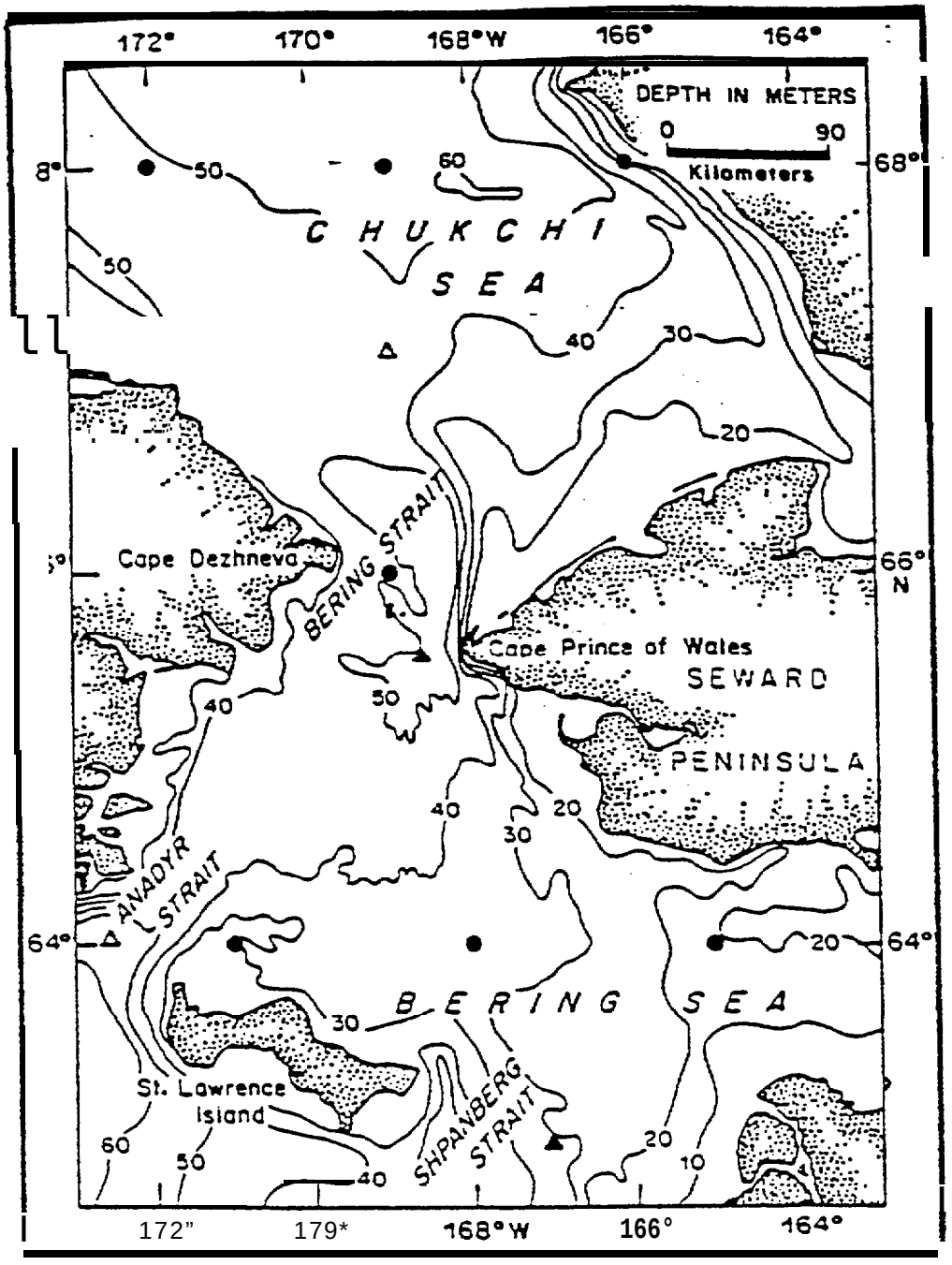

Figure 1. The Anadyr, Shpanberg and Bering Straits study area. Bathymetric contours (m) are shown.

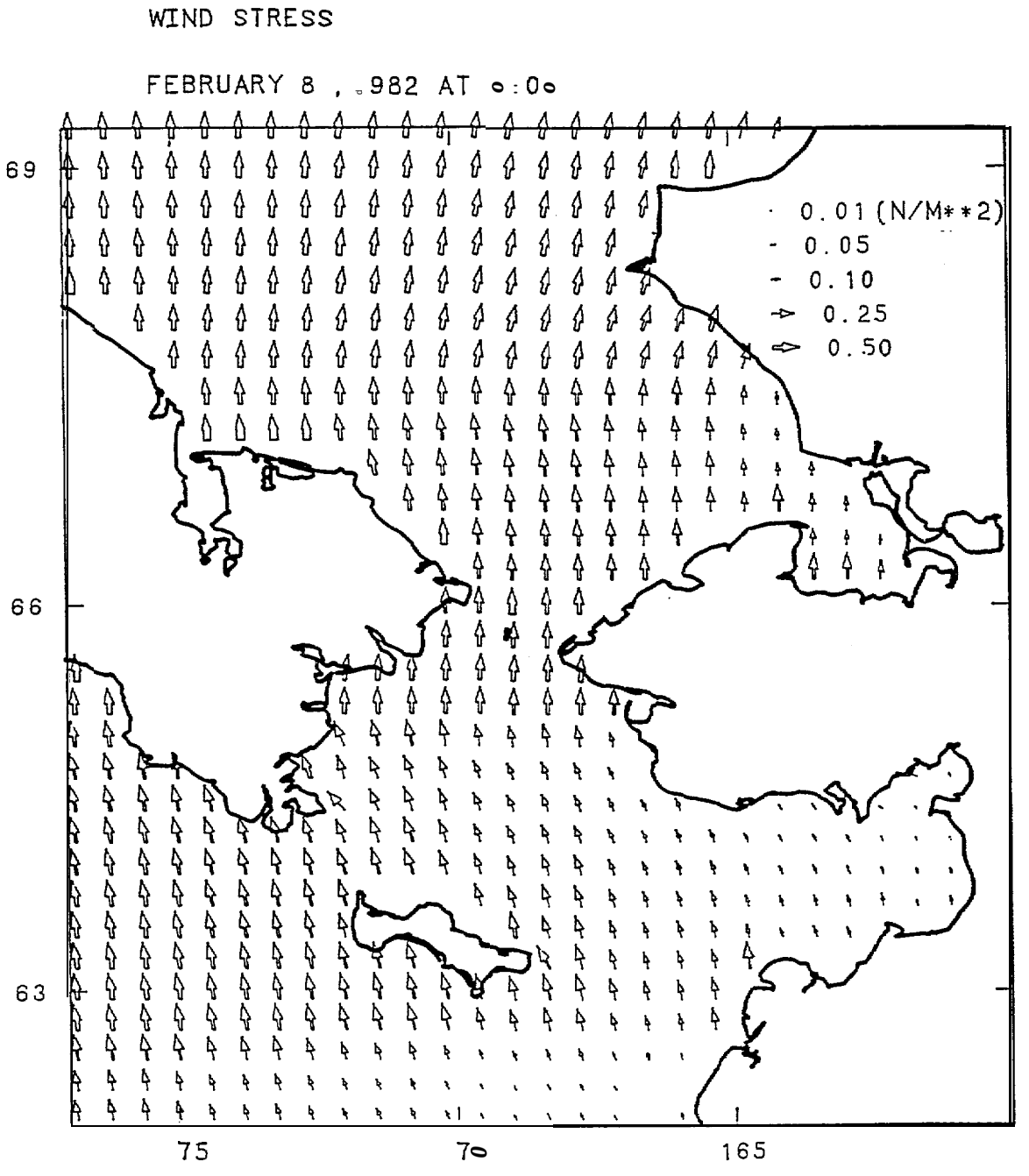

Figure 2. Typical Fleet Numerical Oceanographic Center (FNOC) model predicted wind forcing field (2.5° degree resolution).

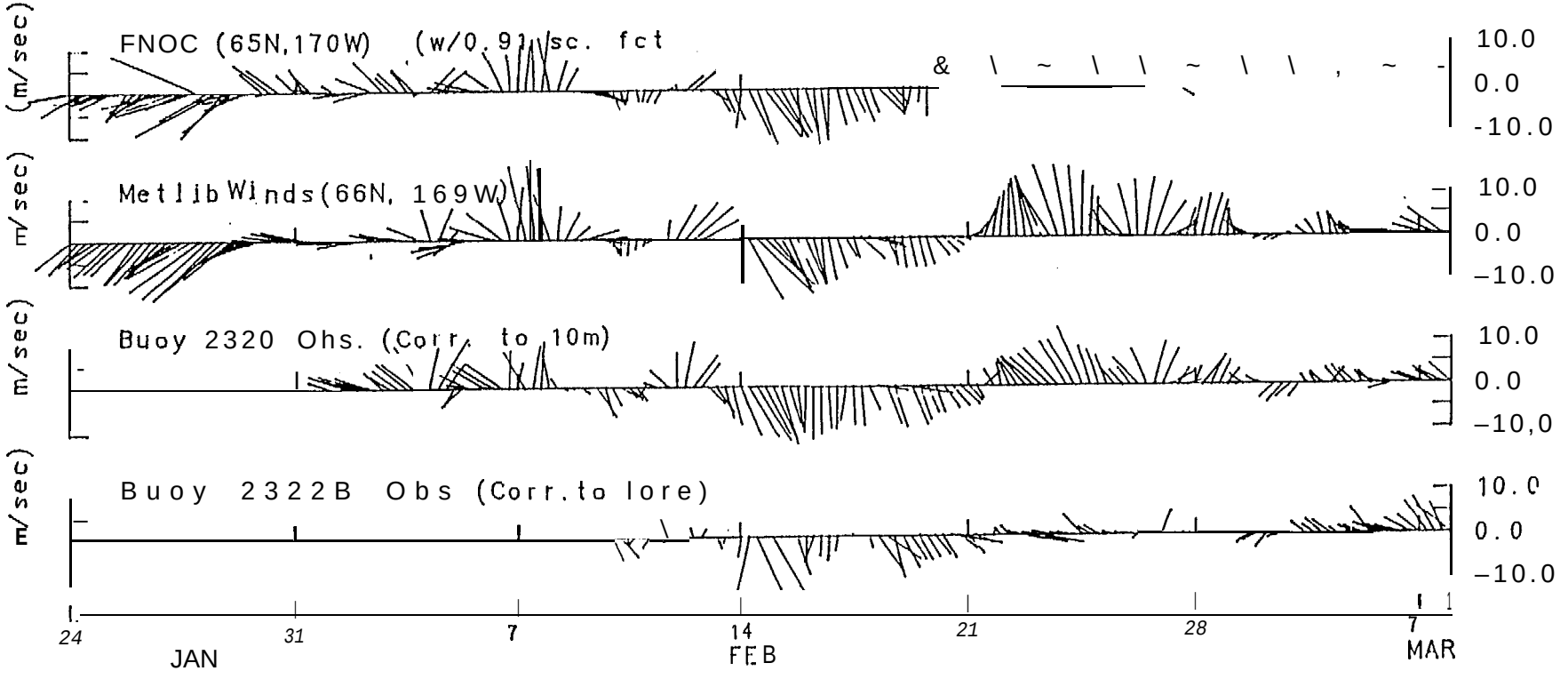

FNOC Winds vs. PMEL data:
Jan 24 - Mar 7 1982.

Figure 3. Comparison of Fleet Numerical Oceanographic Center (FNOC) model predicted winds, Metlib winds, and observations from buoys (2320, 2322B) (Reynolds and Pease, 1984) for February 1982.

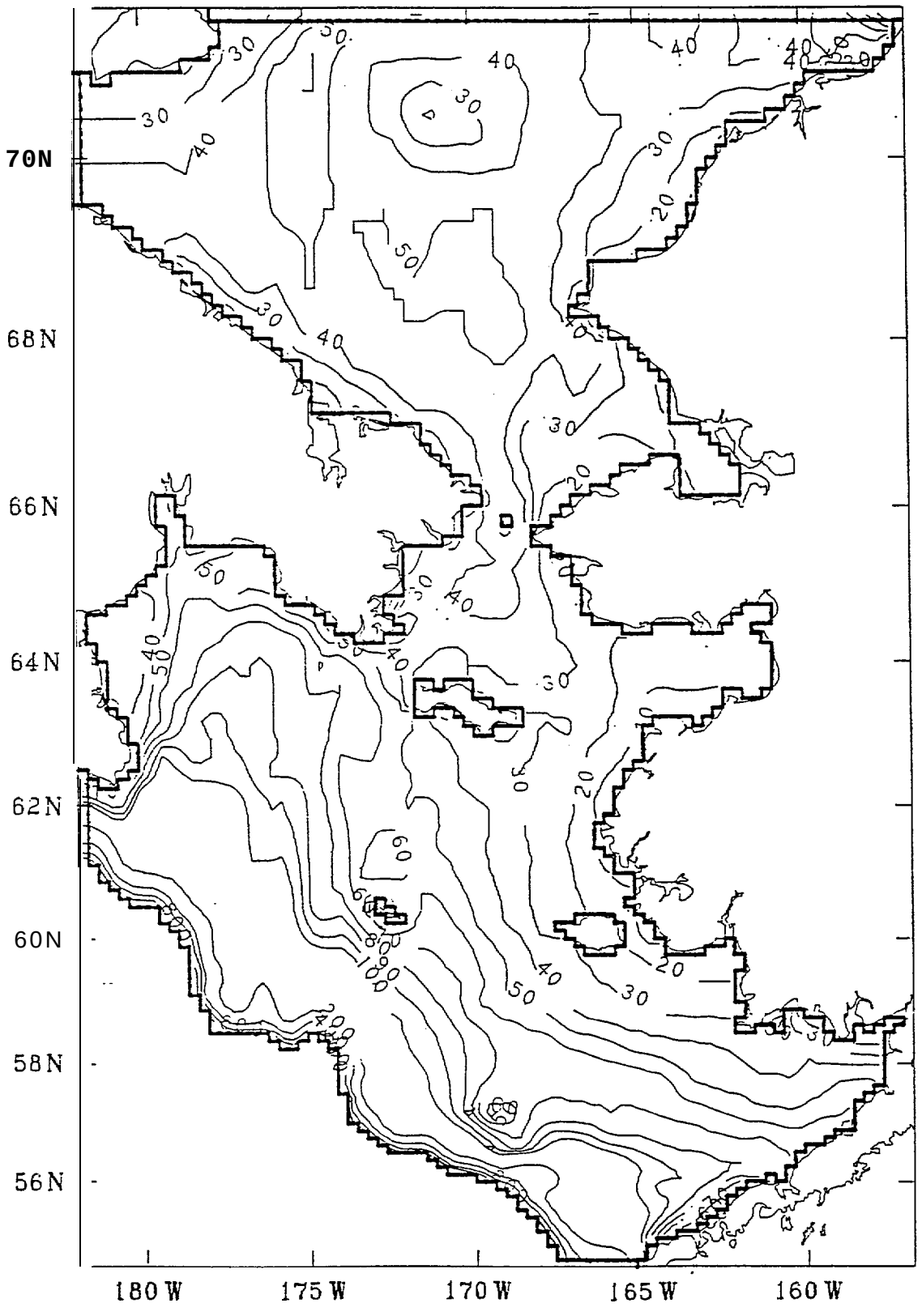

Figure 4 Fine grid (0.125° latitude by 0.3° longitude resolution) hydrodynamic model grid system for study area.

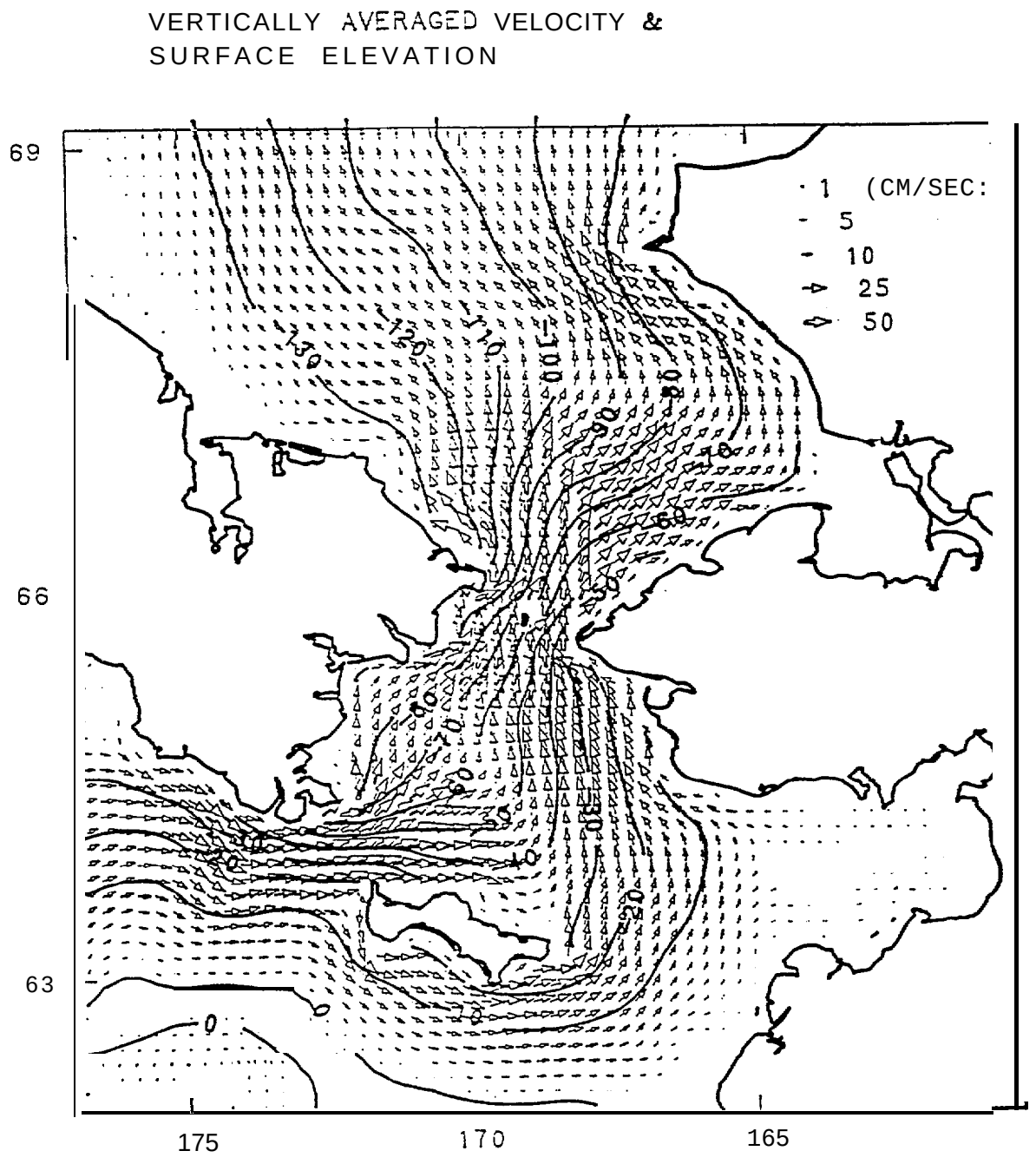

Figure 5. **Fine grid hydrodynamic model predicted steady** state vertically averaged current and sea elevation contours "in response to an imposed sea surface slope of 10 6.

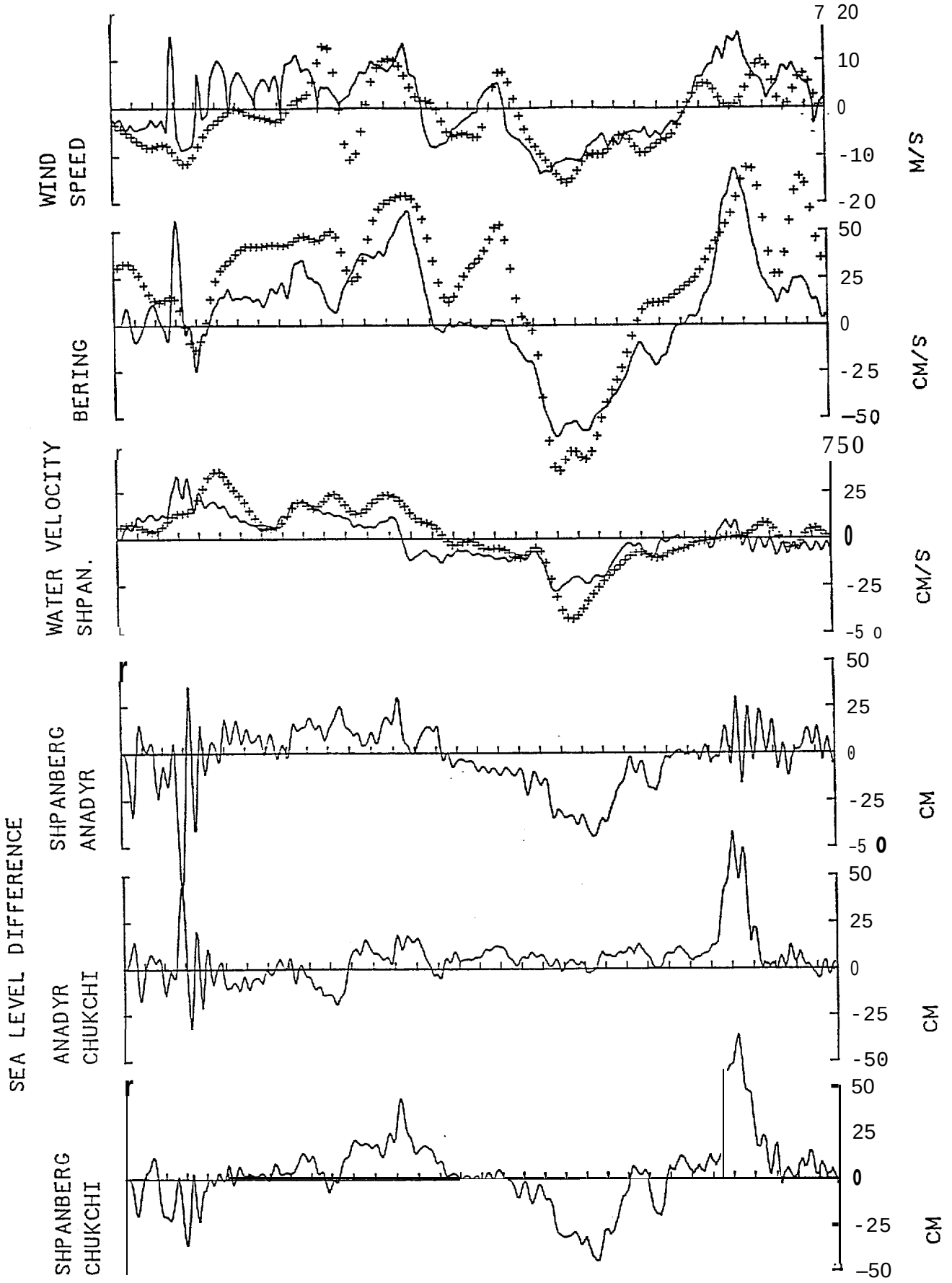

Figure 6. Comparison of model predictions to observations for winds, currents (Shpanberg and Bering Straits) and pressure differences (Shpanberg - Anadyr, Anadyr - Chukchi, Shpanberg - Chukchi). Model predictions use the fine grid simulation and **the** data is derived and presented in the same from ***as*** Figure 3 of Aagaard et al (1985). Wind data however is from Tin City, Alaska.

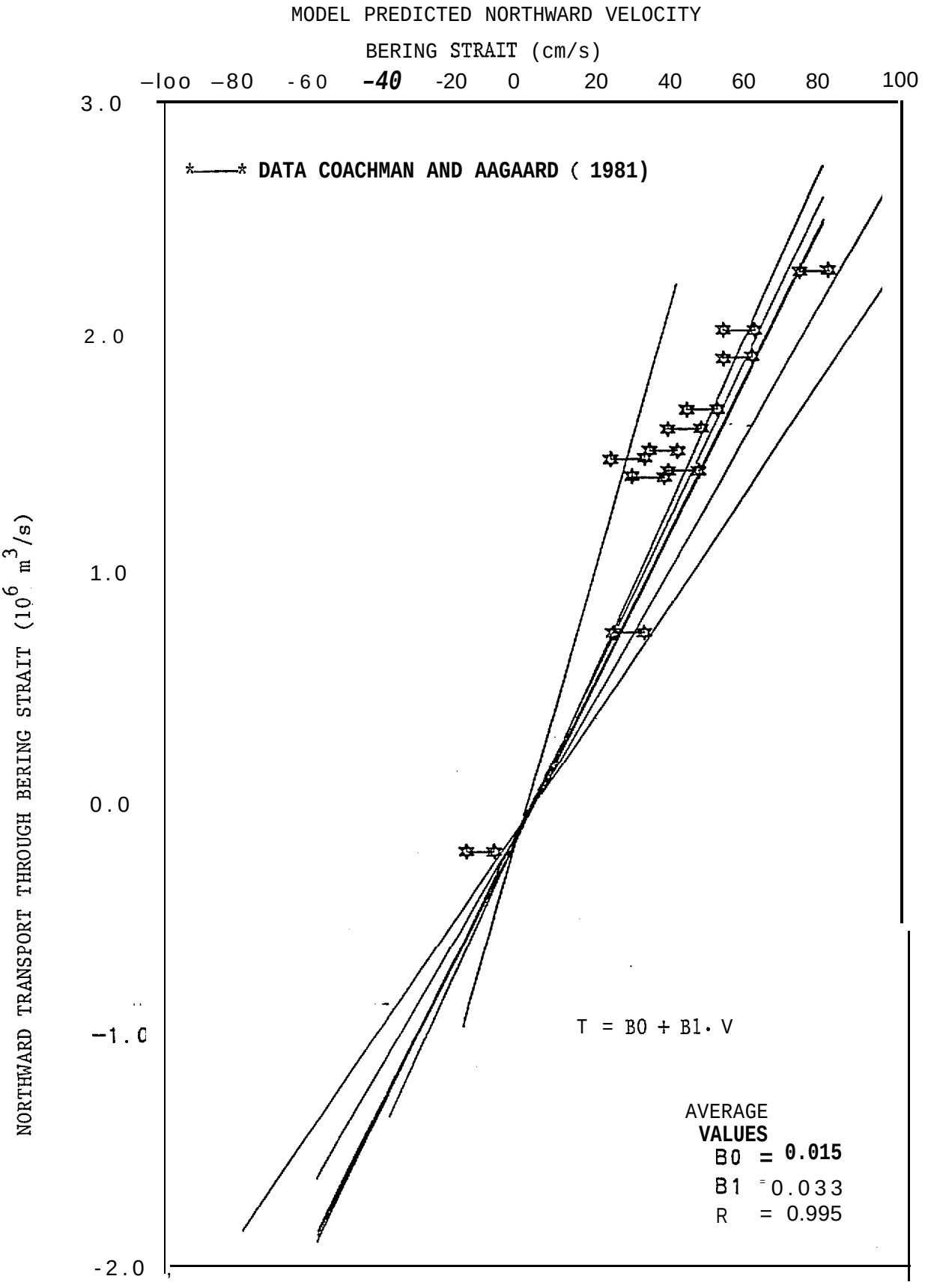

Figure 7. Correlation between hydrodynamic model predicted transport (north positive) and velocity (north positive) for the Bering Straits for the February simulation. Also shown are transport velocity correlation measurements reported in Coachman and Aagaard (1981). The various lines are the correlations using various grid cells in the strait to specify the velocity.

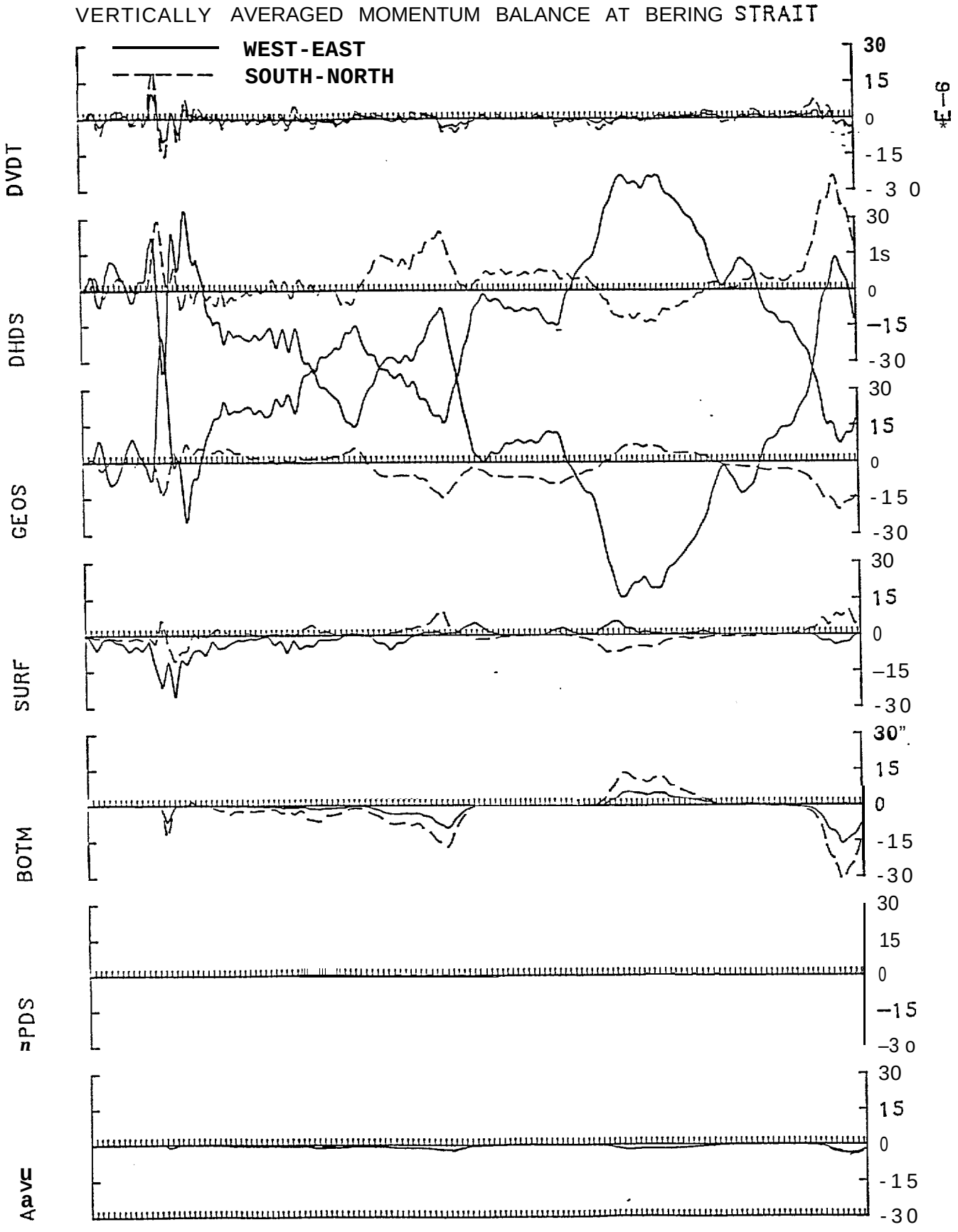

Figure 8(a). East - west and north - south momentum balances versus time for the February simulation including acceleration (DVDT), surface slope (DHDS), coriolis (GEOS), surface stress (SURF), bottom stress (BOTM) atmospheric pressure gradient (DPDS) and advective (ADV) terms. (a) Bering Straits, (b) Anadyr Straits, and (c) Shpanberg Straits.

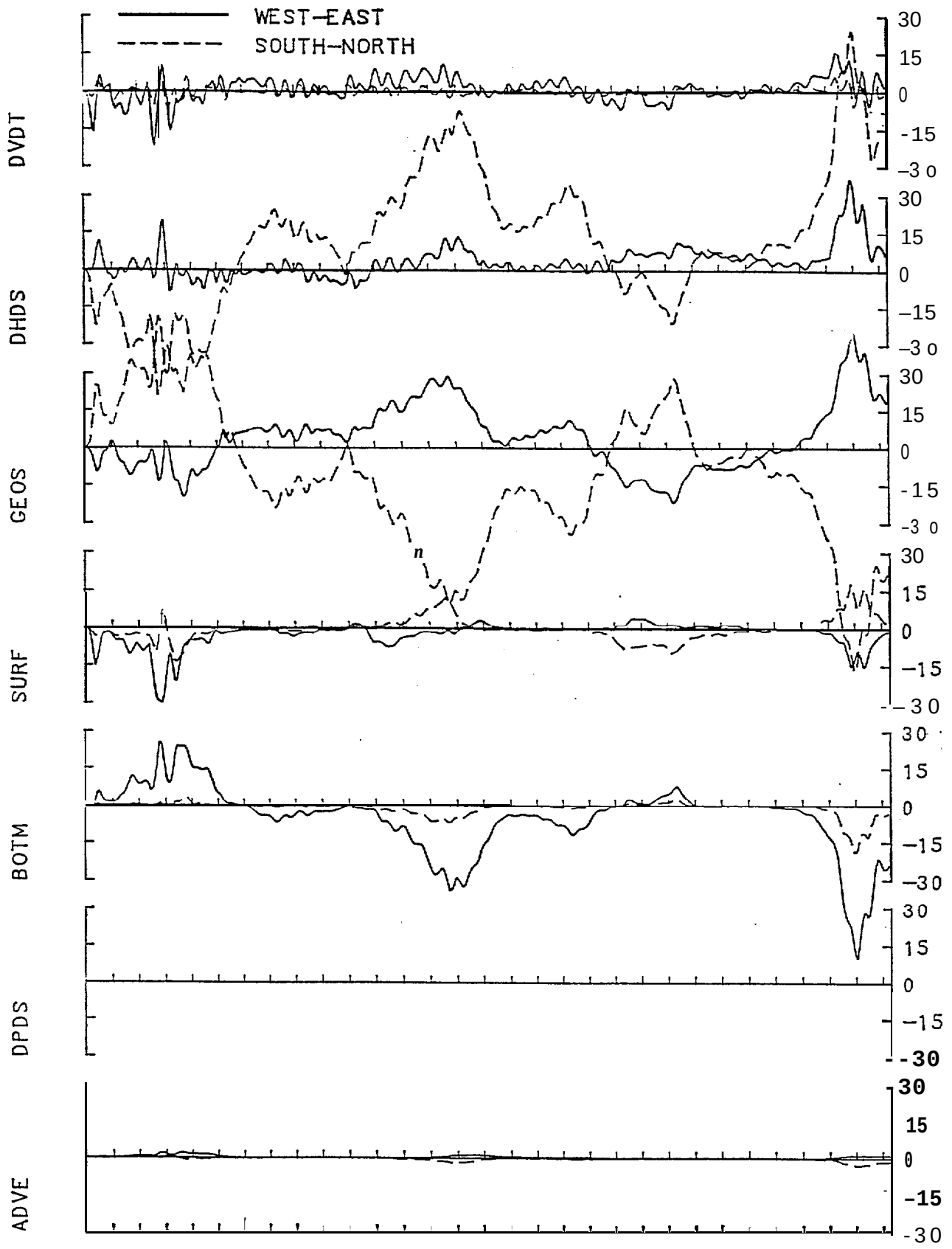

Figure 8(b). East -west and north - south momentum balances versus time for the February simulation including acceleration (DVDT), surface slope (DHDS), coriolis (GEOS), surface stress (SURF), bottom stress (BOTM) atmospheric pressure gradient (DPDS) and advective (ADV) terms. (a) Bering Straits, (b) Anadyr Straits, and (c) Shpanberg Straits.

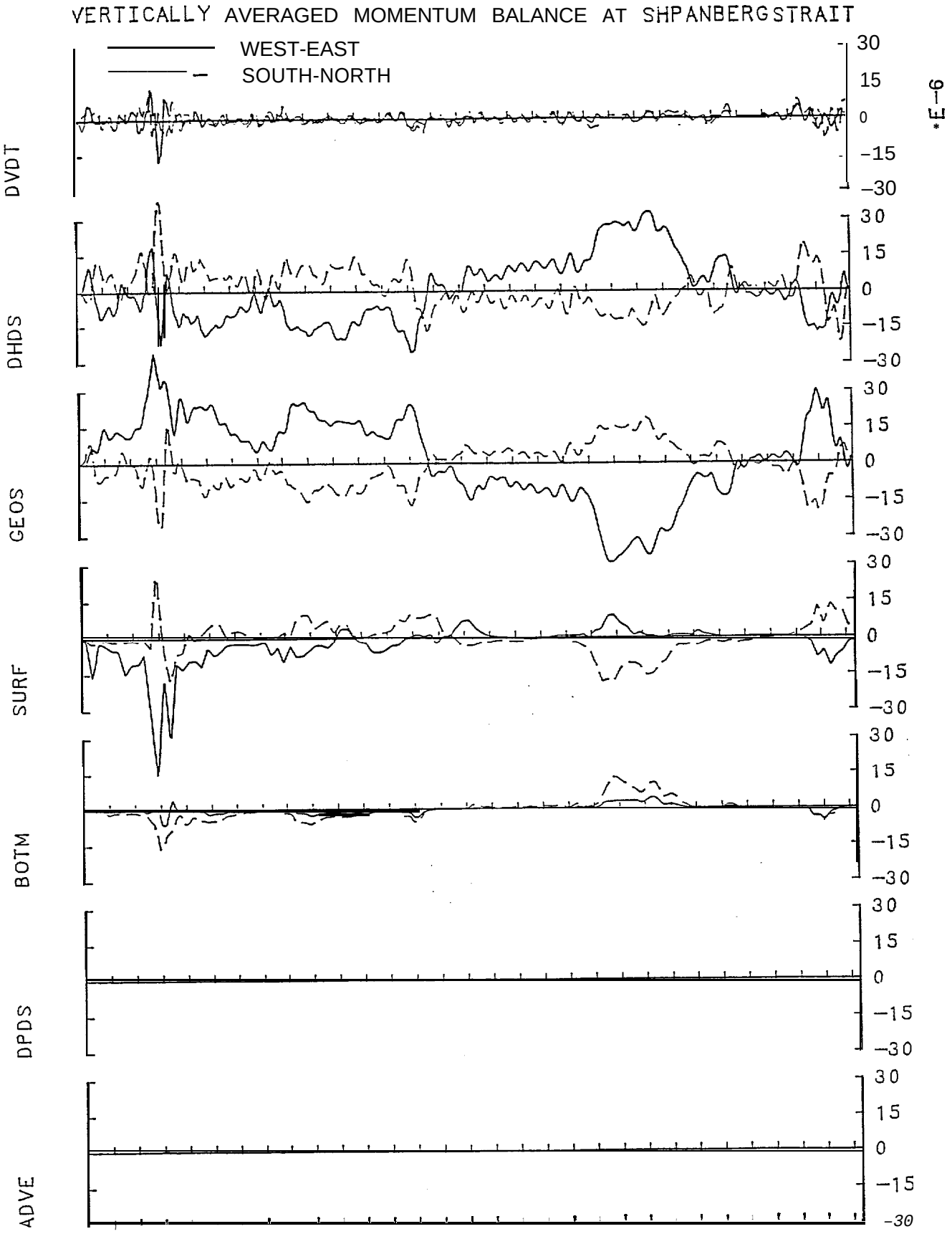

Figure 8(c). East - west and north – south momentum balances versus time for the February simulation including acceleration (DVDT), surface slope (DHDS), coriolis (GEOS), surface stress (SURF), bottom stress (BOTM) atmospheric pressure gradient (DPDS) and advective (ADV) terms. (a) Bering Straits, (b) Anadyr Straits, and (c) Shpanberg Straits.

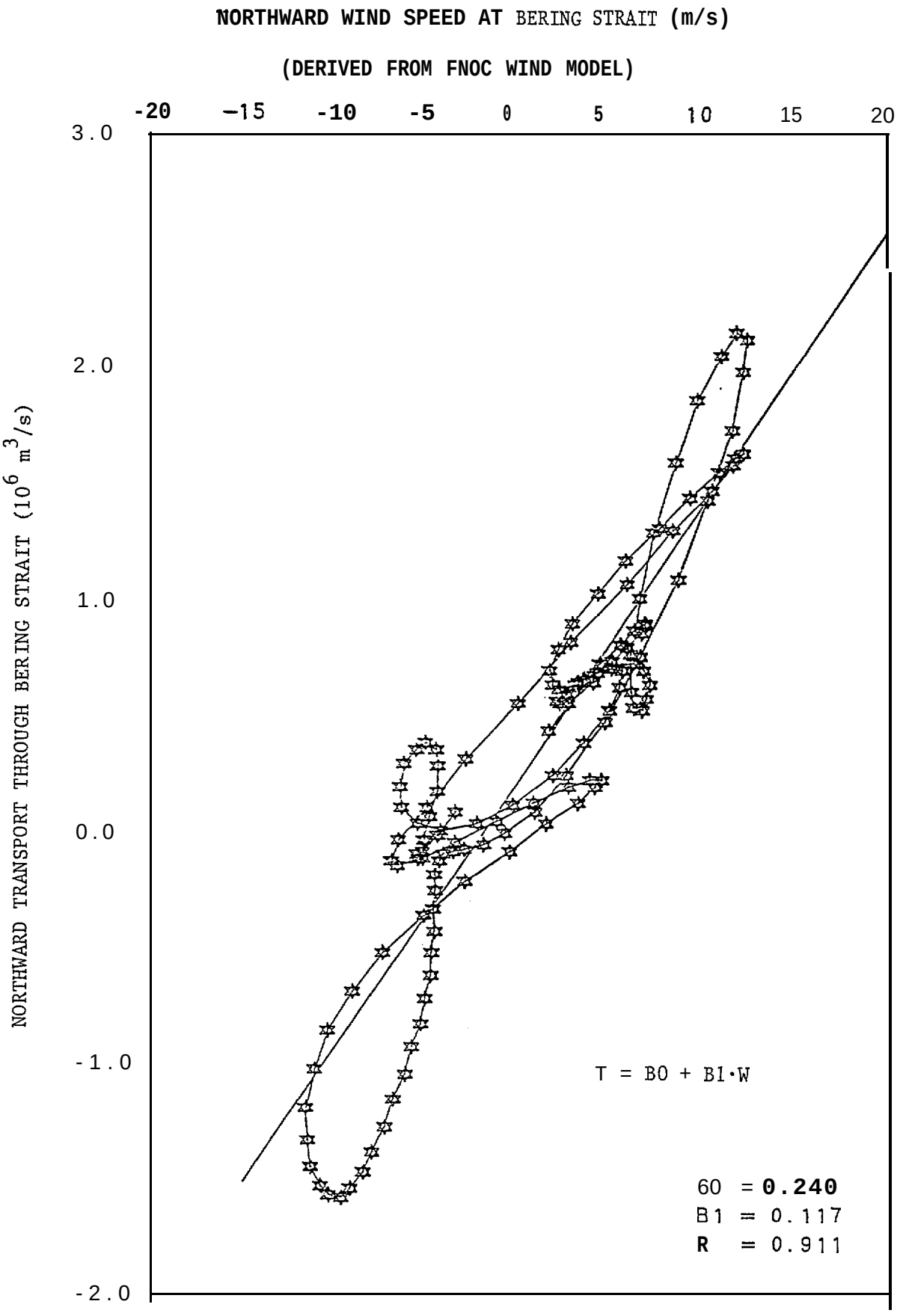

Figure 9. Correlation between the hydrodynamic model predicted transport and local (along axis 192° T) wind speed for the Bering Strait.

Table 1. Comparison of the hydrodynamic model predicted transports and mean velocities for the Bering', Anadyr, and Shpanberg Straits with an imposed sea surface slope of 10^{-6}, fine and coarse grid cases.

	Coarse Grid			Fine Grid			
Passage	**Transport (Sv)**	**Mean Speed (m/s)**	**Cross Sectional Area (m' x 10')**	**Transport (Sv)**	**Mean Speed (cm/s)**	**Cross Sectional (m^2 x 10^{-6})**	**Mean Depth (m)**
Anadyr	1.17 (66.5%)*	36(49)**	3.2	1.35 (68.2%)	44(54)	3.0	40
Shpanberg	0.59 (33.5%)	11(11)	4.6	0.63 (31.8%)	12(13)	4.4	24
Bering	1.76 (100%)	41(46)	3.6	1.98 (loo%)	49(52)	3.9	34

* Indicates % of transport referenced to the Bering **Straits.**
** **The first numbers gives the mean current speed** normal **to the transect while the second entry in parentheses** *is* the mean velocity magnitude across the transect.

Guide to Appendices

For interested researchers we have documented the simulations performed by providing spatial plots of the wind forcing field and the corresponding vertically averaged currents and surface elevation contours as a function of time. Plots are presented every day starting at midnight.

Appendices A and B contain the Fleet Numerical Oceanographic Center (FNOC) wind model predictions on a 2.5 degree resolution for February and June 1982, respectively. Appendices C and D show the hydrodynamic model predicted vertically averaged currents and sea surface elevation contours for February and June 1982, respectively.

All plots have the same scale to facilitate comparison between the wind forcing fields and the corresponding current and surface elevation response.

APPENDIX A

WIND STRESS

FEBRUARY 1 , 1982 AT 0:00

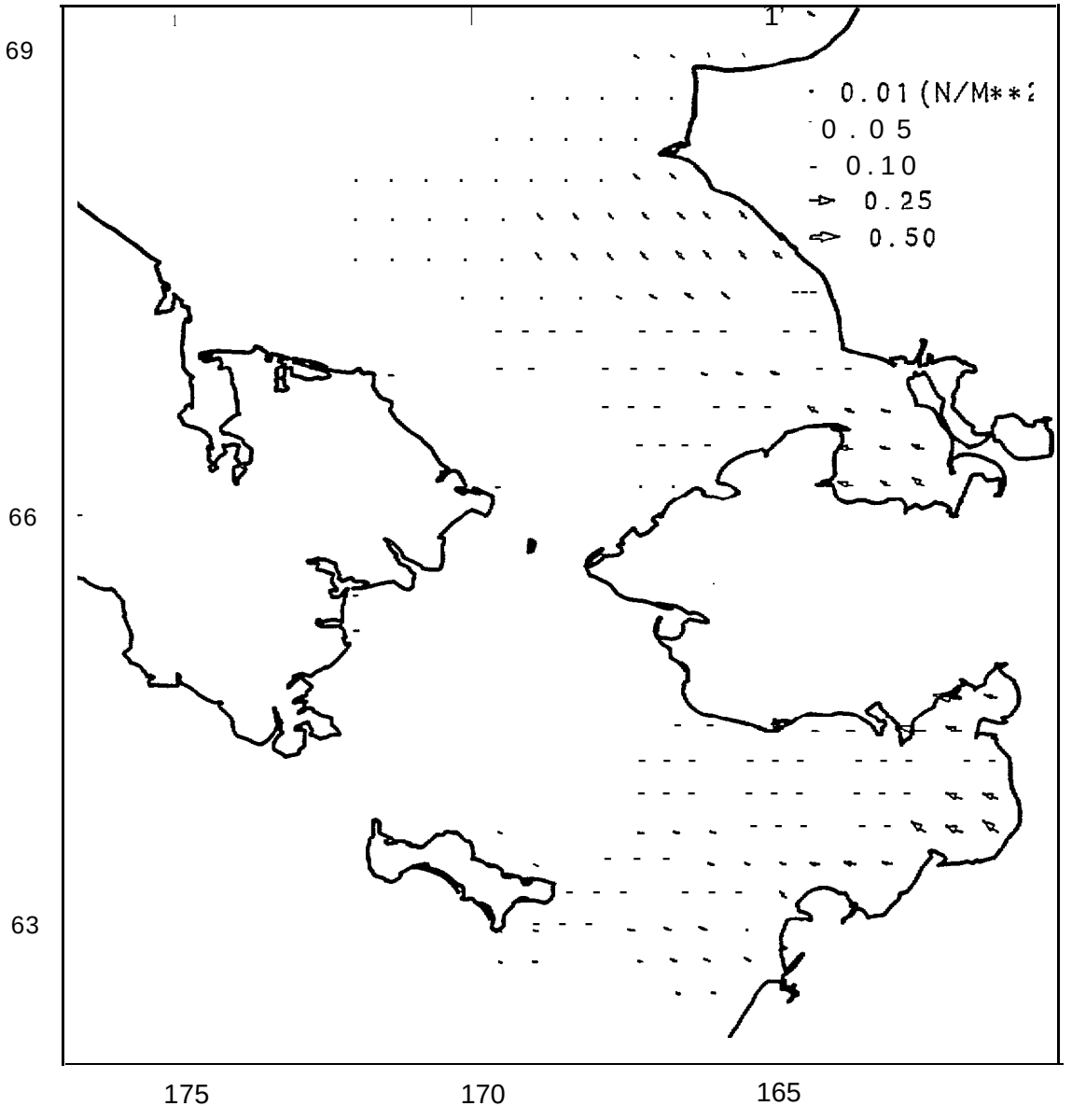

AIT_F1

WIND STRESS

FEBRUARY 2 , 1982 AT 0:00

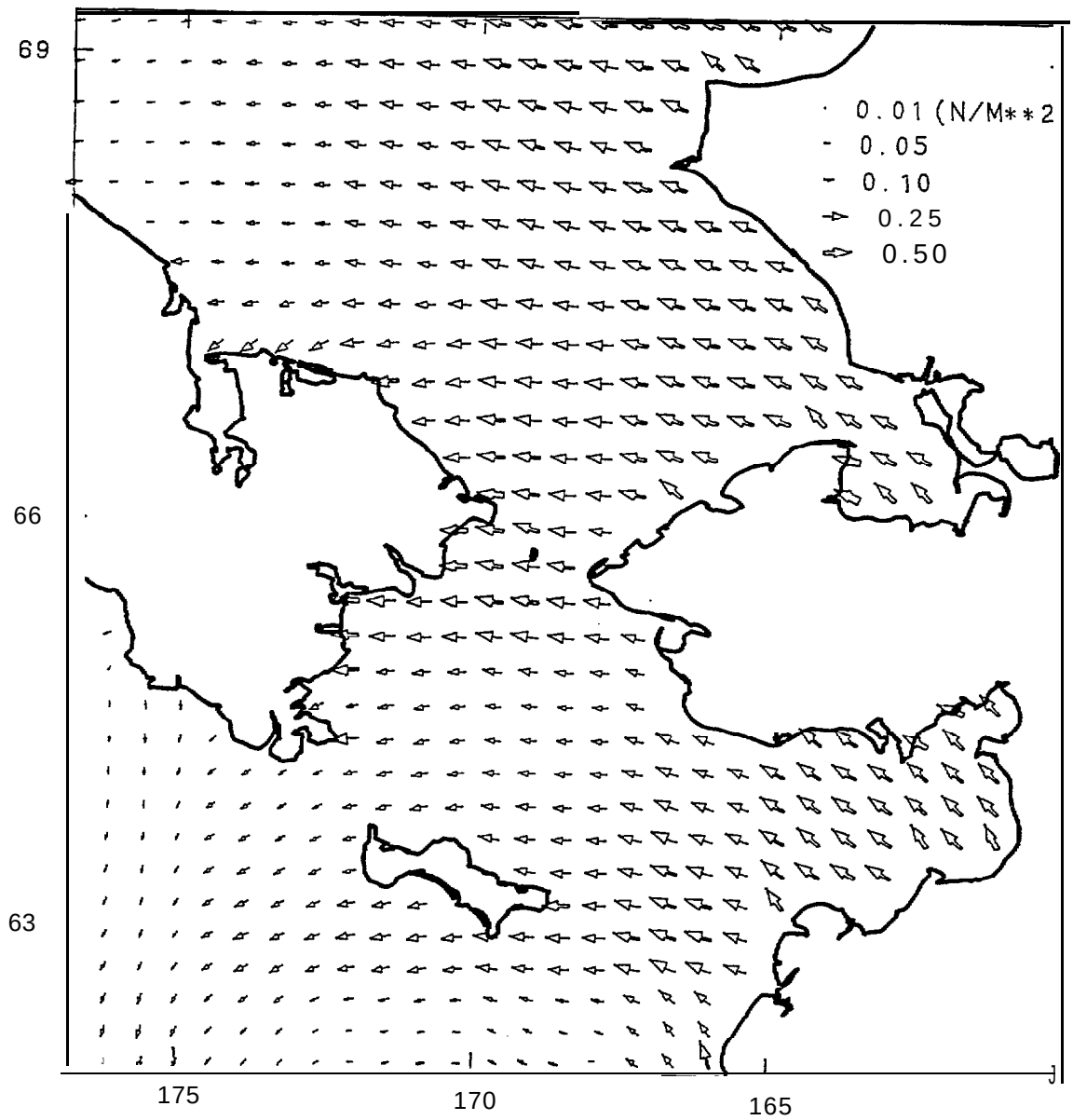

STRAIT_F1

WIND STRESS

FEBRUARY 3 , 1982 AT O:Oo

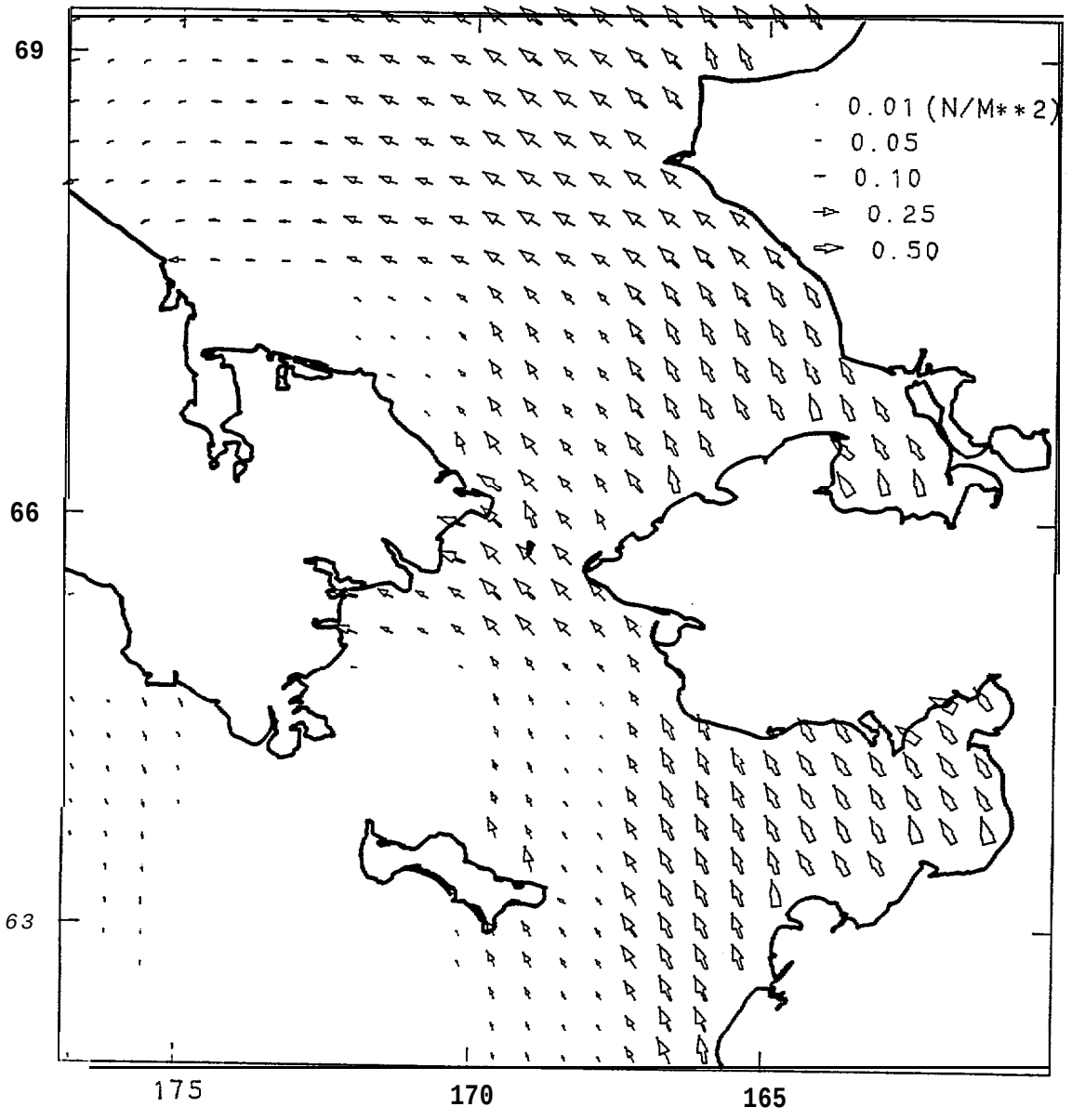

AIT_F1

WIND STRESS

FEBRUARY 4 , 1982 AT 0:00

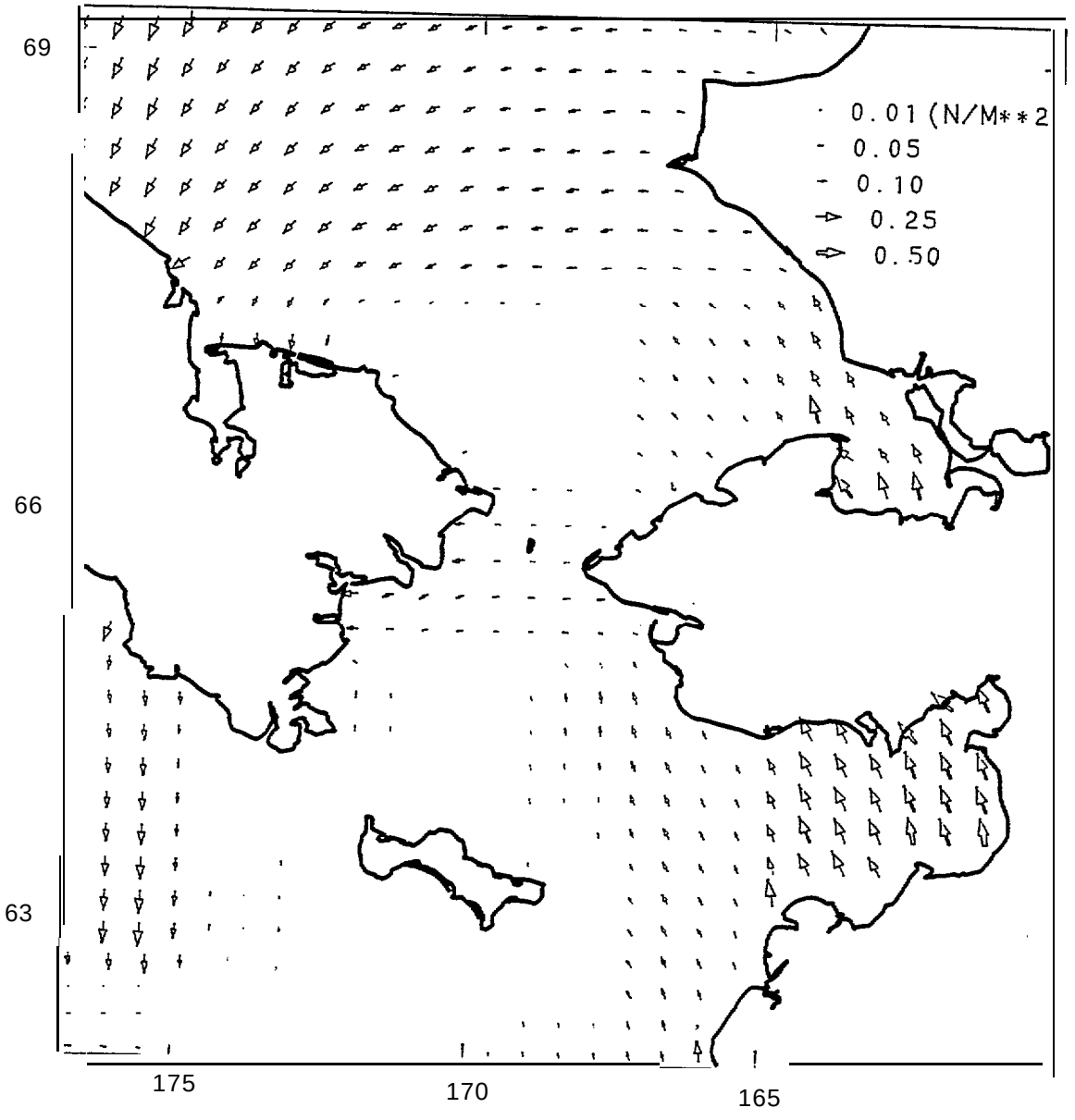

WIND STRESS

FEBRUARY 5 , 1982 AT 0:00

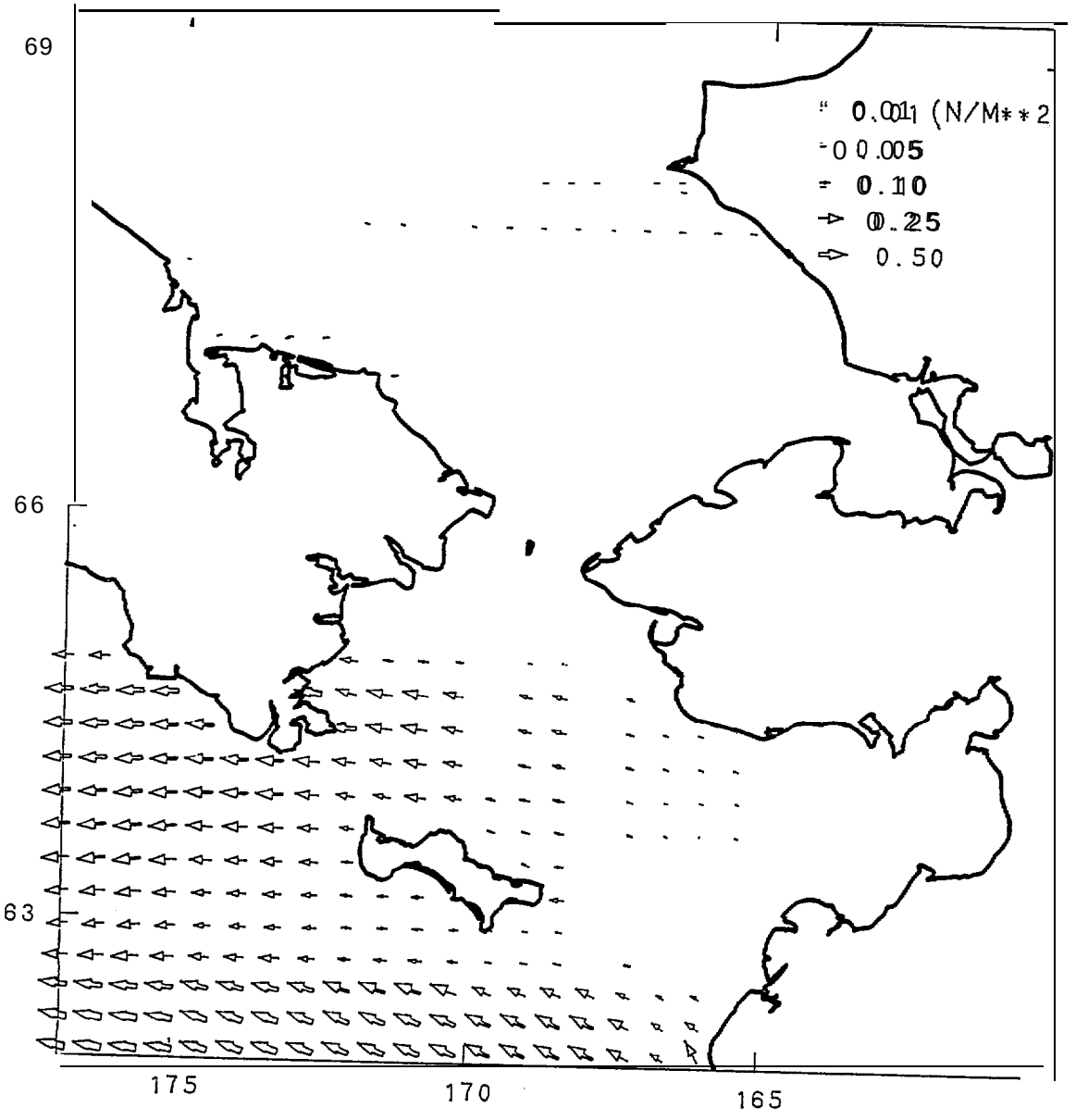

STRAIT_F1

WIND STRESS

FEBRUARY 6 982 AT 0.00

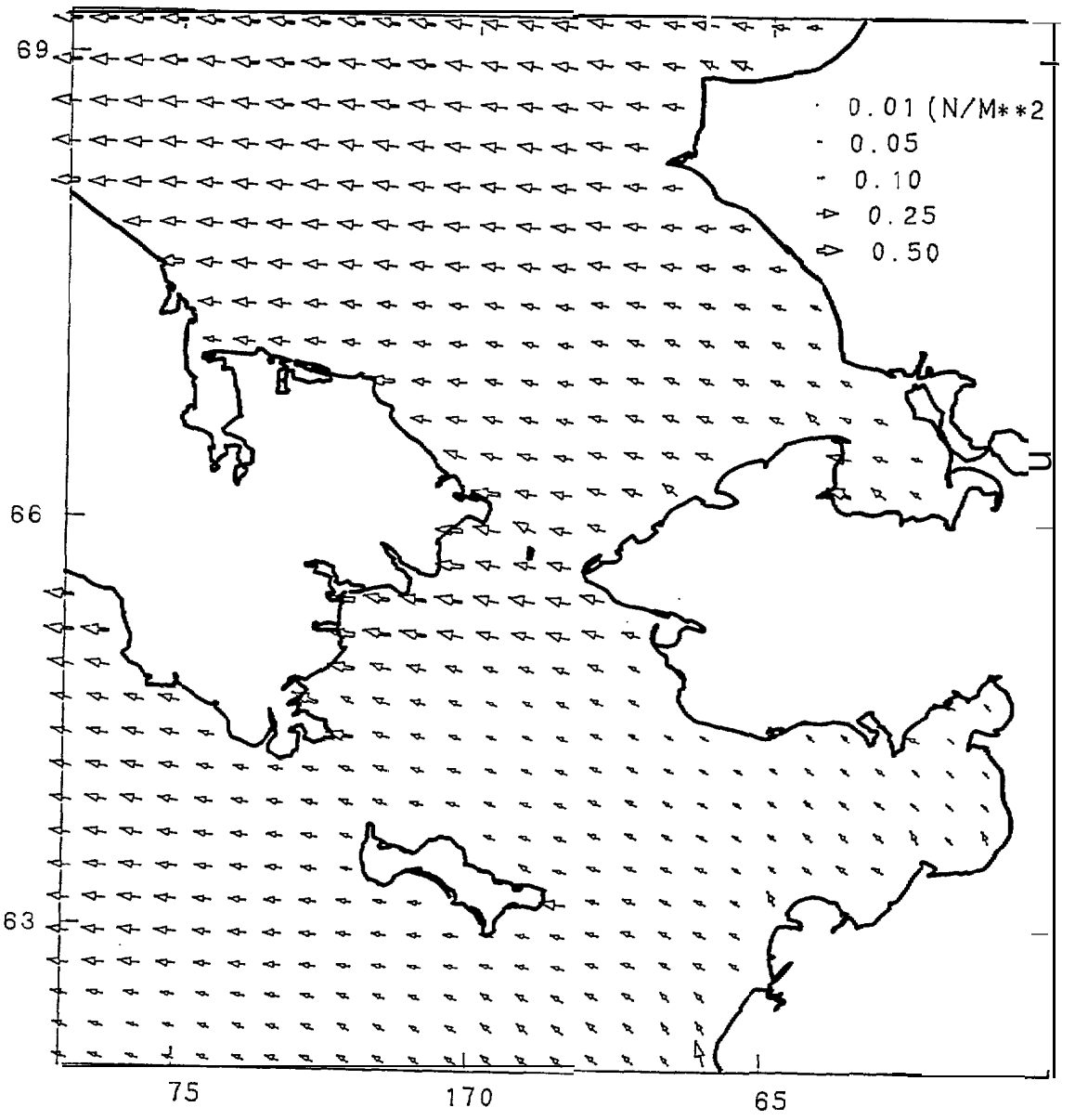

WIND STRESS

FEBRUARY 7 , 982 AT 0:00

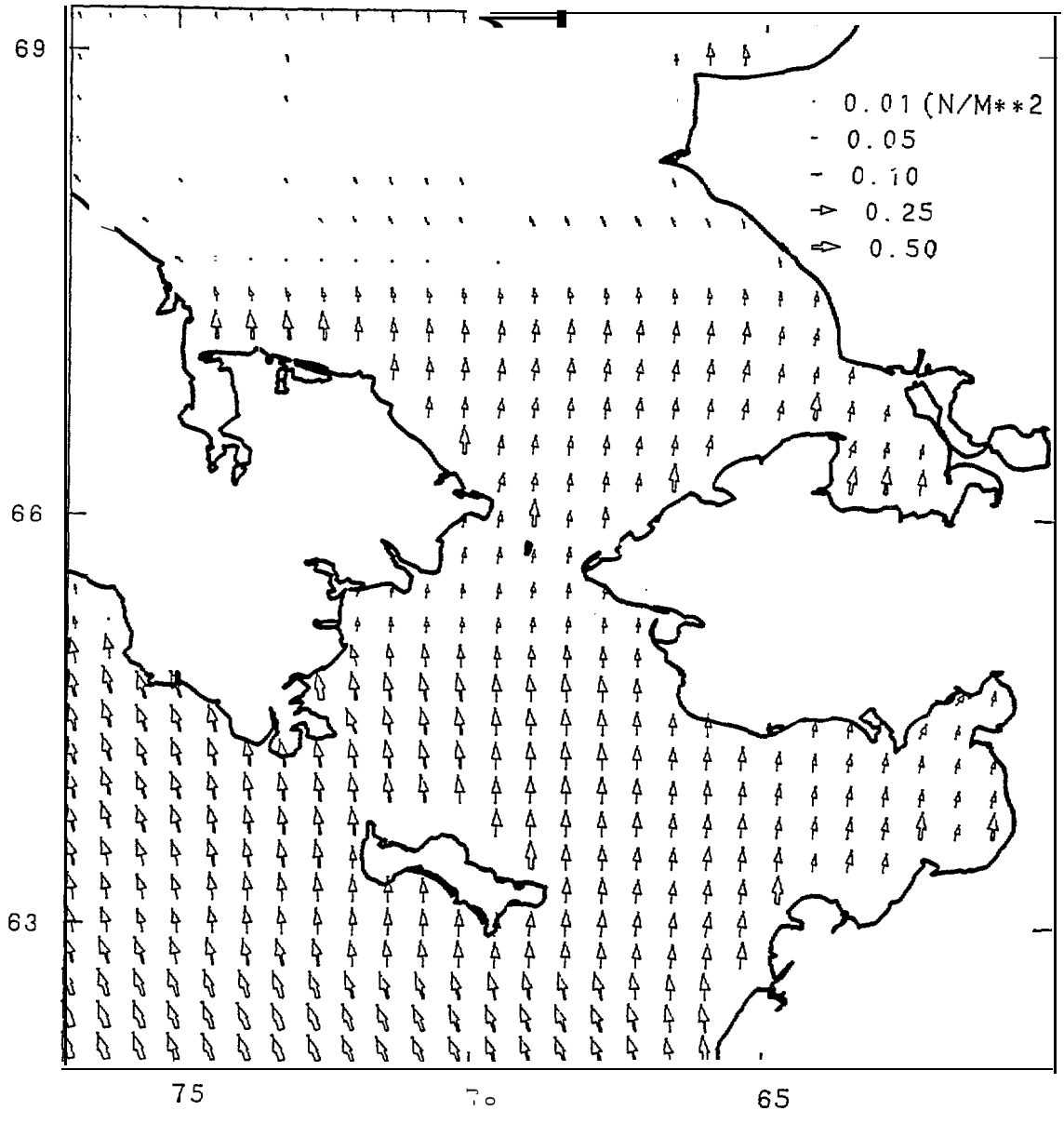

STRAIT_F

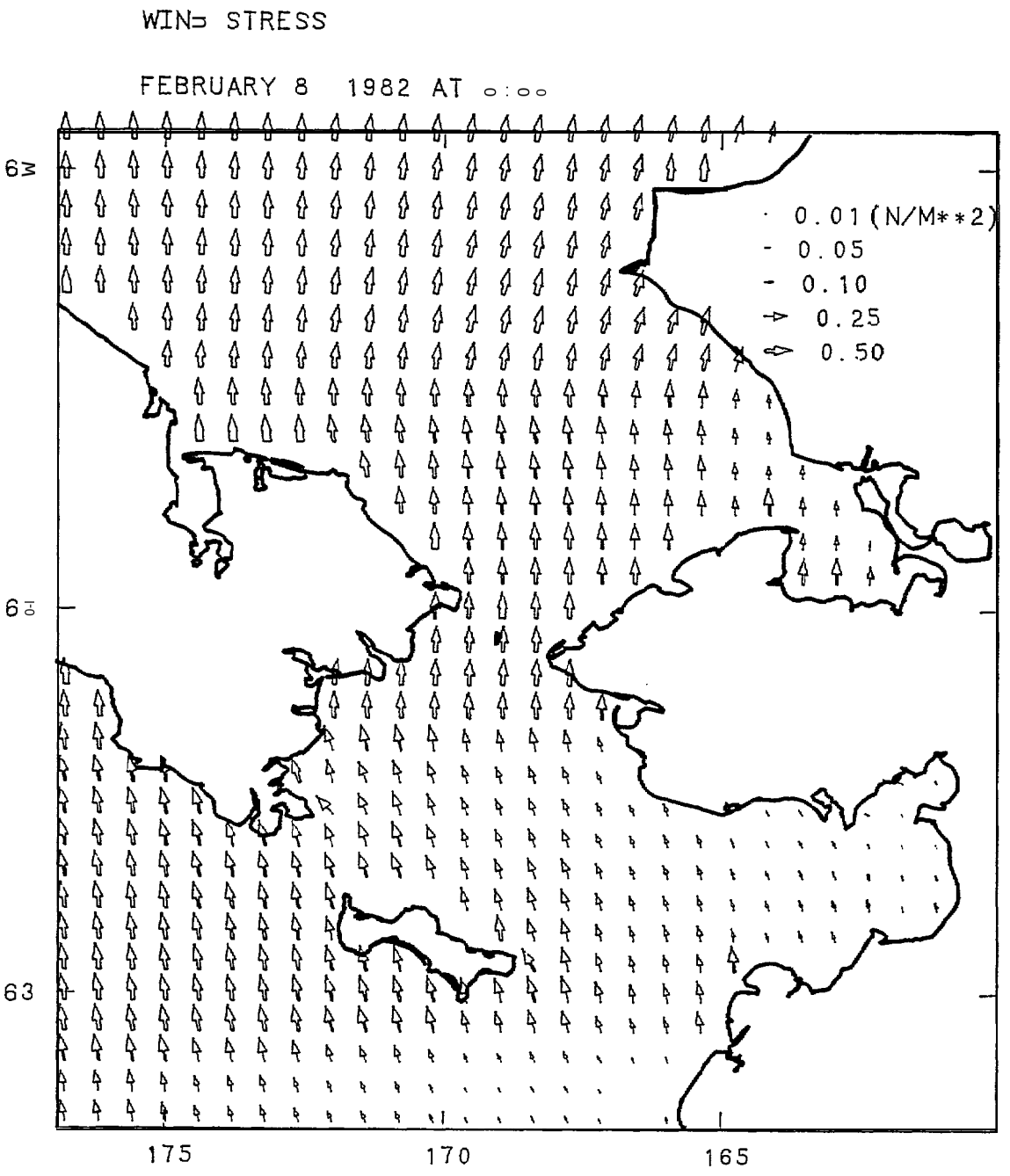
WIND STRESS
FEBRUARY 8 1982 AT 0:00
0.01 (N/M**2)
0.05
0.10
0.25
0.50
65
60
63
175
170
165

WIND STRESS

FEBRUARY 9 ,1982 AT 0:00

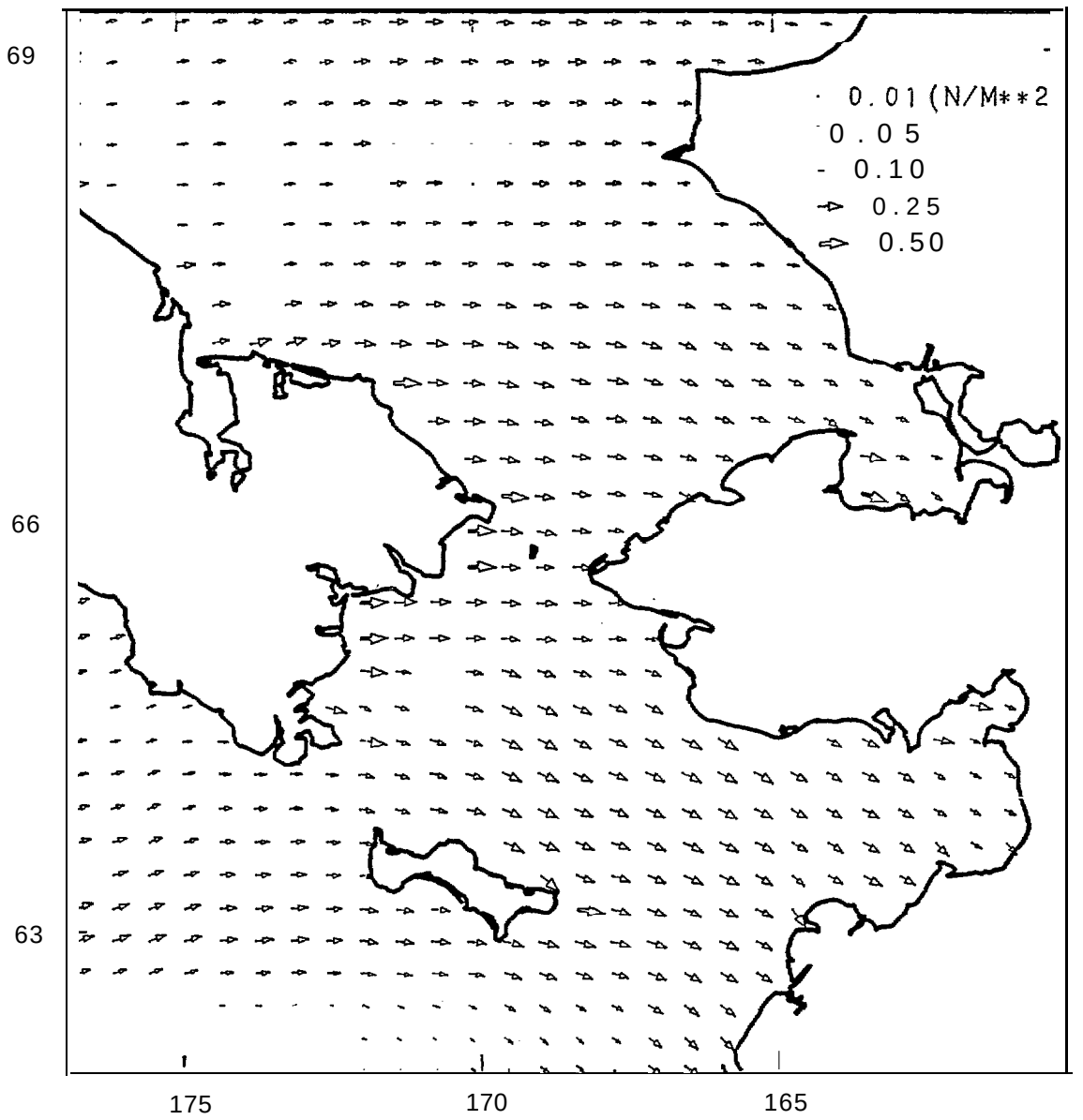

STRAIT_F1

WIND STRESS

FEBRUARY 10 , 1982 AT 0:00

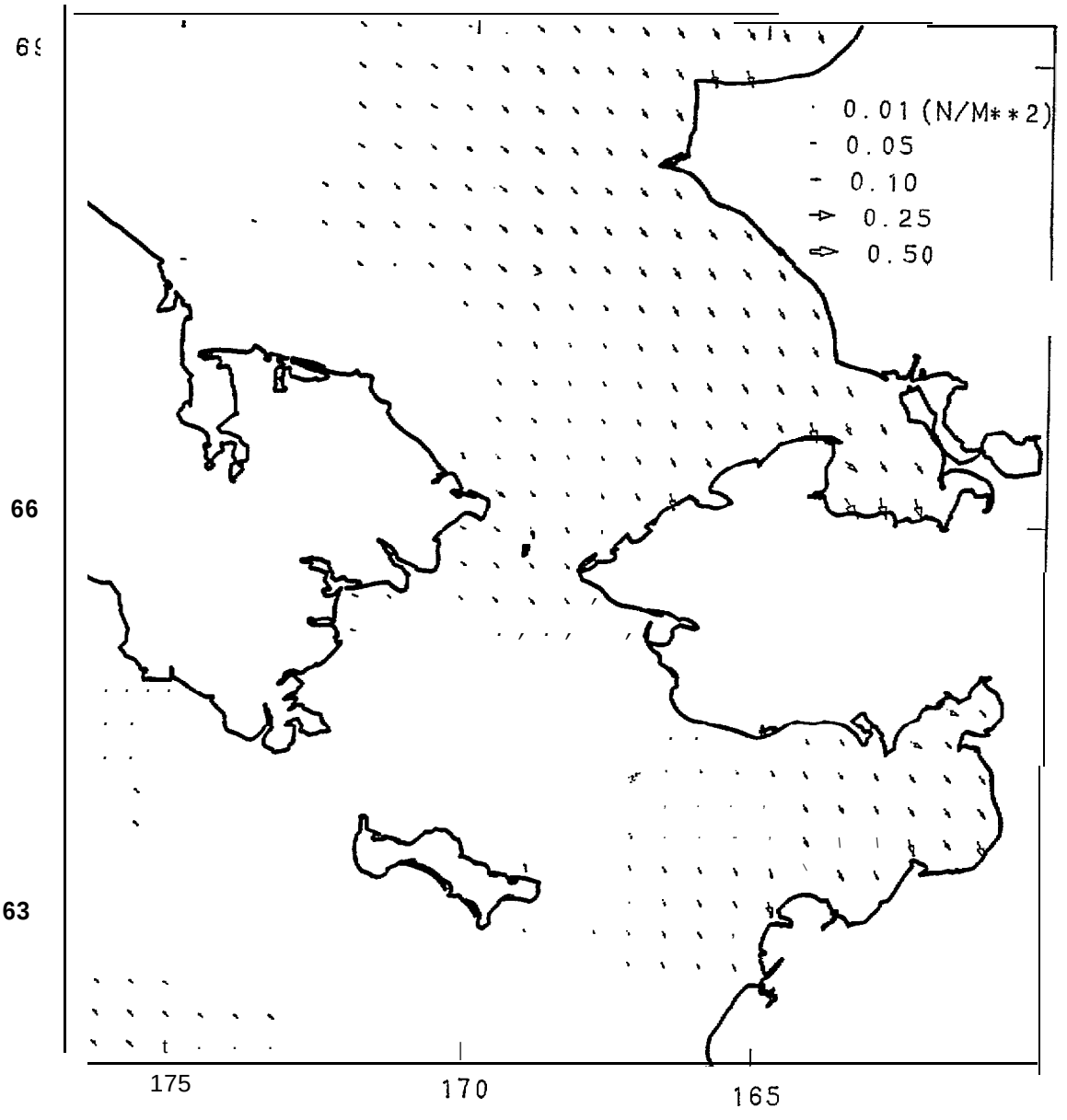

STRAIT_F1

WIND STRESS

FEBRUARY 11 , 1982 AT 0:00

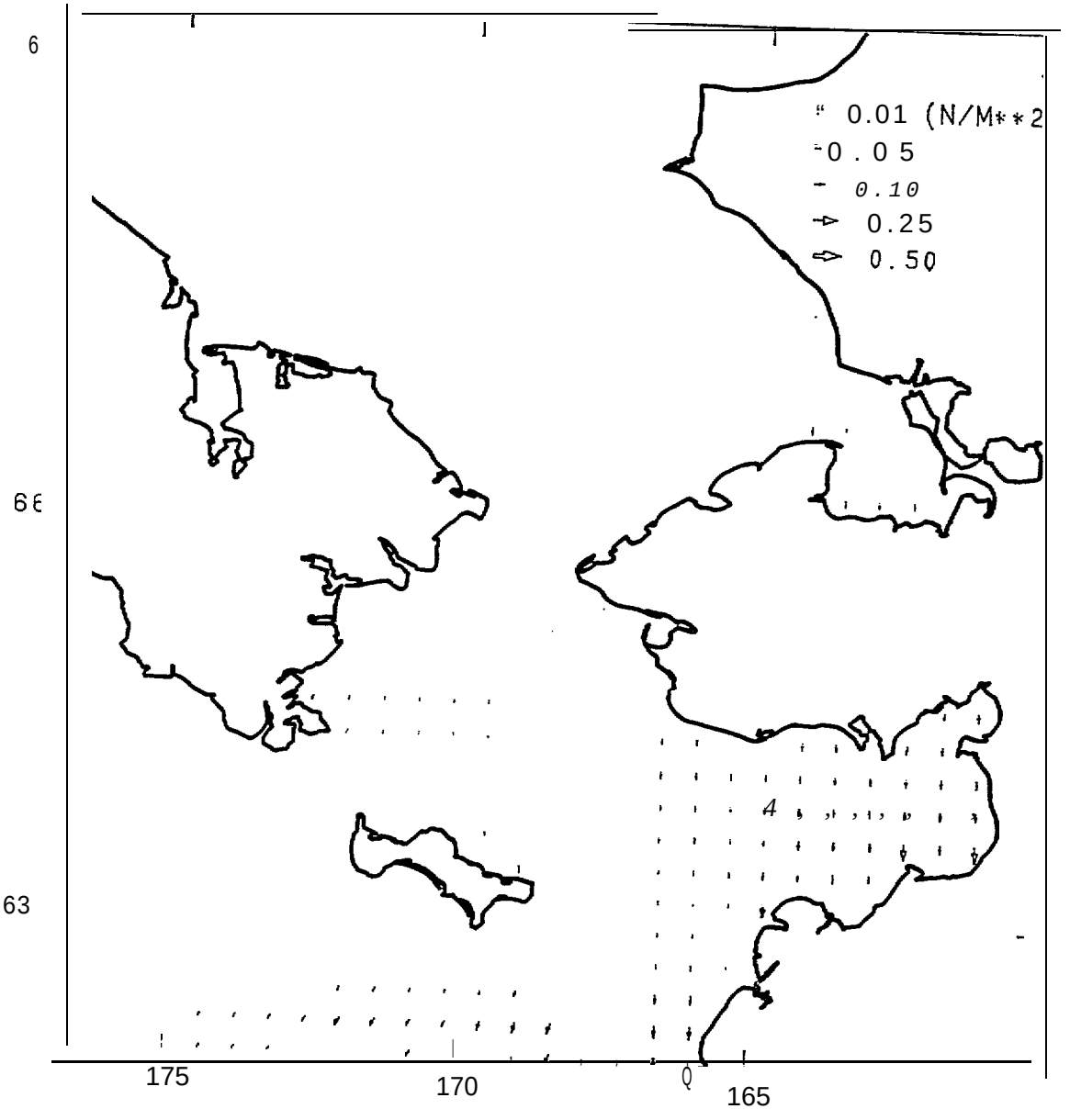

STRAIT_F1

WIND STRESS

FEBRUARY 14 .982 ΔT o:oo

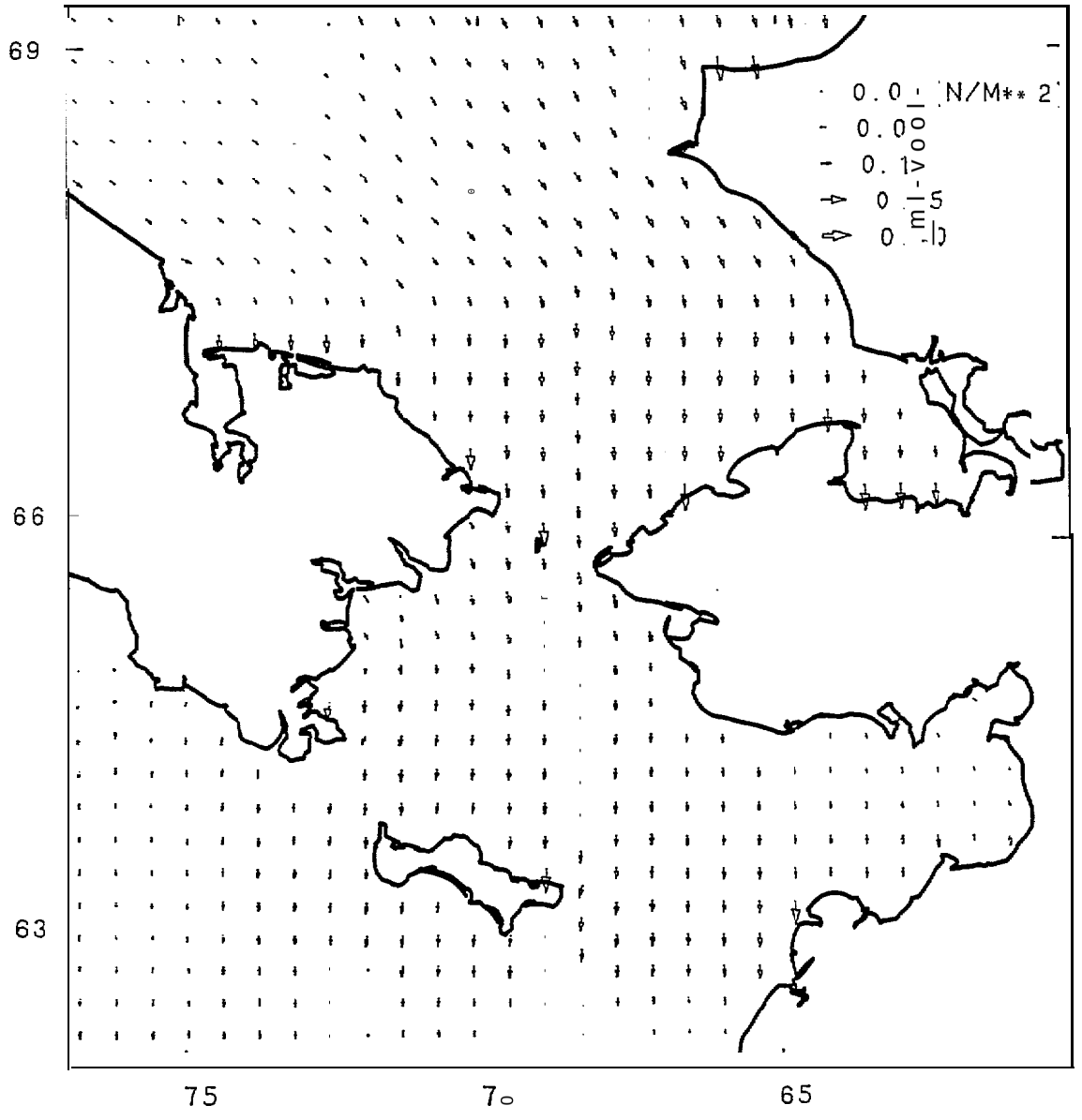

wIND STRESS

FEBRUARY 13 , 1982 AT 0:00

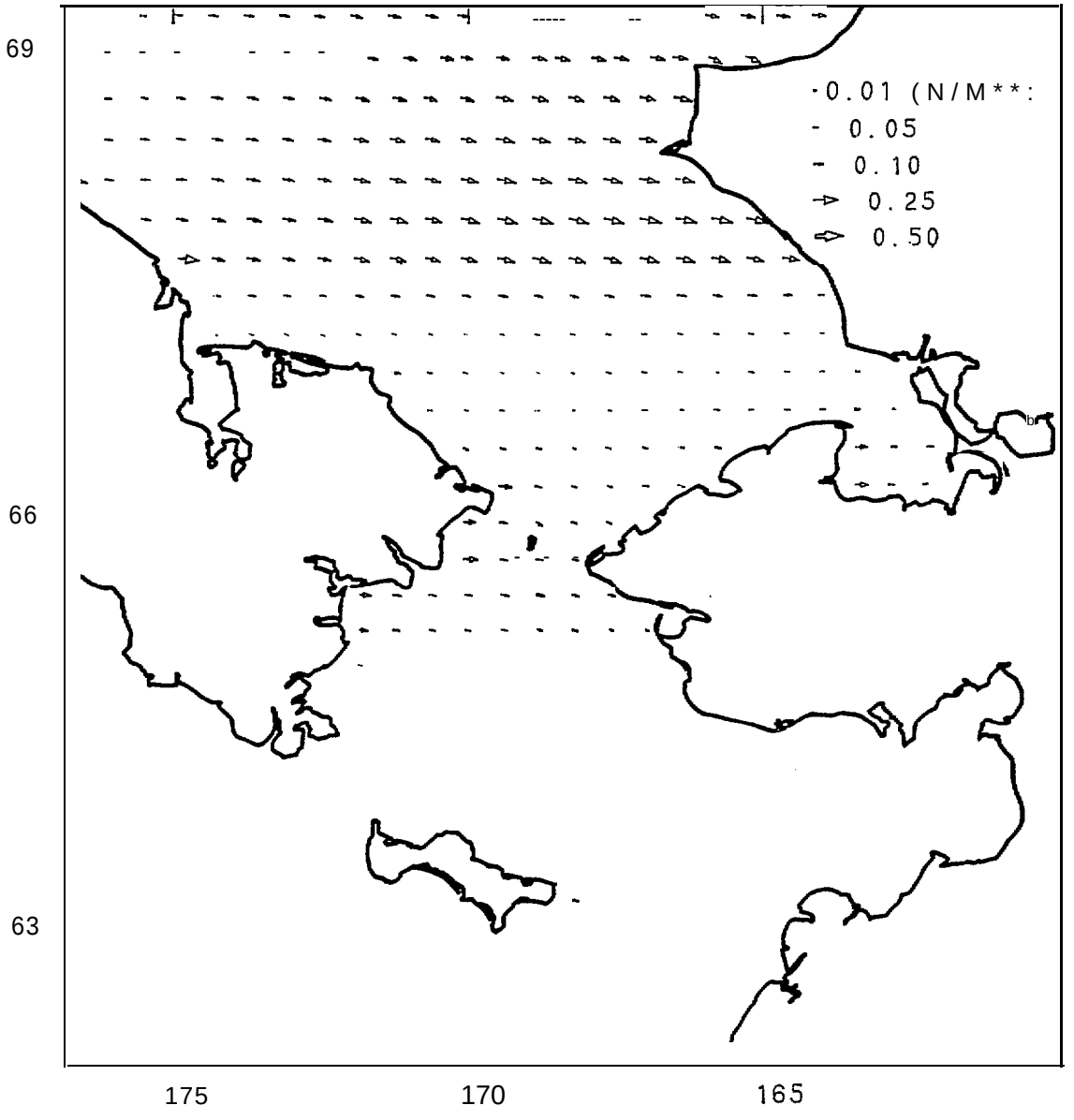

WIND STRESS

FEBRUARY 12 , 1982 AT 0:00

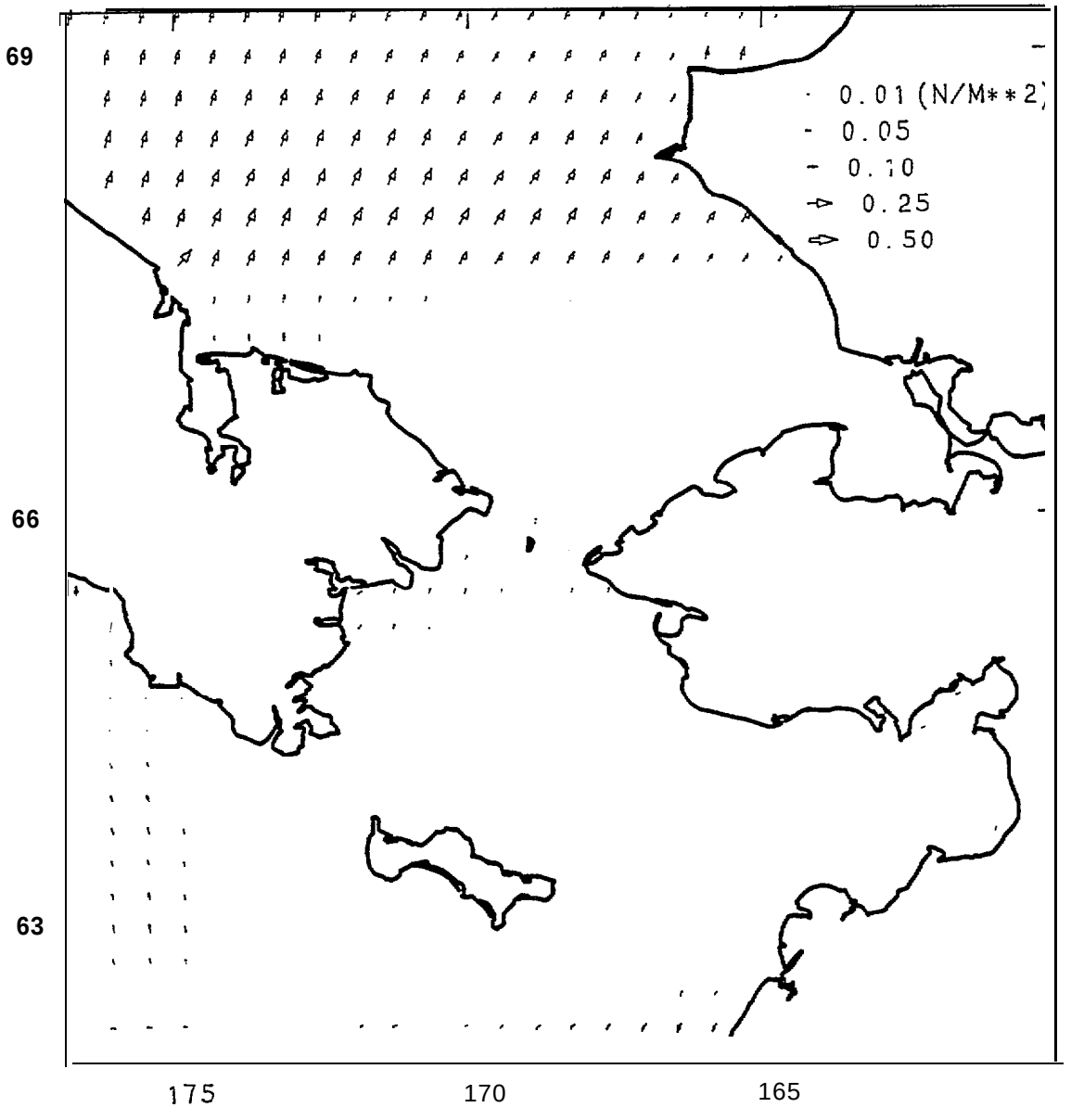

WIND STRESS

FEBRUARY 15 , 1982 AT 0:00

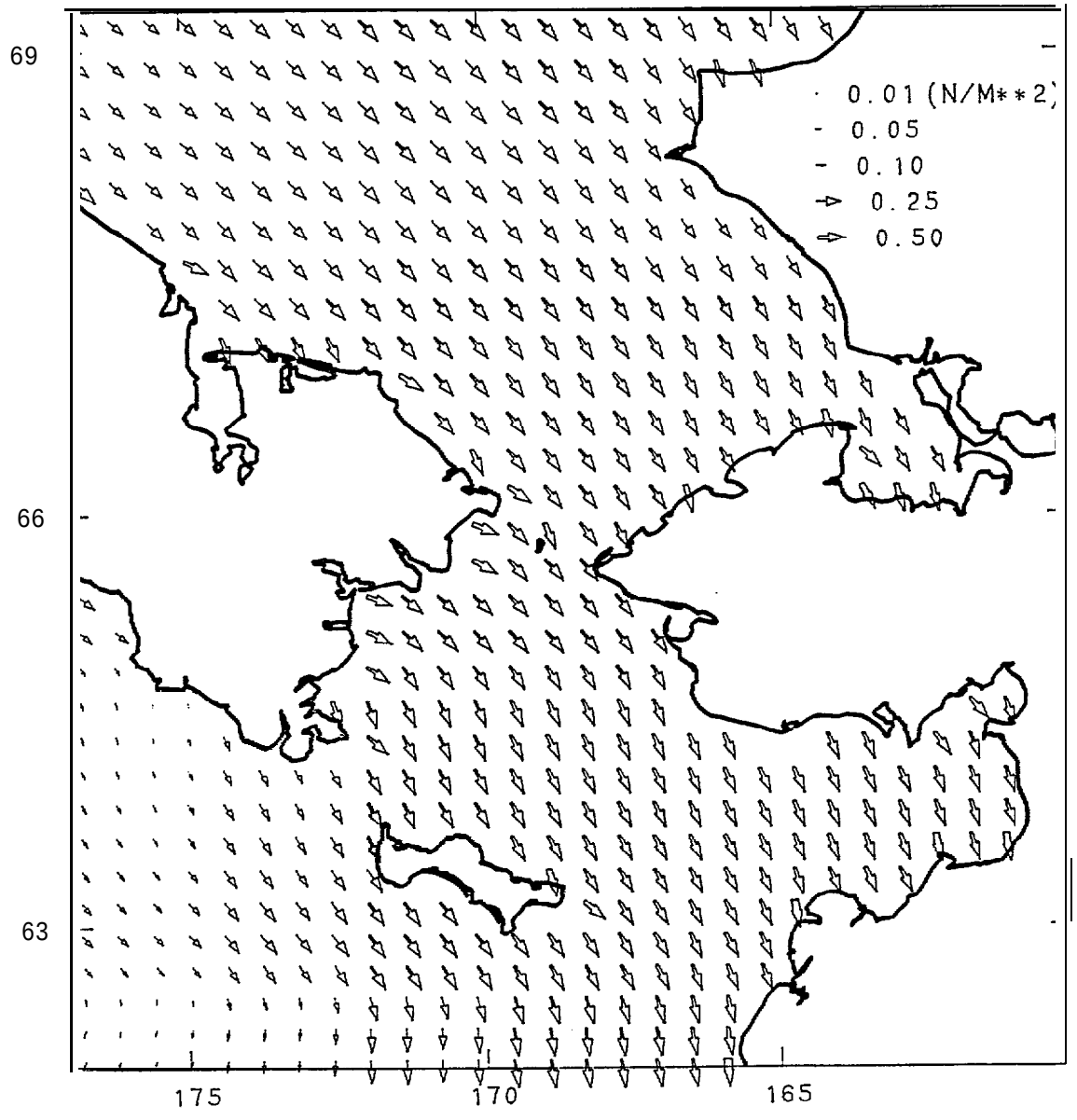

WIND STRESS

FEBRUARY 16 , 1982 AT 0:00

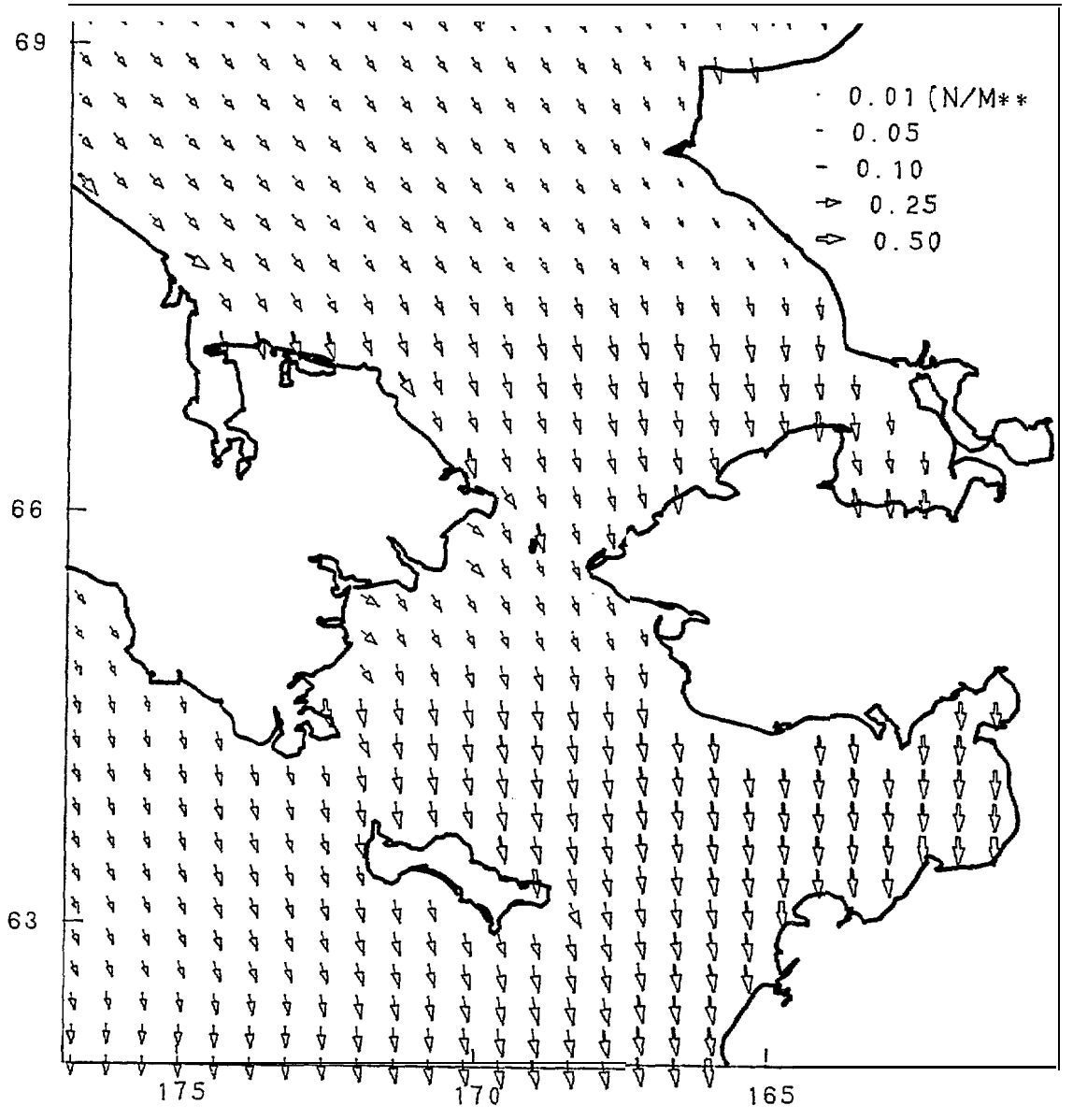

WIND STRESS

FEBRUARY 17 98≥ AT ₀.0₀

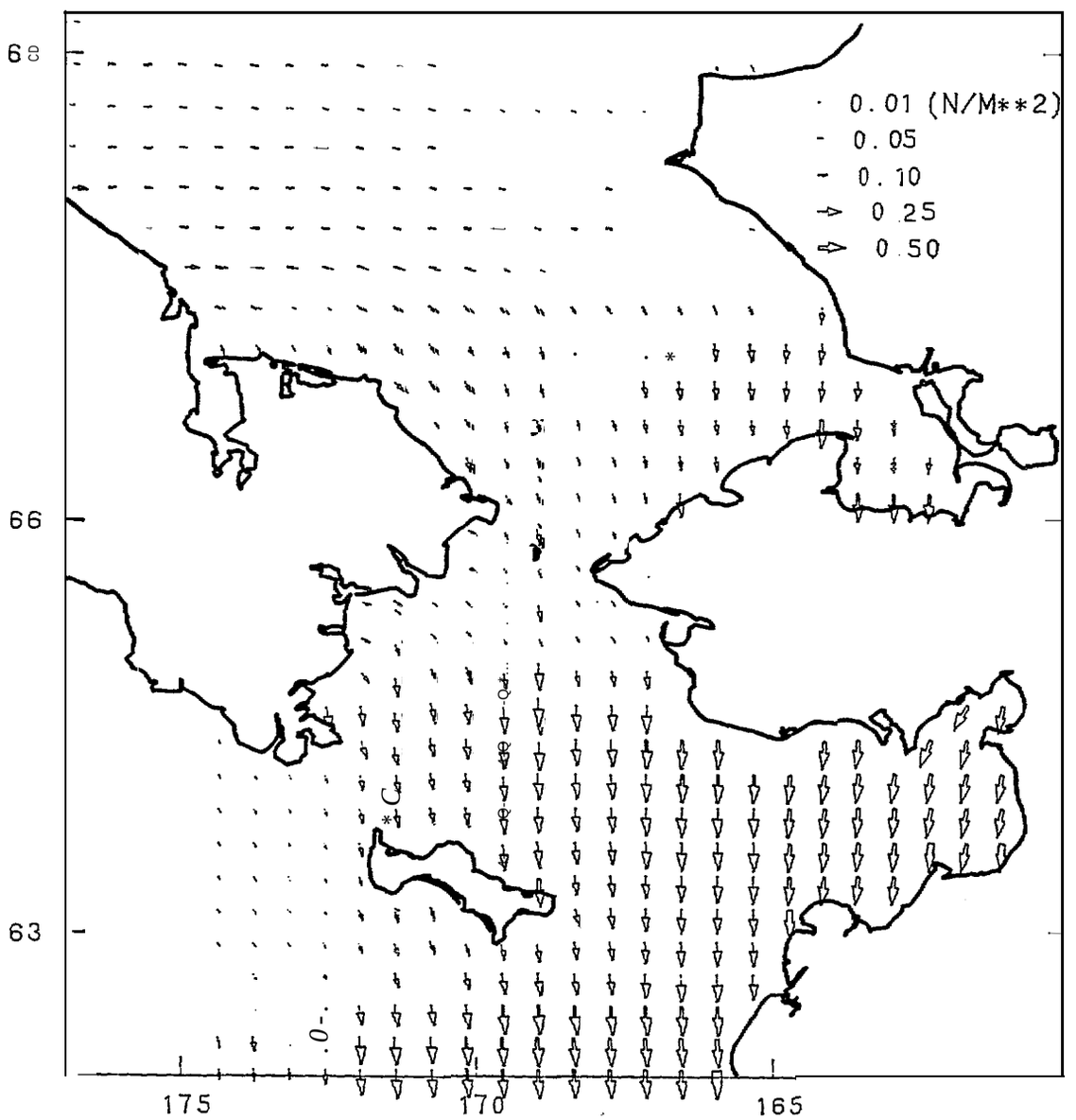

STRAIT_F

WIND STRESS

FEBRUARY 18 : 982 AT 0 oo

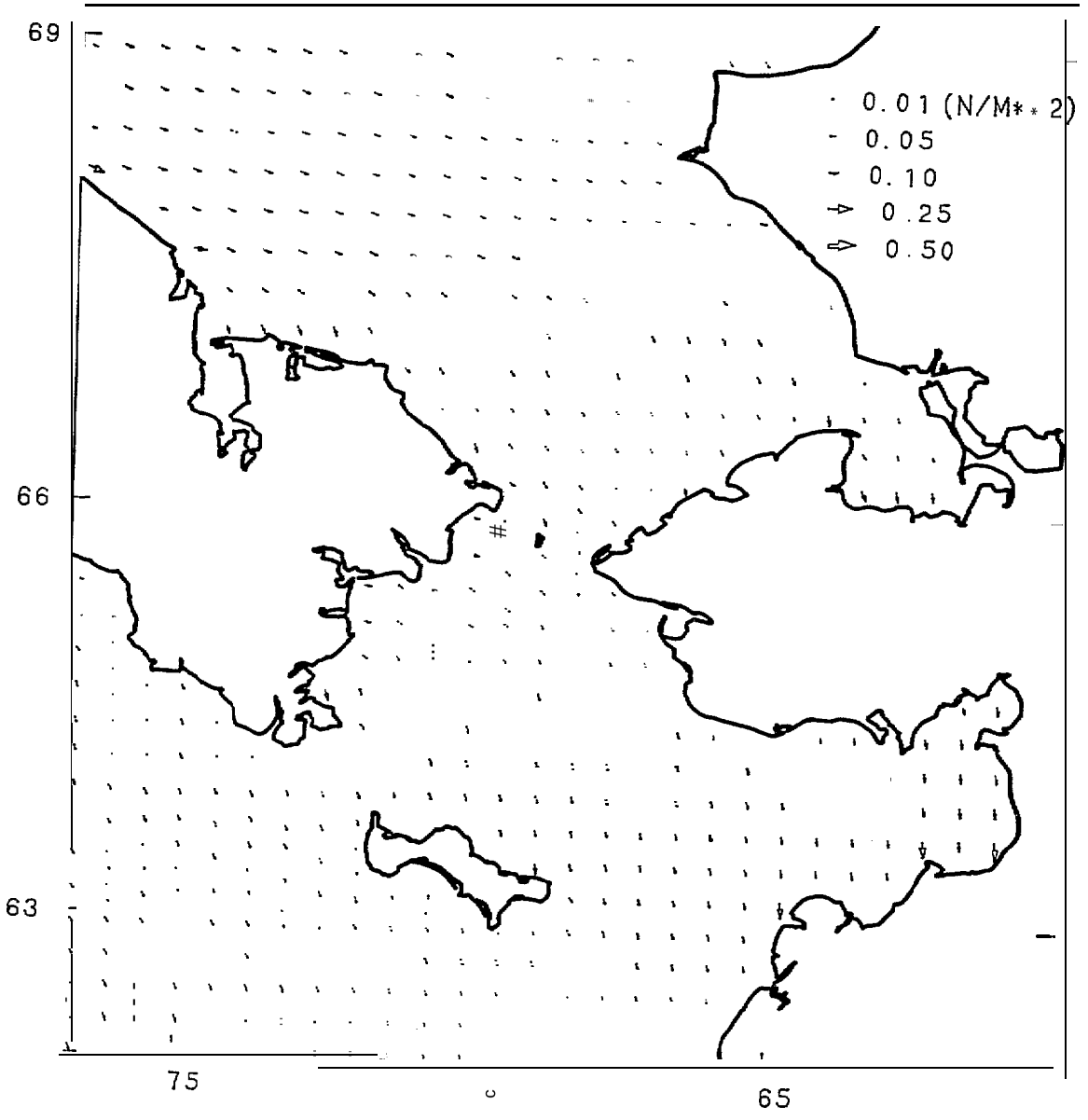

STRAIT_F

WIND STRESS

FEBRUARY 19 , 1982 AT 0:00

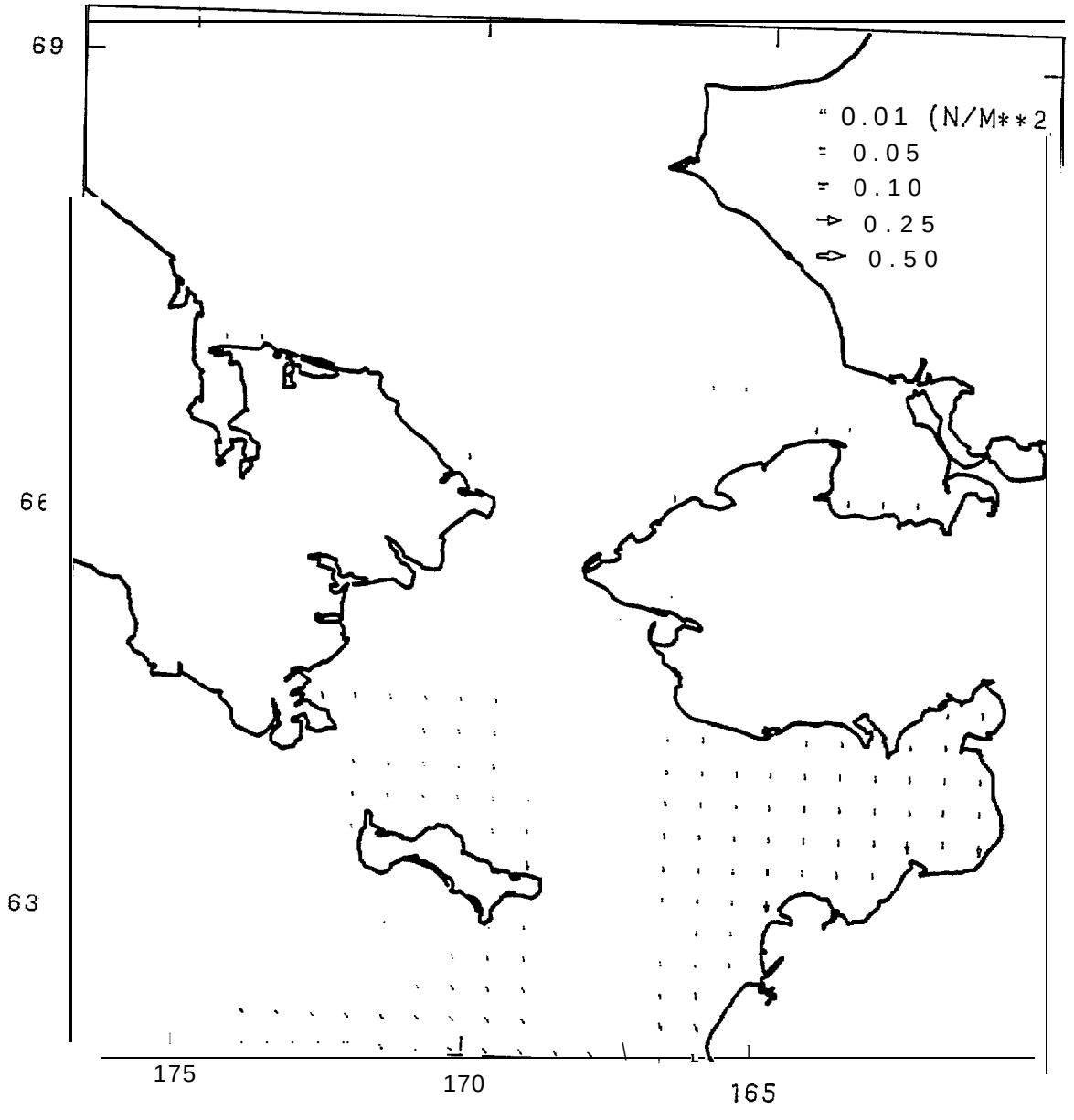

WIND STRESS

FEBRUARY 20 , 1982 AT 0:00

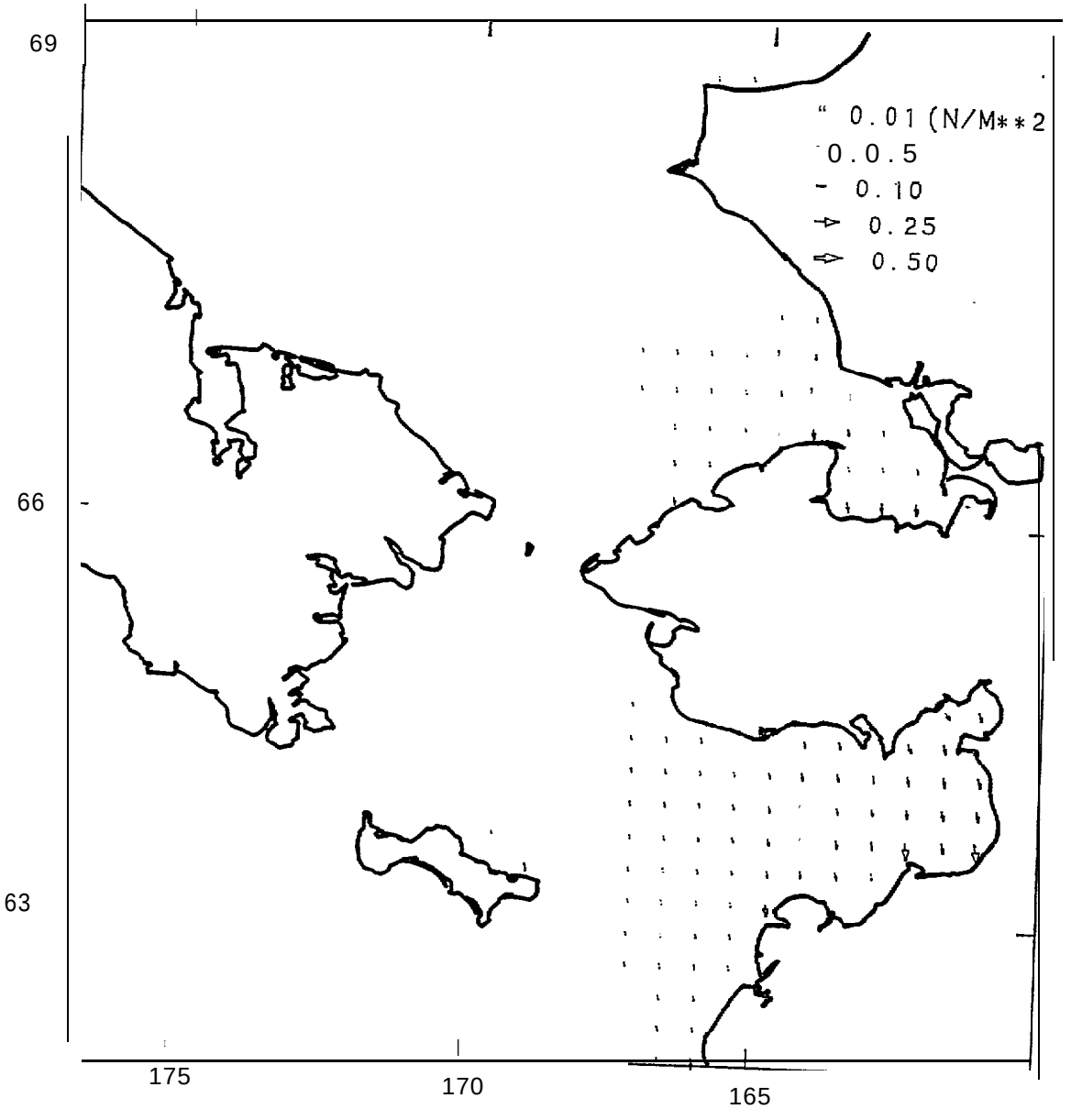

STRAIT_F1

WIND STRESS

FEBRUARY 21 , 1982 AT 0:00

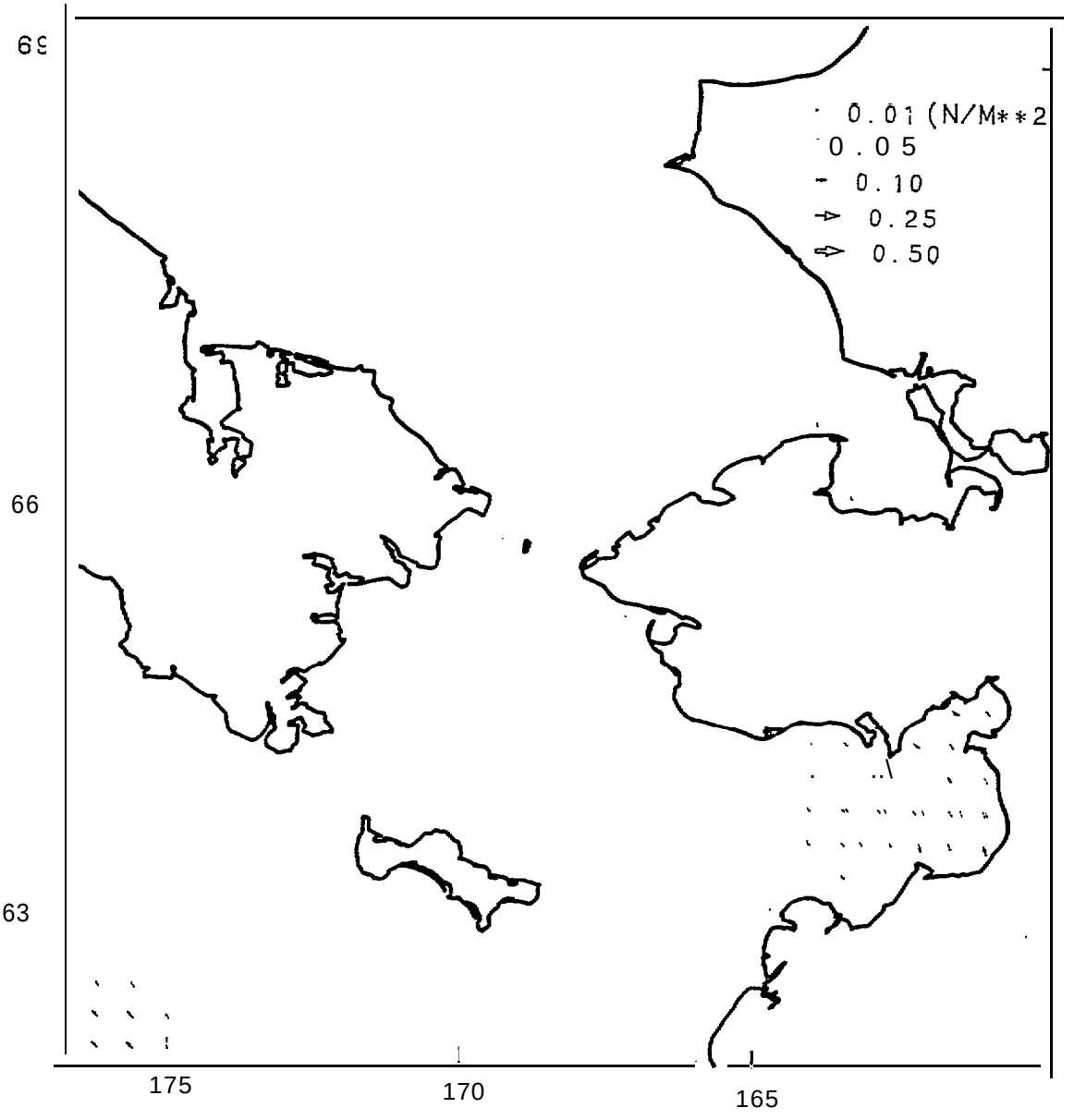

WIND STRESS

FEBRUARY 22 ,1982 AT 0:00

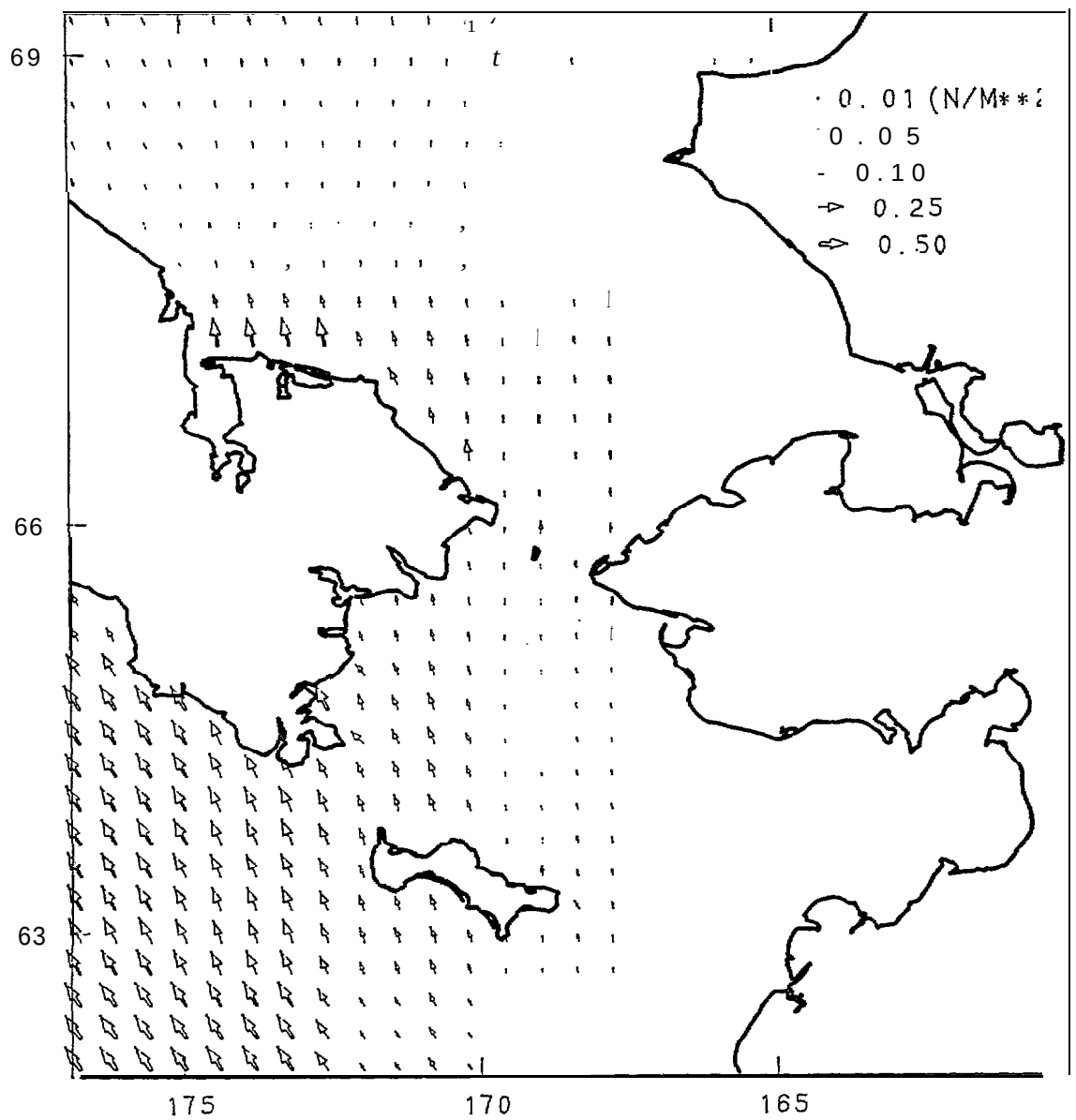

STRAIT_F1

WIND STRESS

FEBRUARY 23 , 1982 AT 0:00

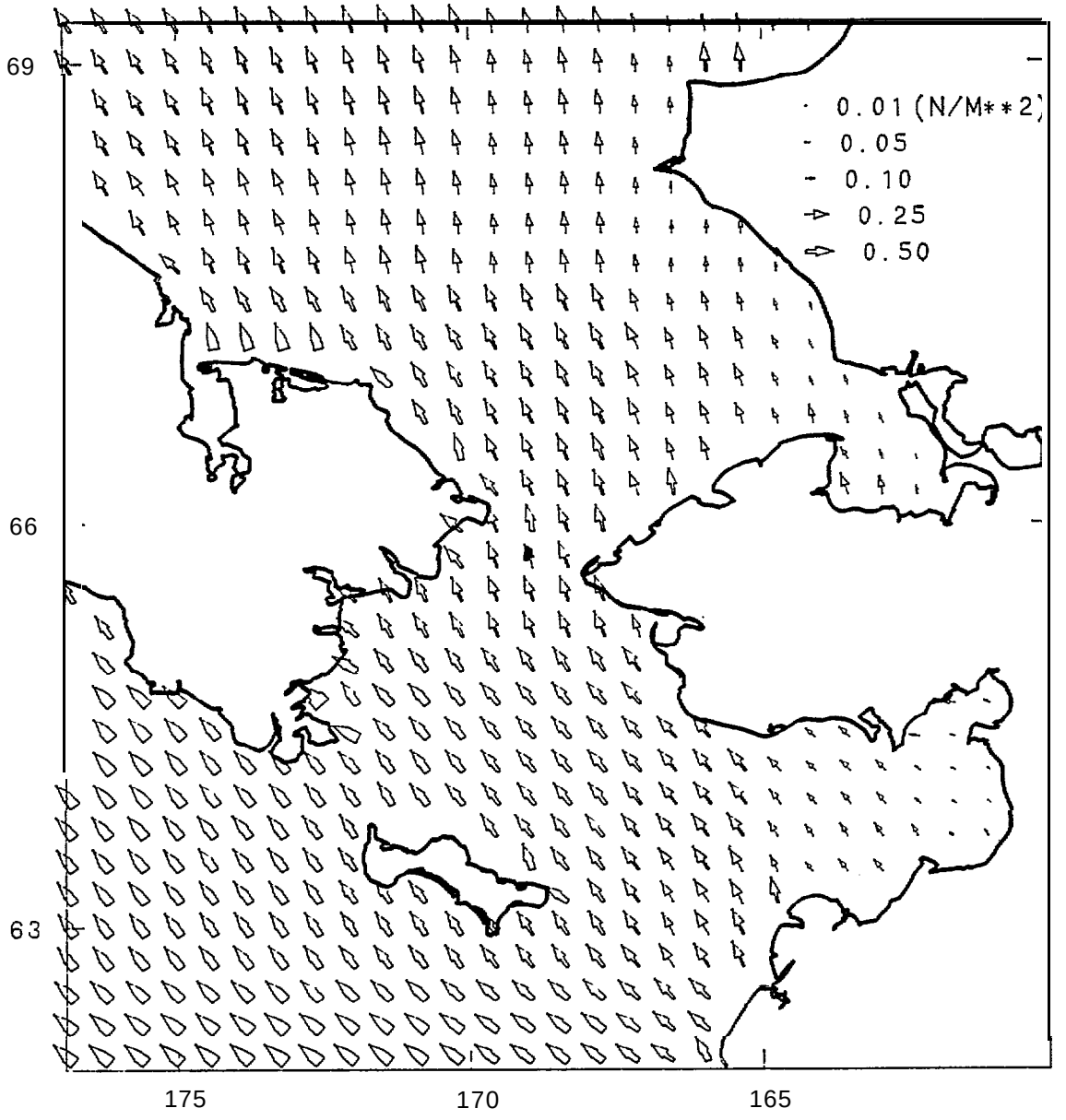

AIT_F1

WIND STRESS

FEBRUARY 24 1982 AT 0:00

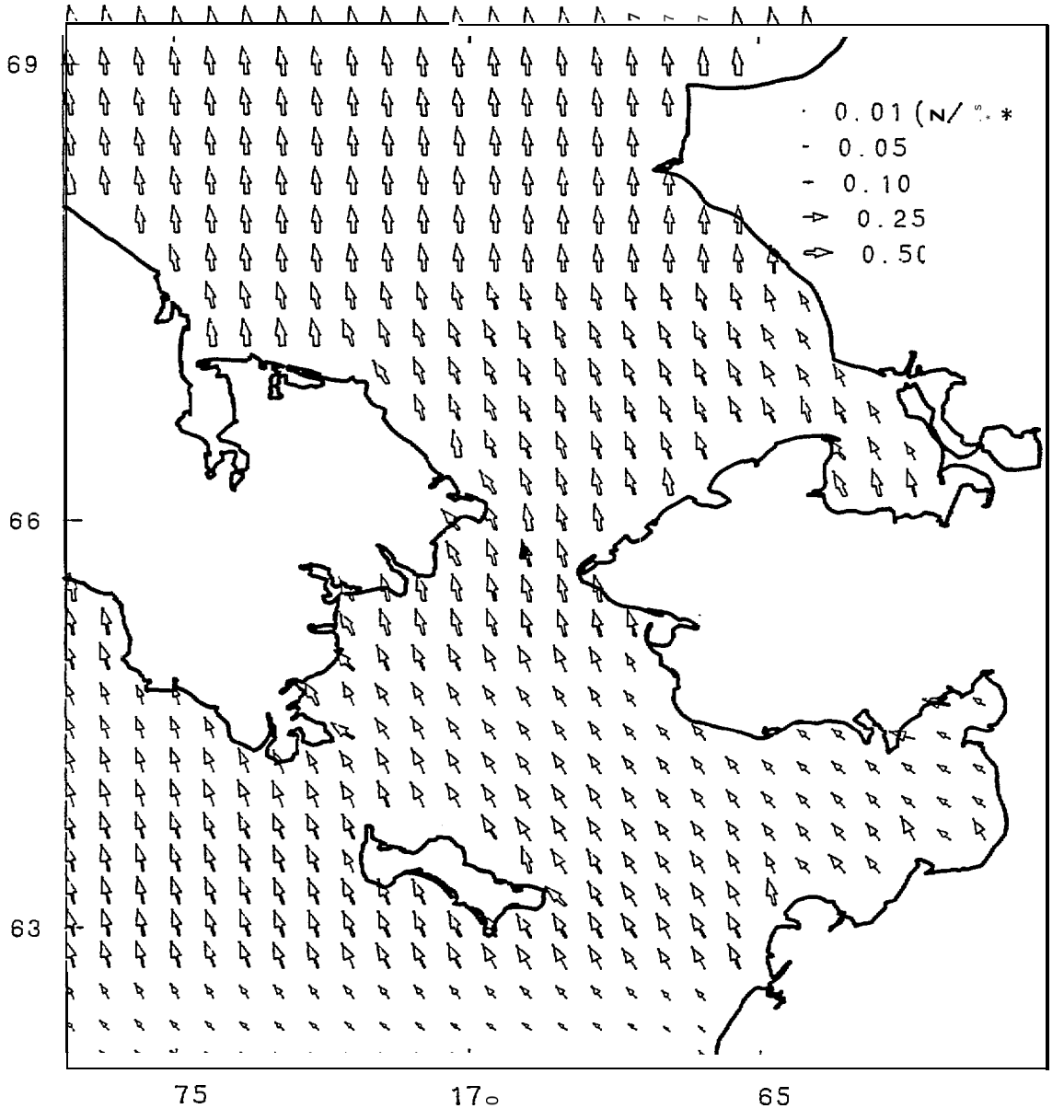

WIND STRESS

FEBRUARY 25 , 1982 AT 0:00

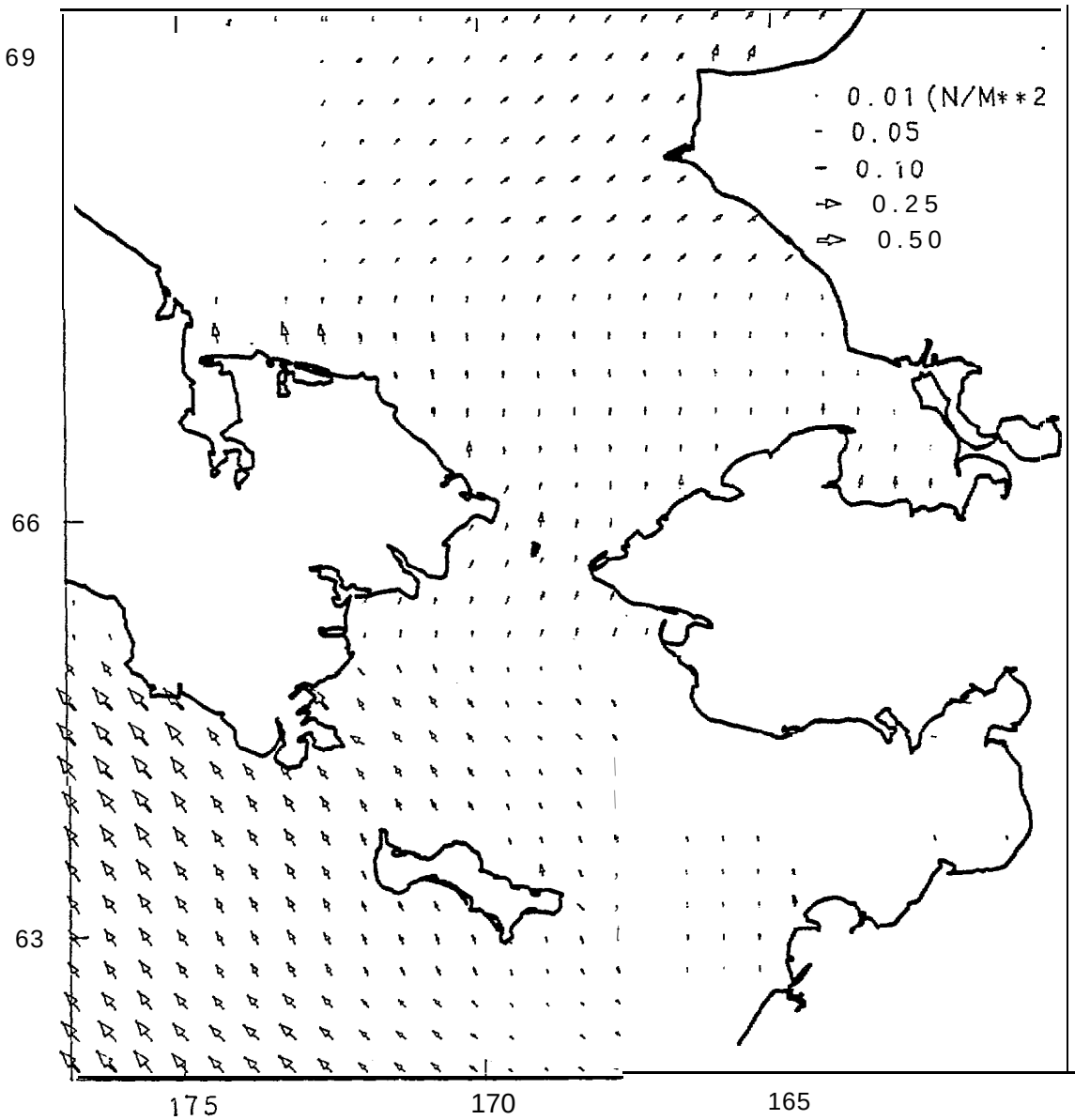

STRAIT_F1

WIND STRESS

FEBRUARY 26 ,1982 AT 0:00

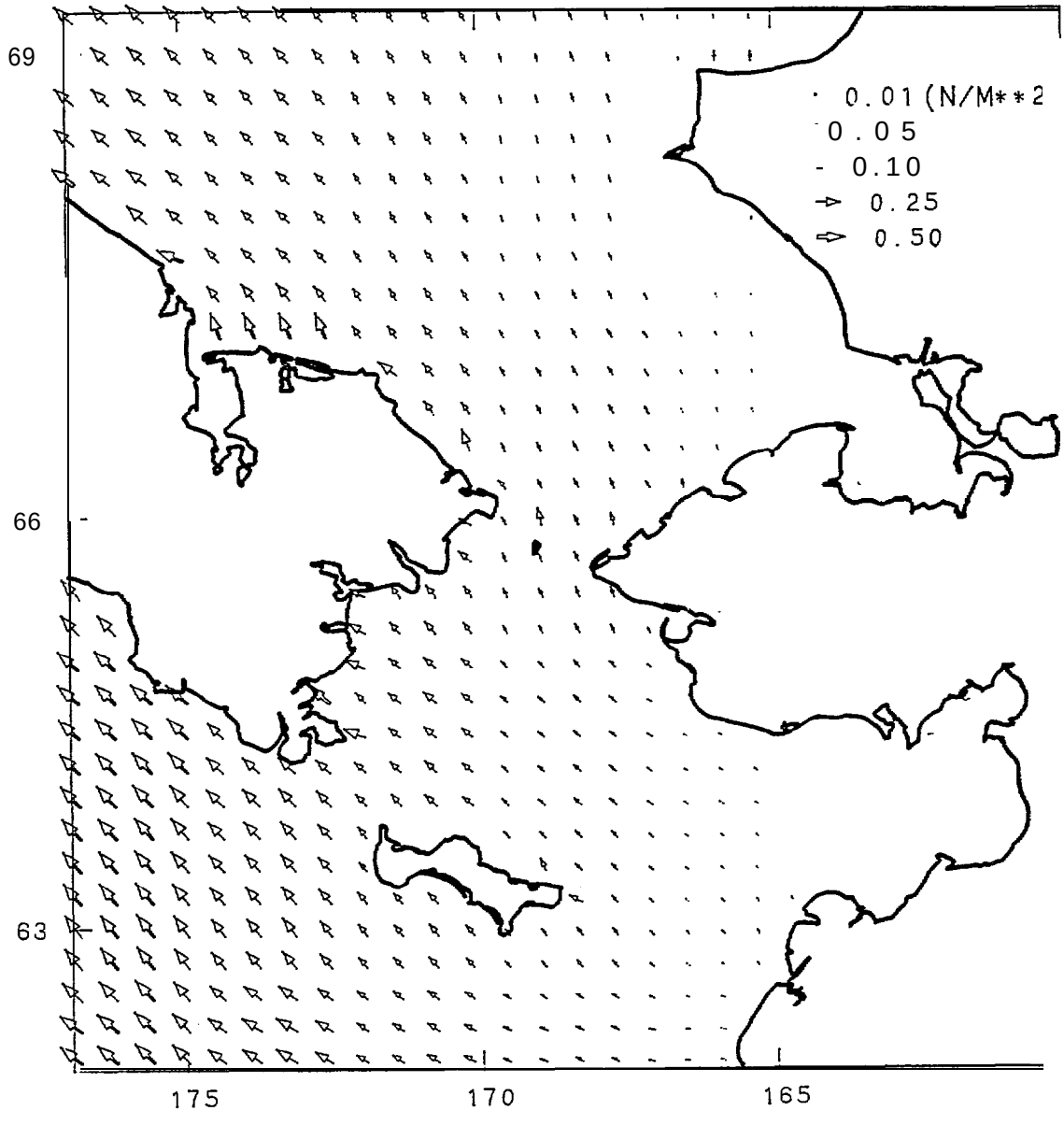

WIND STRESS

FEBRUARY 27 ,1982 AT 0:00

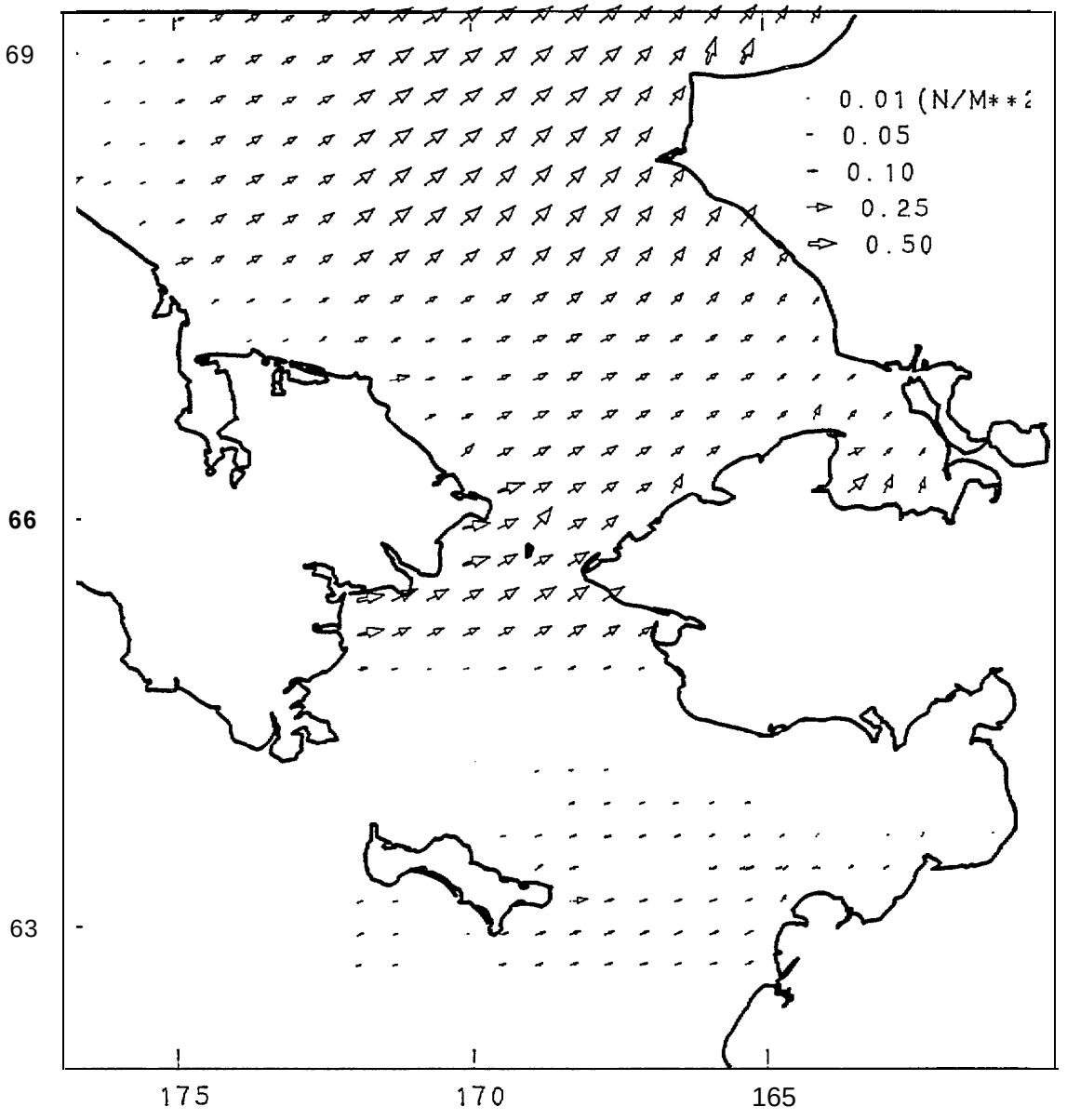

'WIND STRESS

FEBRUARY **28** , 1982 AT 0:00

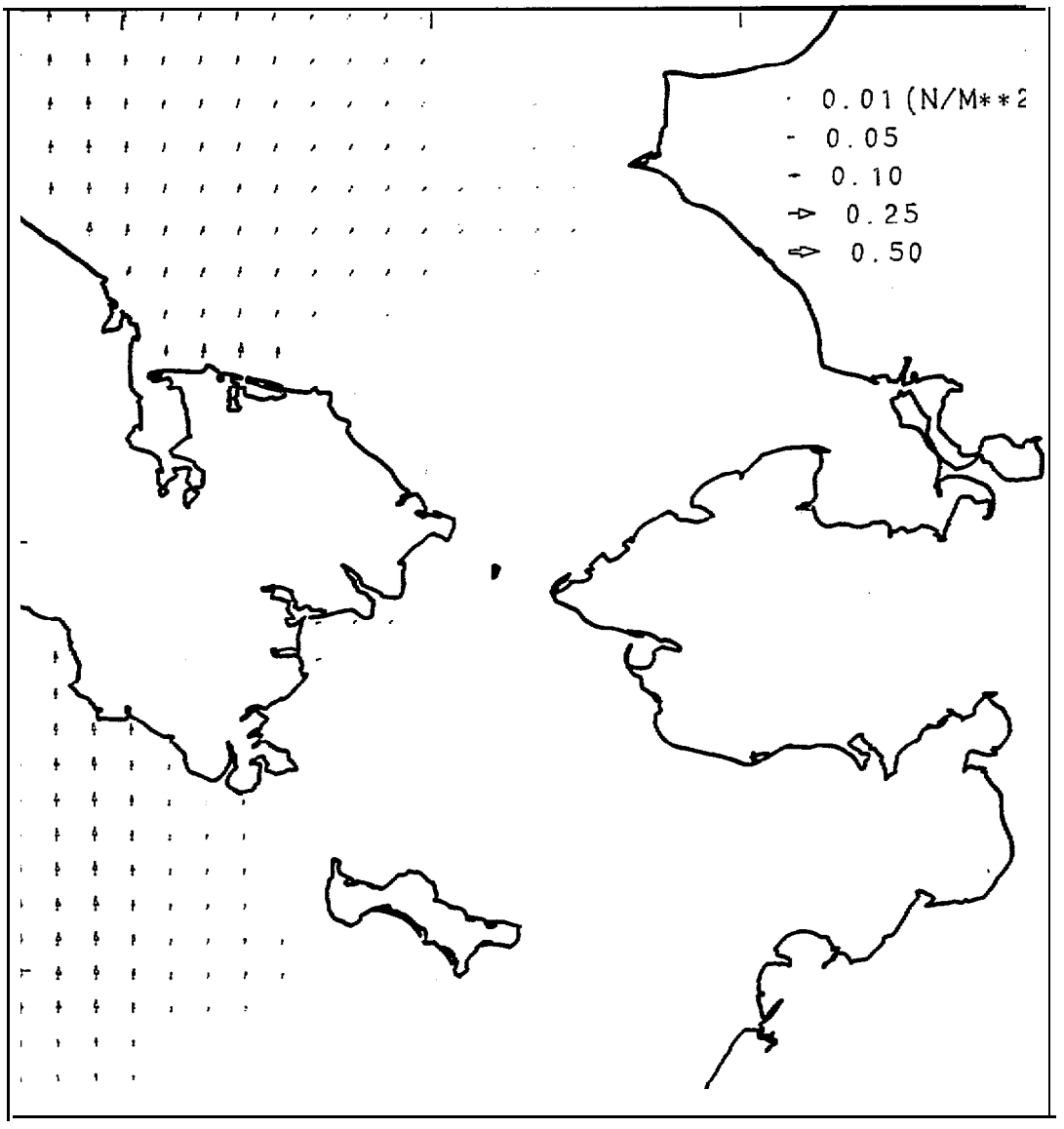

RAIT_F1

APPENDIX C

VERTICALLY AVERAGED VELOCITY &
SURFACE ELEVATION
FEBRUARY 1 ,1982 AT 0:00

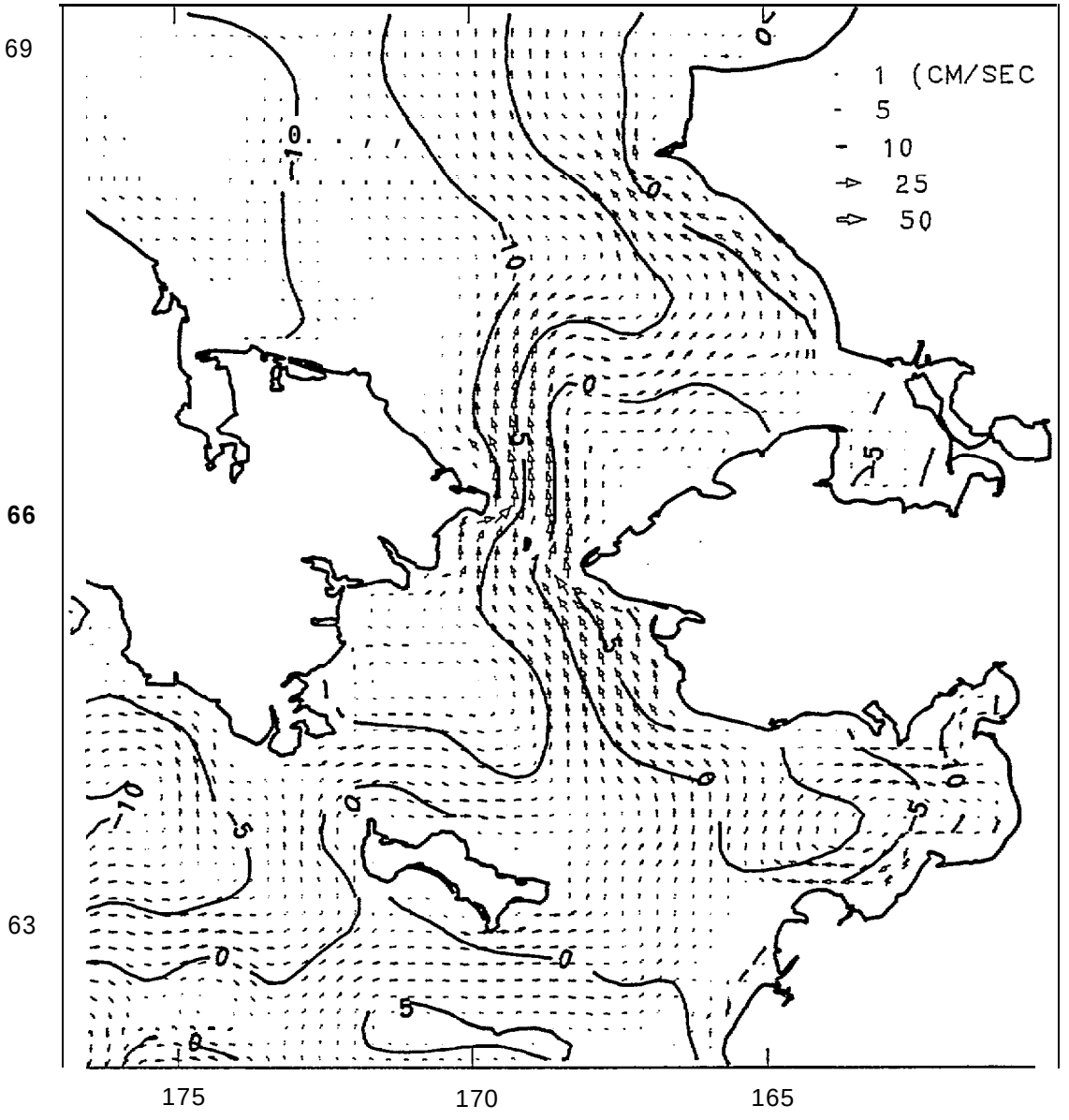

VERTICALLY AVERAGED VELOCITY &
SURFACE ELEVATION(CM)
FEBRUARY 2 , 1982 AT 0:00

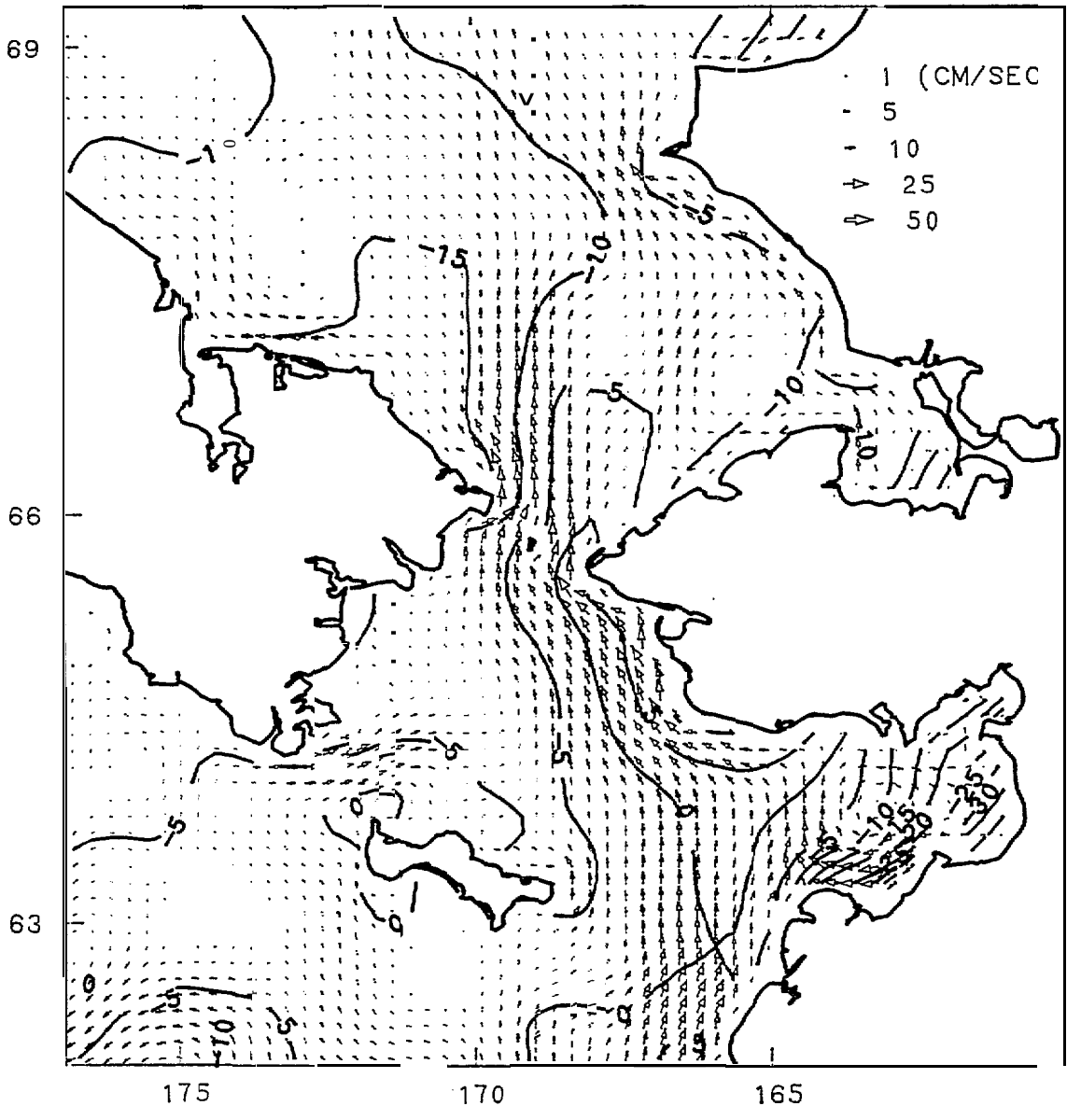

AIT_F1

VERTICALLY AVERAGED VELOCITY &
SURFACE ELEVATION
FEBRUARY 3 ,1982 AT 0:00

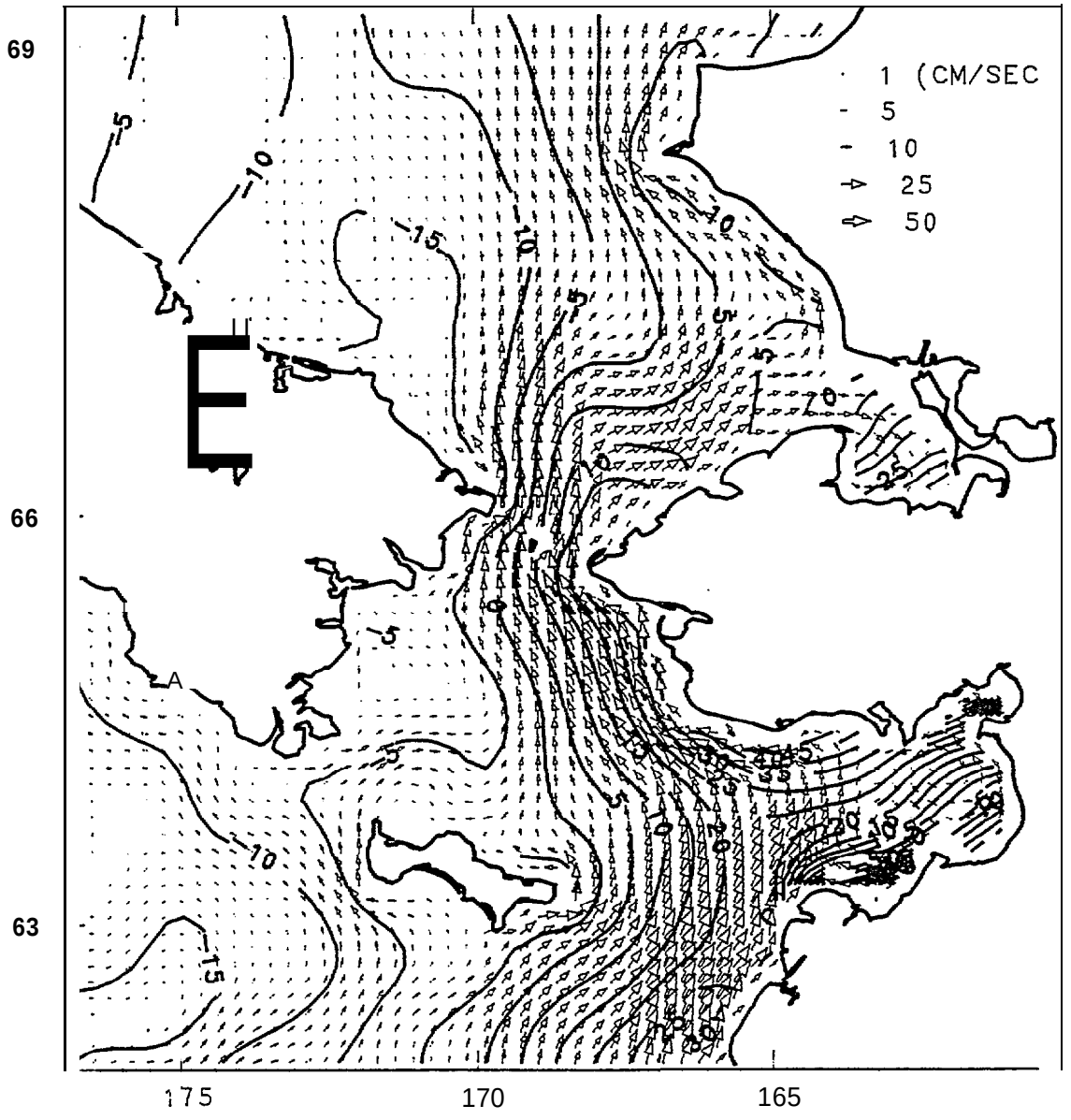

VERTICALLY AVERAGED VELOCITY &
SURFACE ELEVATION
FEBRUARY 4 ,1982 AT 0:00

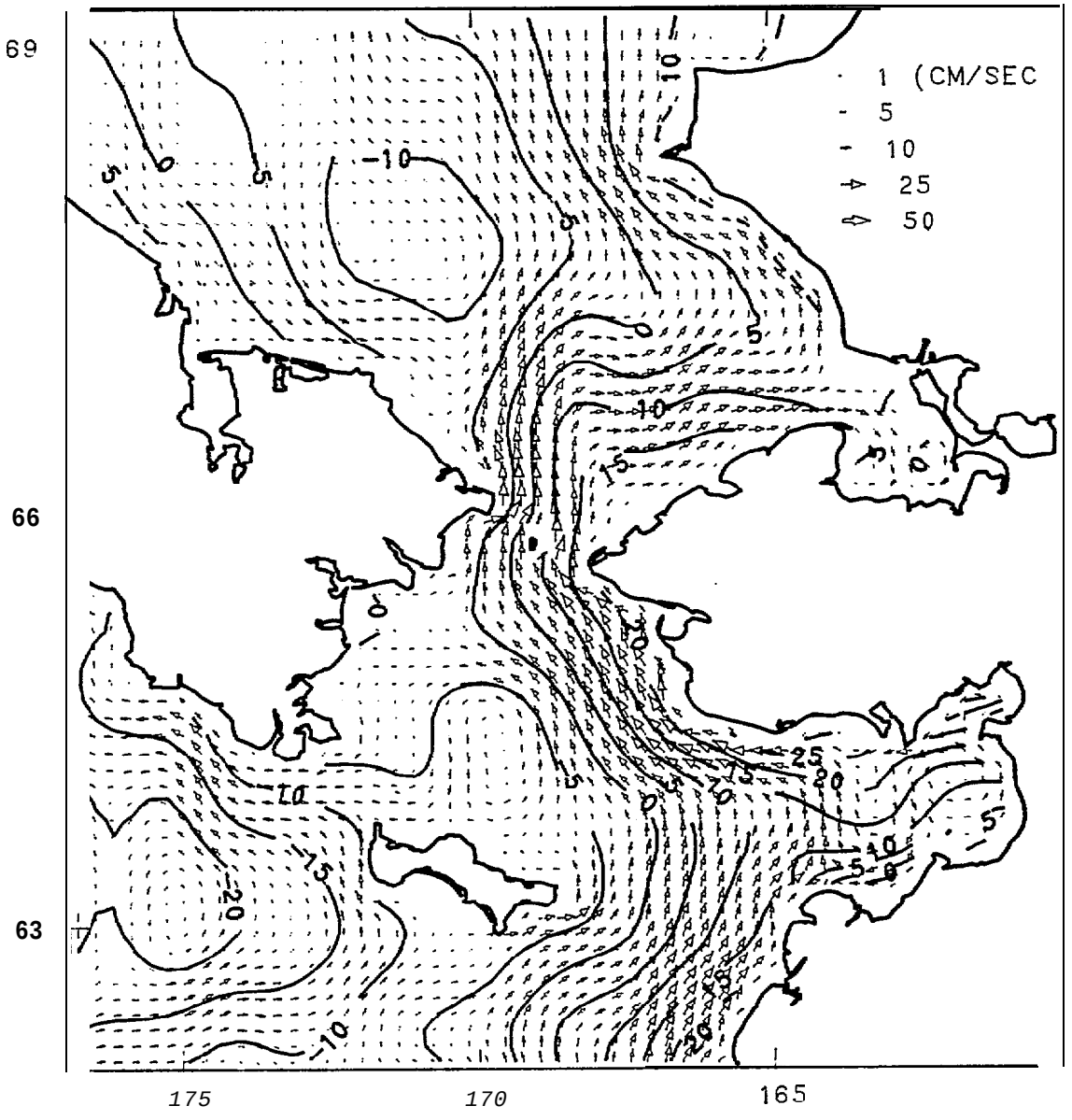

VERTICALLY AVERAGED VELOCITY &
SURFACE ELEVATION
FEBRUARY 5 , 1982 AT 0:00

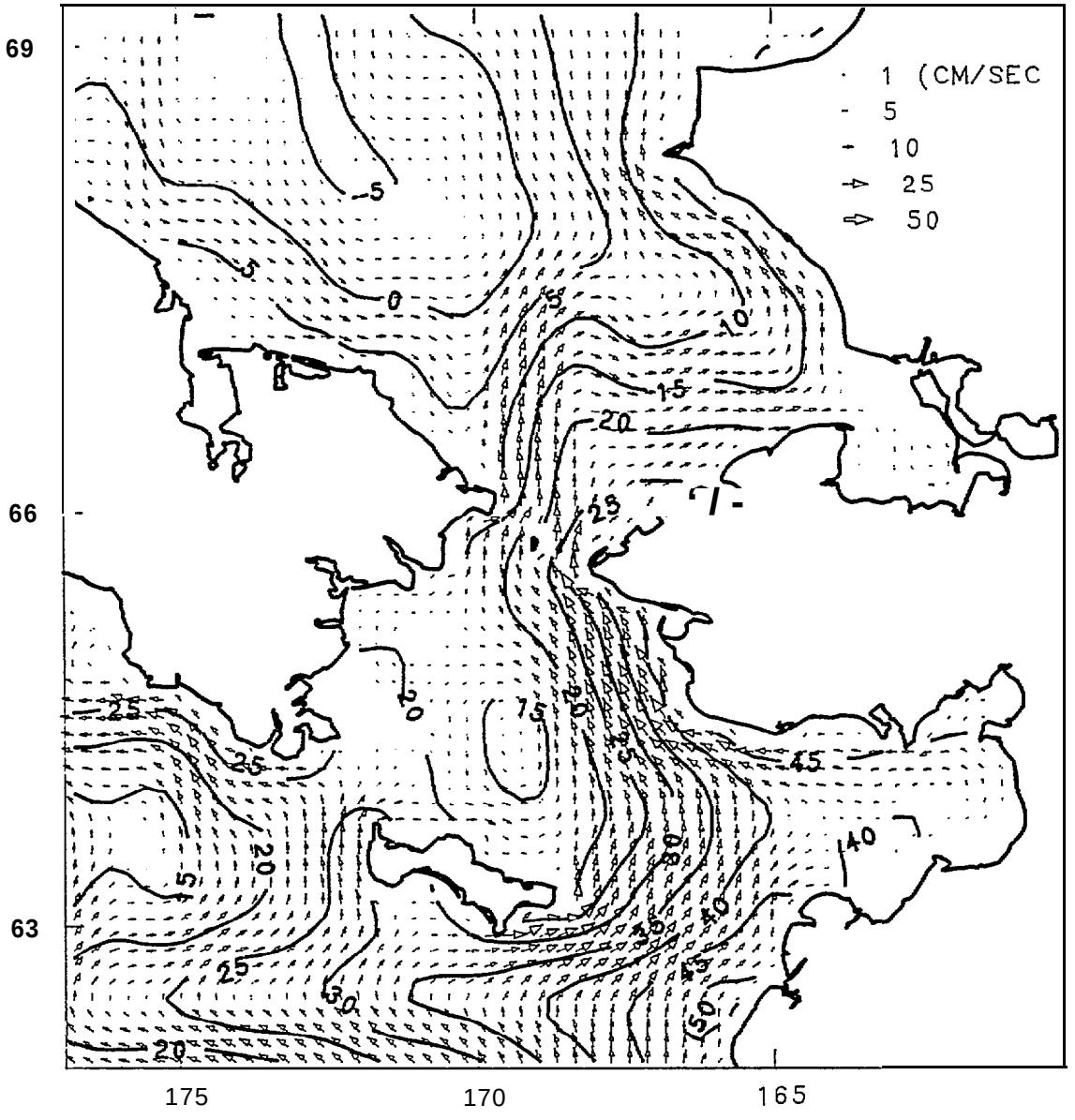

AIT_F1

VERTICALLY AVERAGED VELOCITY &
SURFACE ELEVATION
FEBRUARY 6 ,1982 AT 0:00

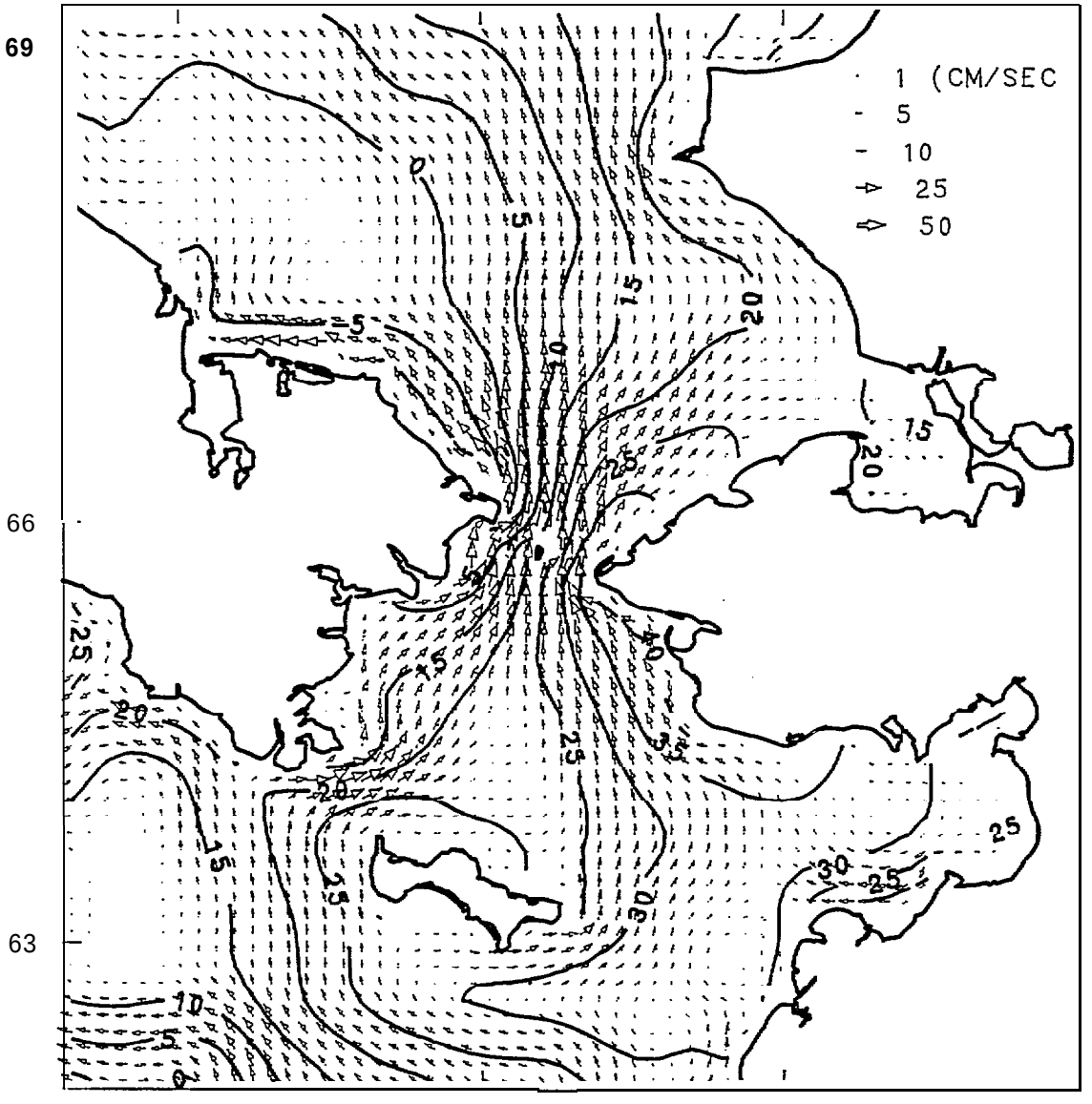

AIT_F1

VERTICALLY AVERAGED VELOCITY &
SURFACE ELEVATION
FEBRUARY 7 ,1982 AT 0:00

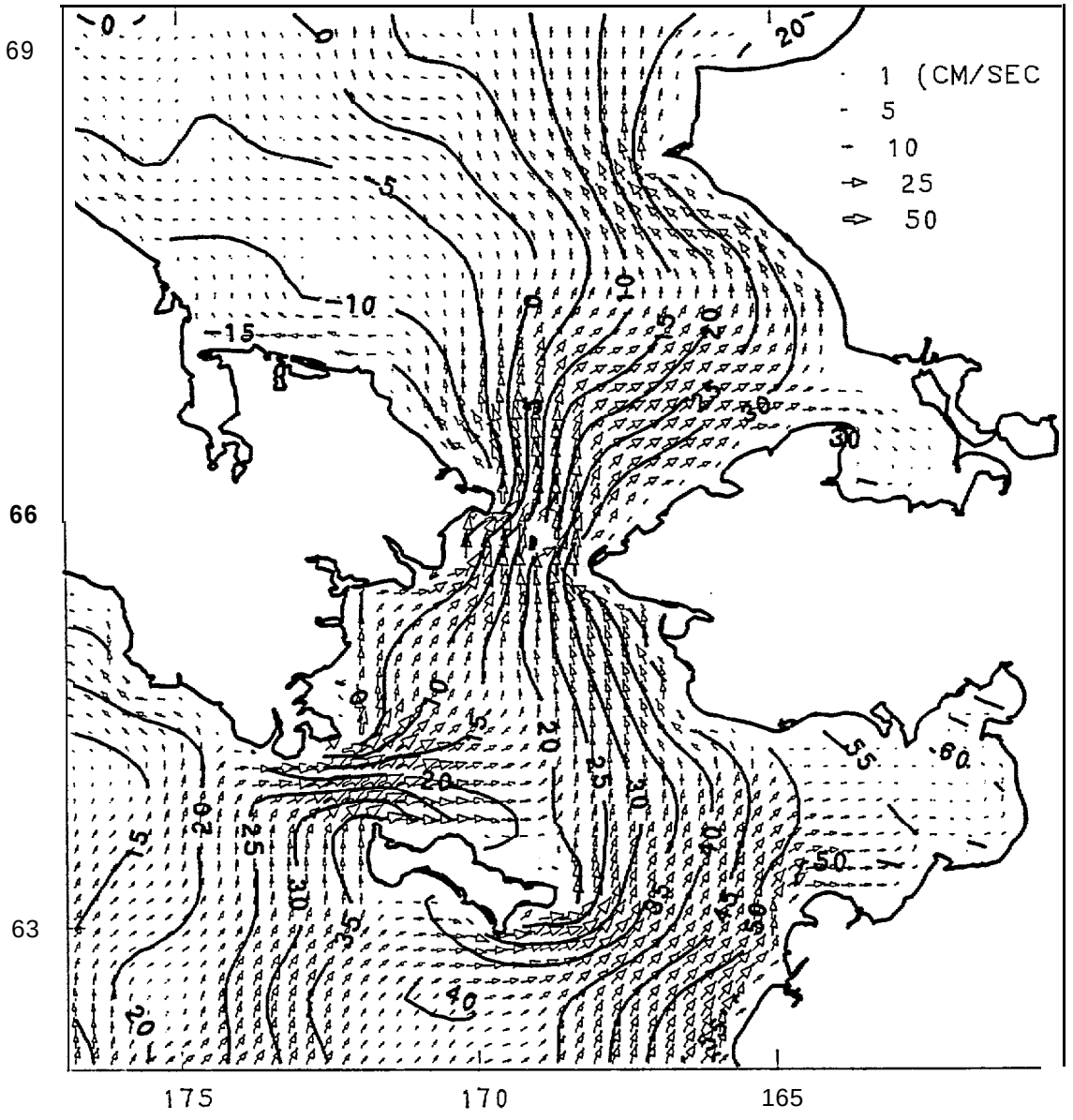

VERTICALLY AVERAGED VELOCITY &
SURFACE ELEVATION
FEBRUARY 8 , 1982 AT 0:00

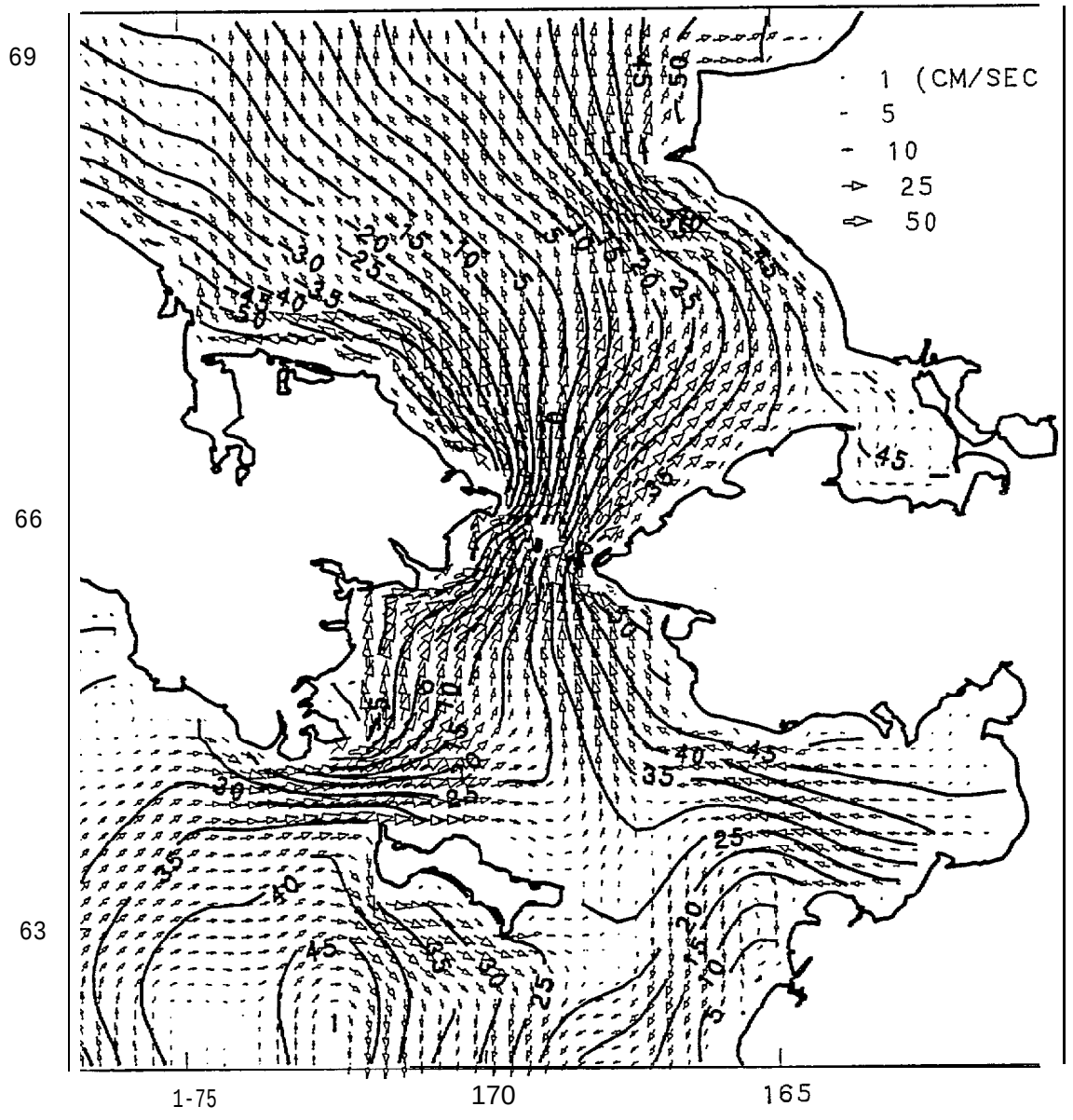

AIT_F1

VERTICALLY AVERAGED VELOCITY &
SURFACE ELEVATION
FEBRUARY 9 ,1982 AT 0:00

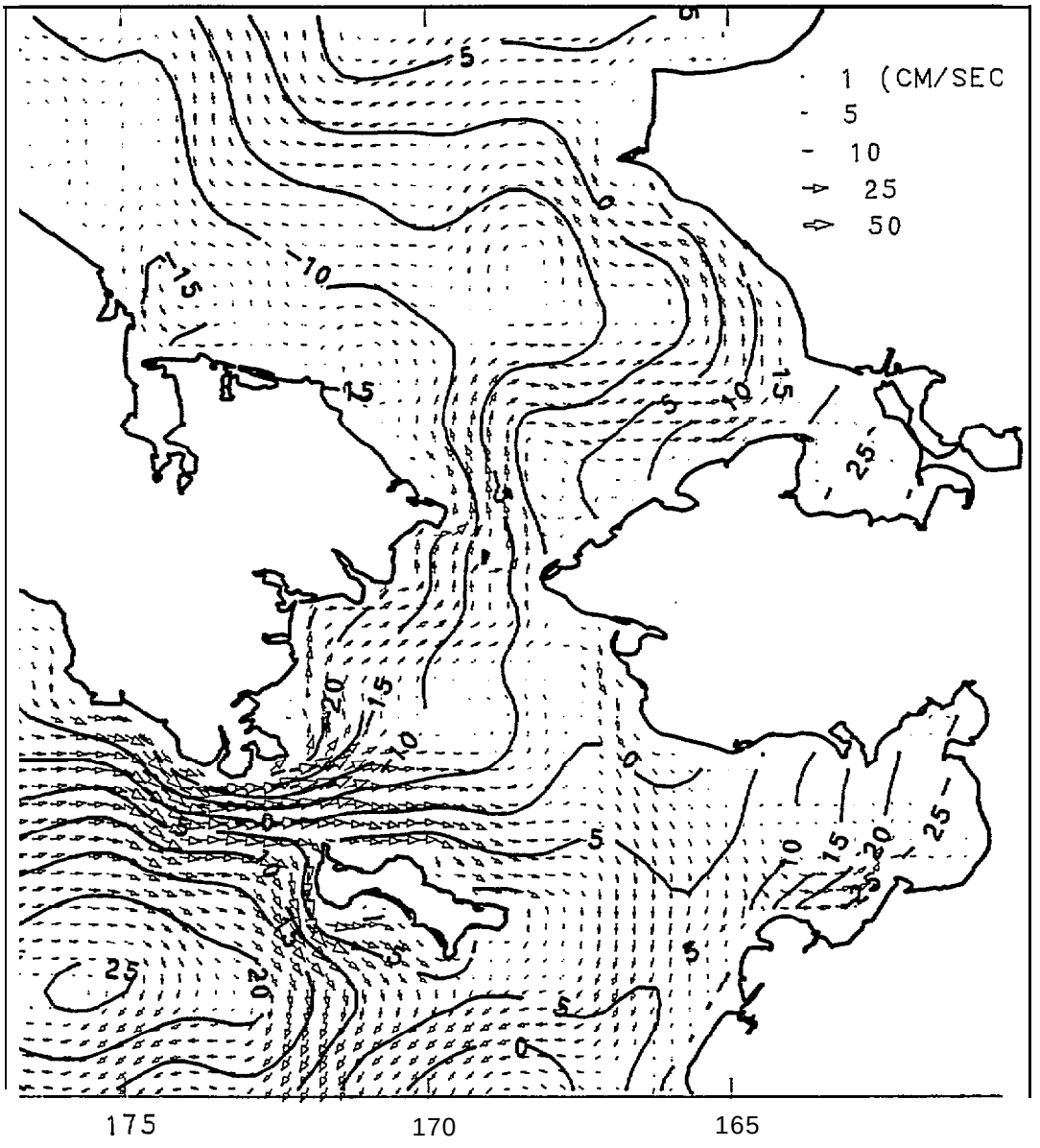

VERTICALLY AVERAGED VELOCITY &
SURFACE ELEVATION
FEBRUARY 10 , 1982 AT 0:00

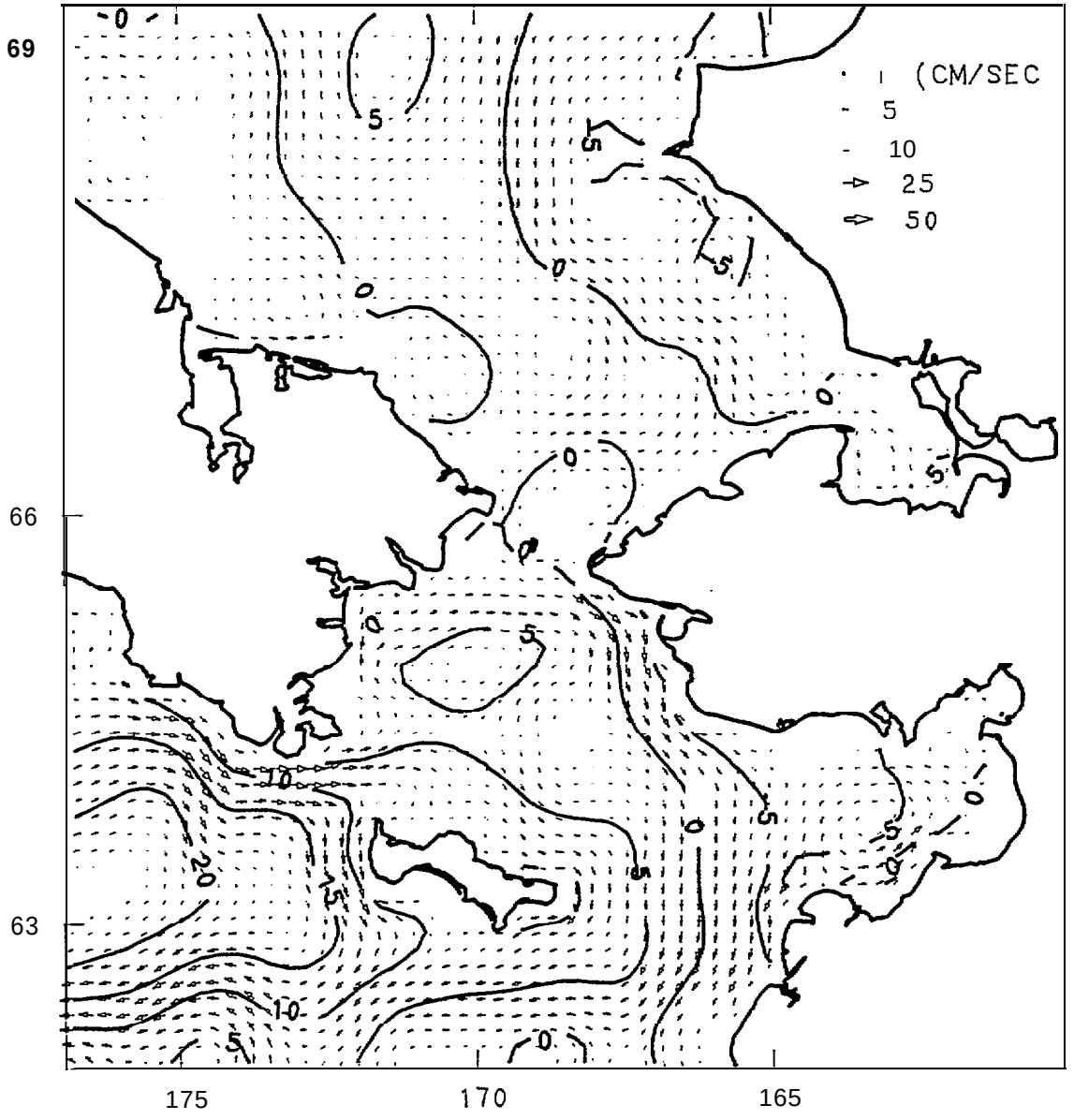

VERTICALLY AVERAGED VELOCITY &
SURFACE ELEVATION
FEBRUARY 11 ,1982 AT 0:00

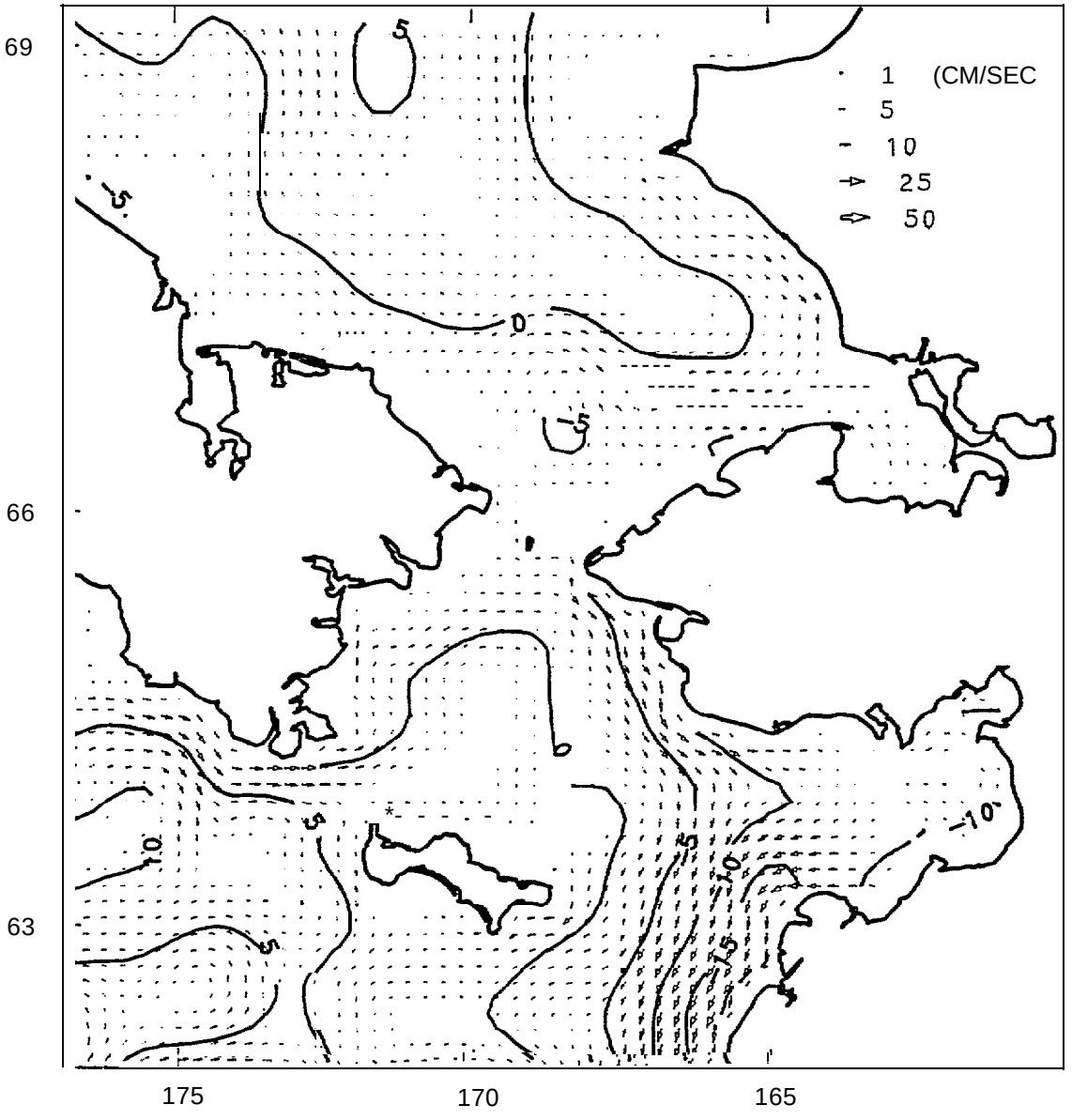

VERTICALLY AVERAGED VELOCITY &
SURFACE ELEVATION
FEBRUARY 12 , 1982 AT 0:00

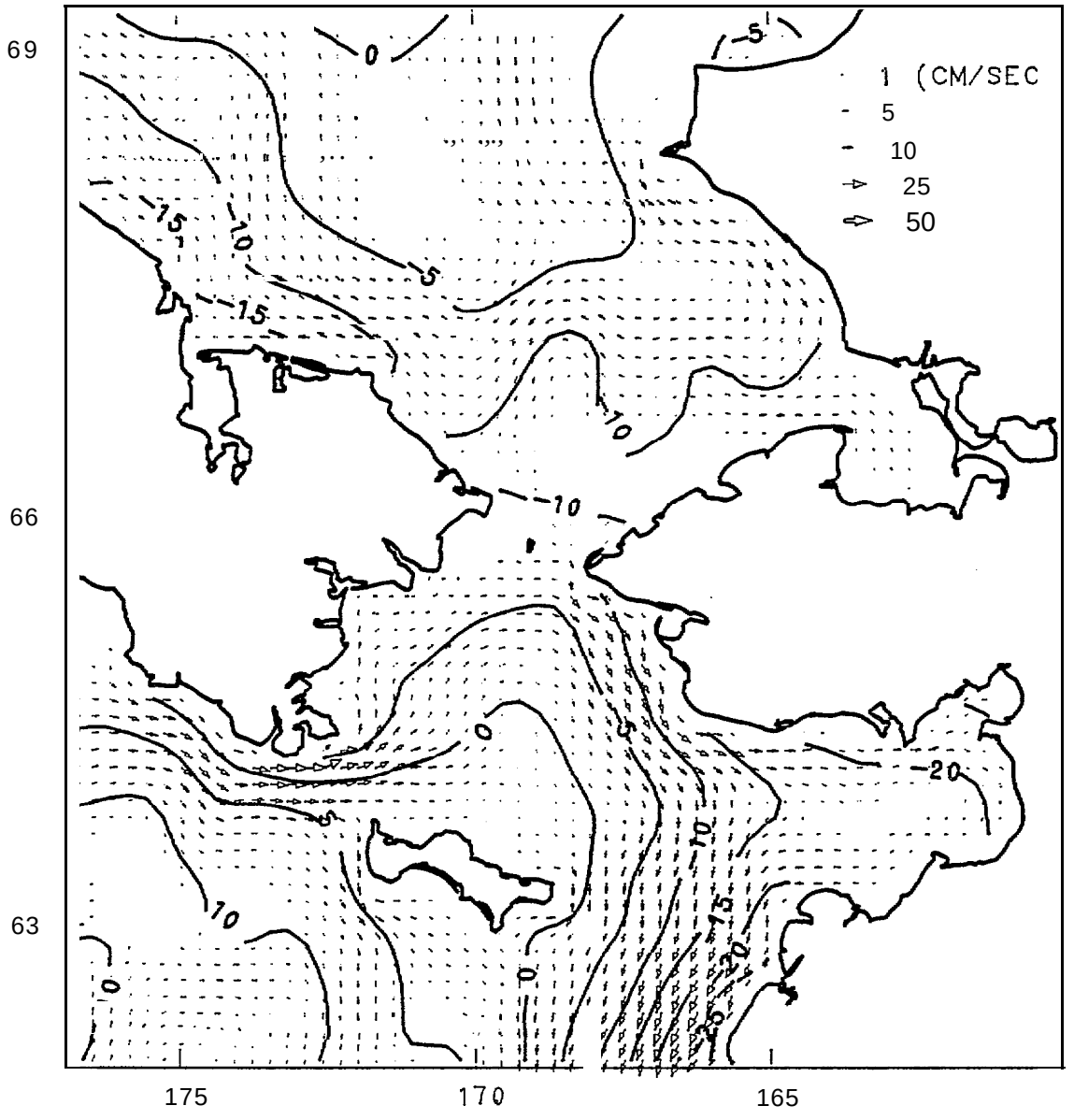

AII_F1

VERTICALLY AVERAGED VELOCITY &
SURFACE ELEVATION
FEBRUARY 13 , 1982 AT 0:00

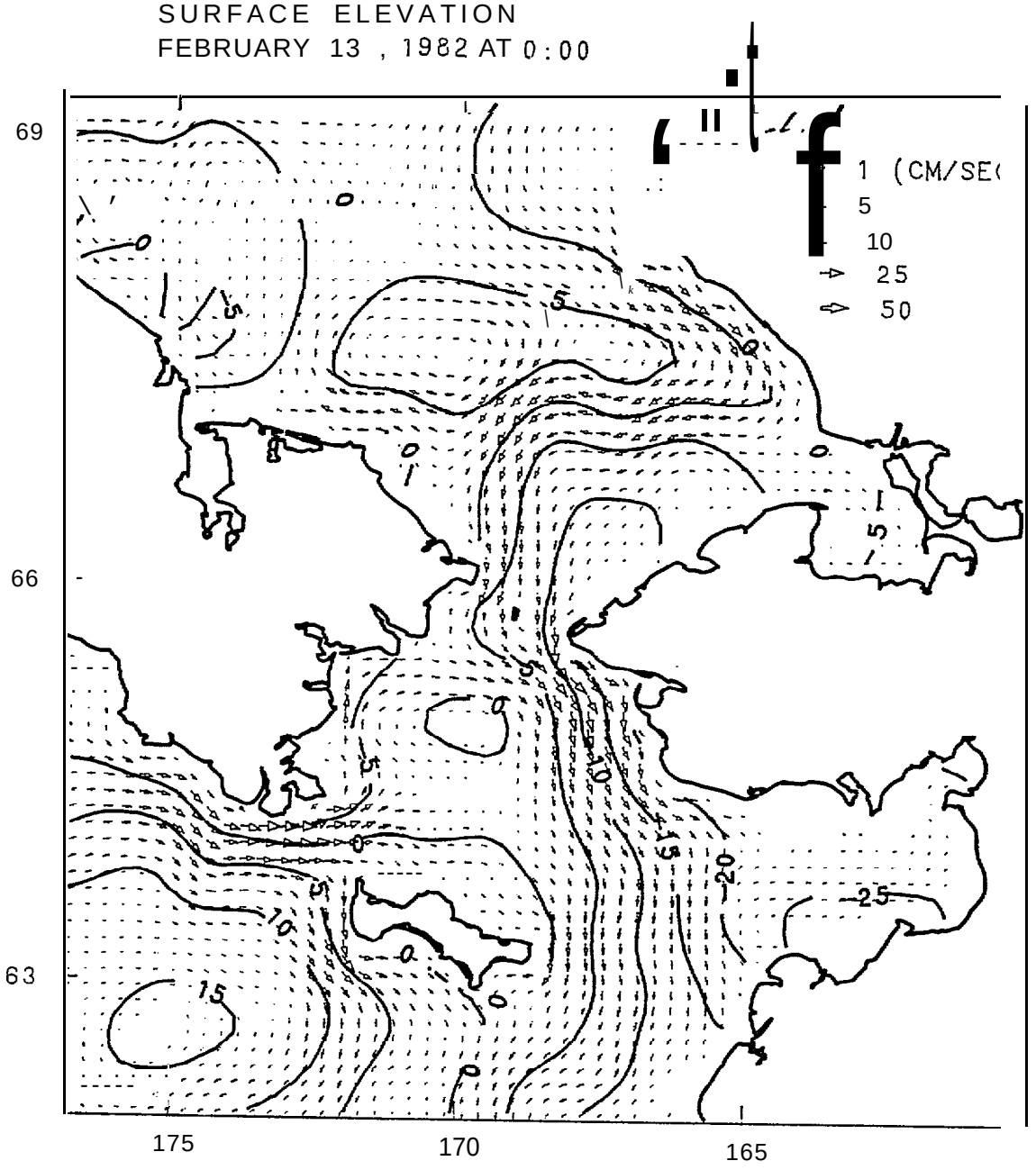

AIT_F1

VERTICALLY AVERAGED VELOCITY &
SURFACE ELEVATION
FEBRUARY 14 , 1982 AT 0:00

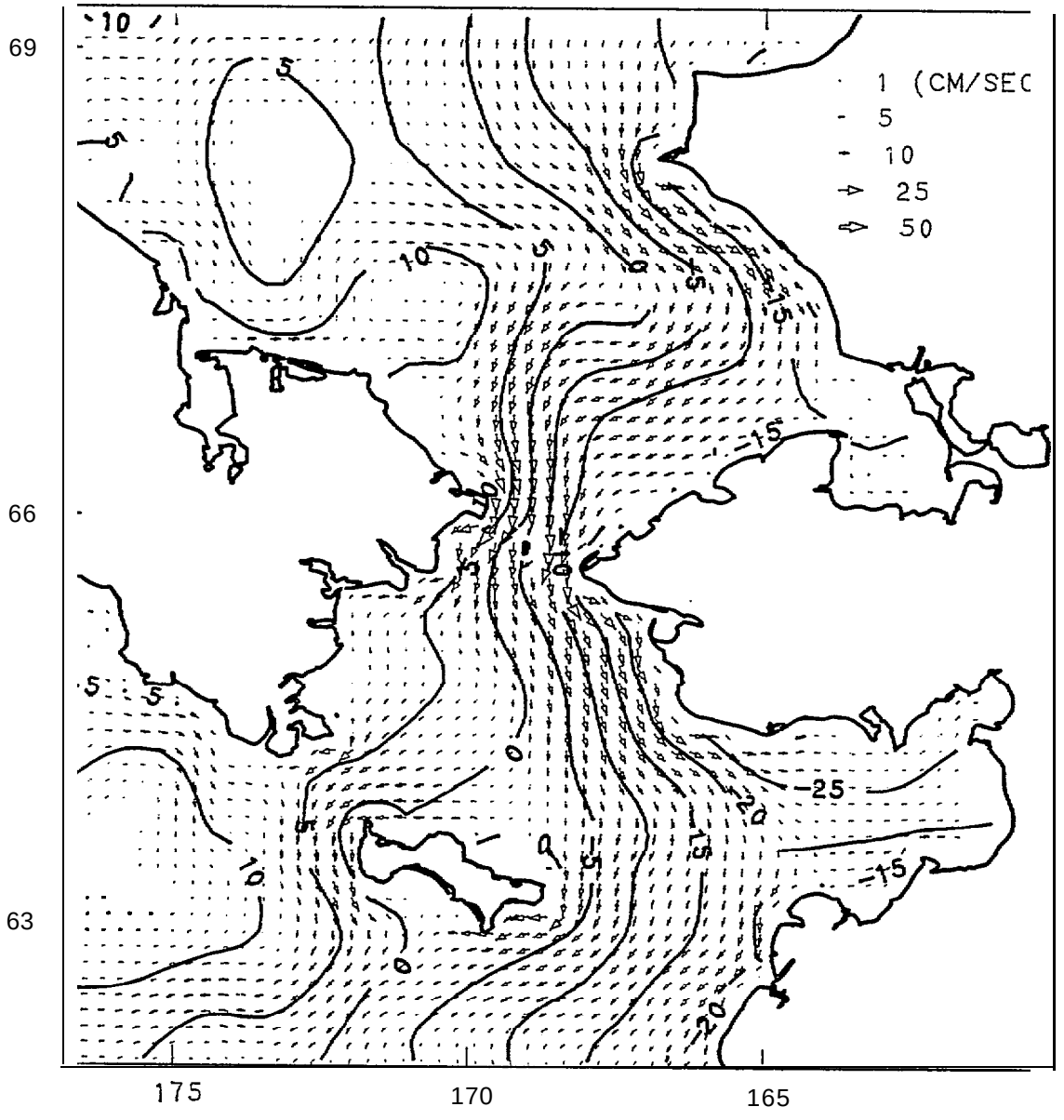

RAIT_F1

VERTICALLY AVERAGED VELOCITY &
SURFACE ELEVATION
FEBRUARY 15 ,1982 AT 0:00

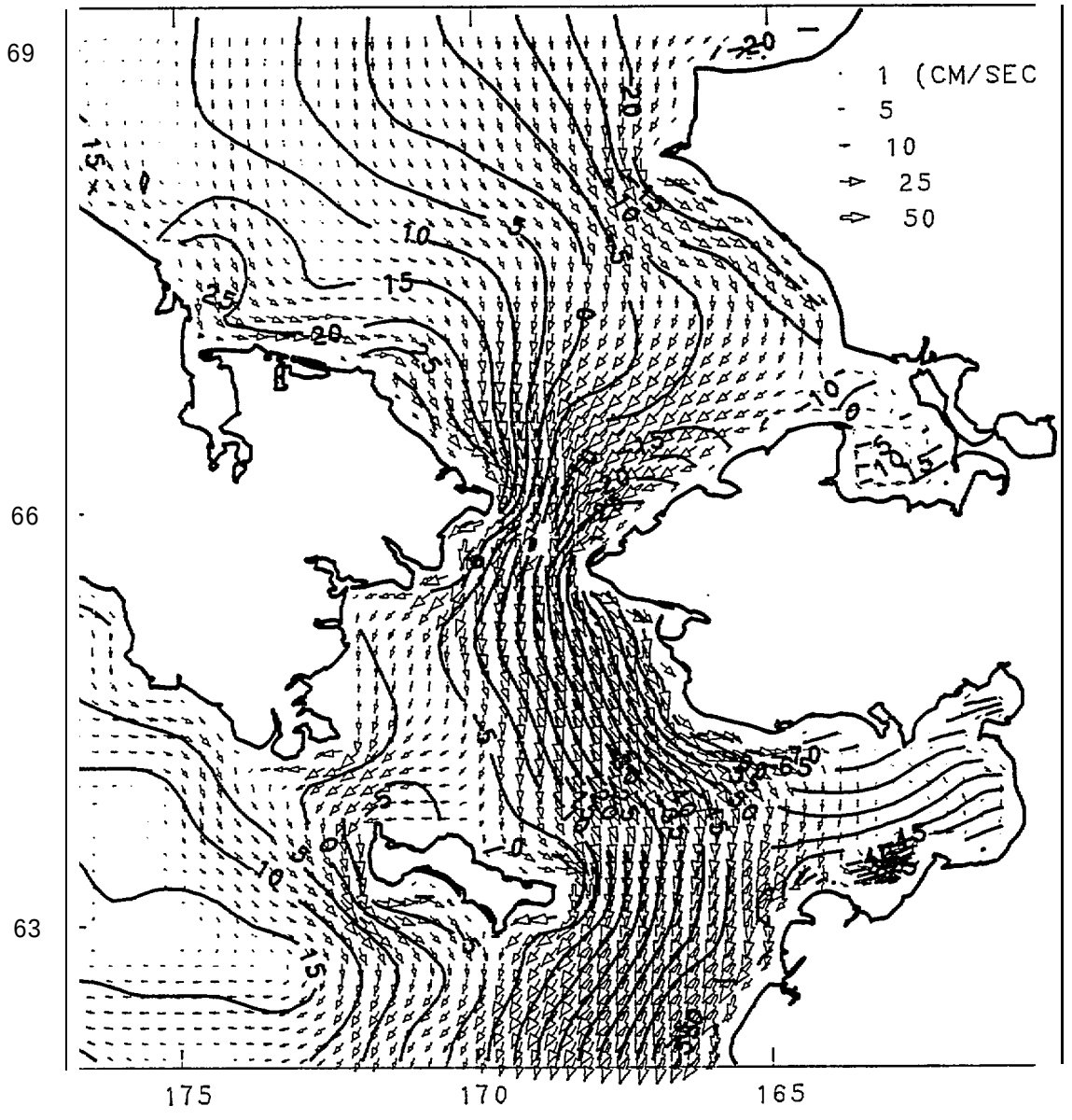

VERTICALLY AVERAGED VELOCITY &
SURFACE ELEVATION(CM,
FEBRUARY 16 , 1982 AT 0:00

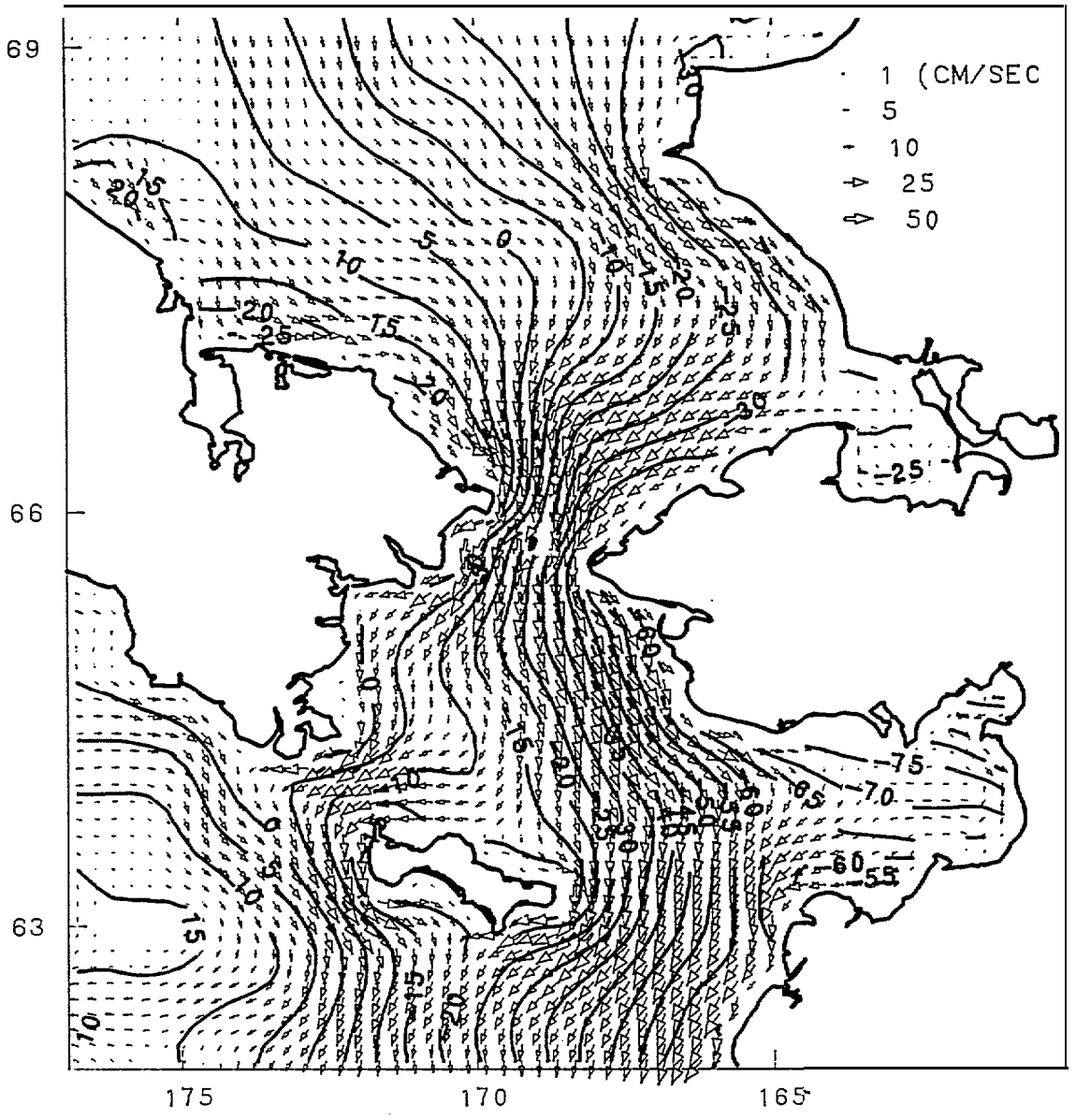

VERTICALLY AVERAGED VELOCITY &
SURFACE ELEVATION
FEBRUARY 17 ,1982 AT 0:00

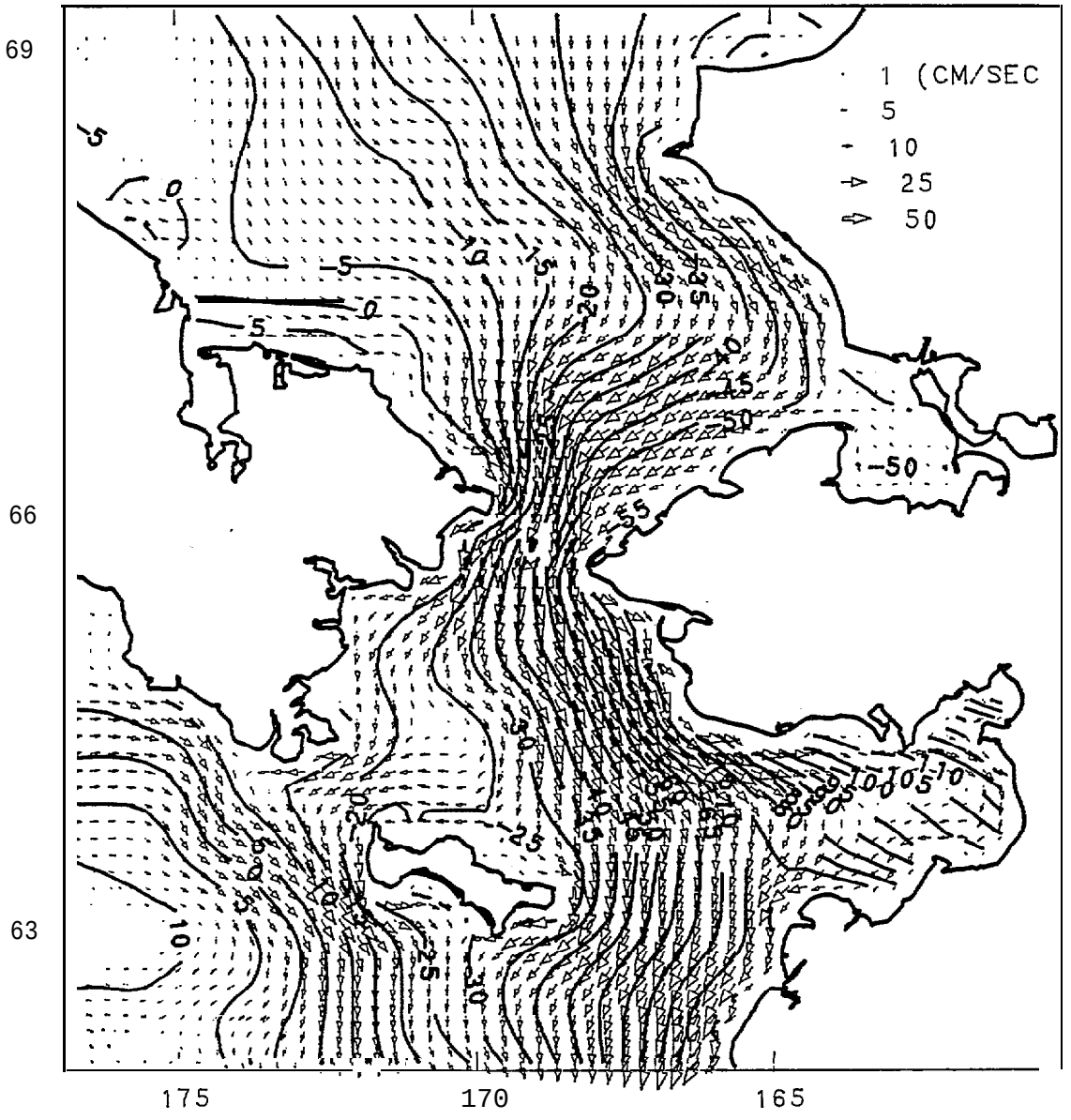

VERTICALLY AVERAGED VELOCITY &
SURFACE ELEVATION
FEBRUARY 18 , 1982 AT 0:00

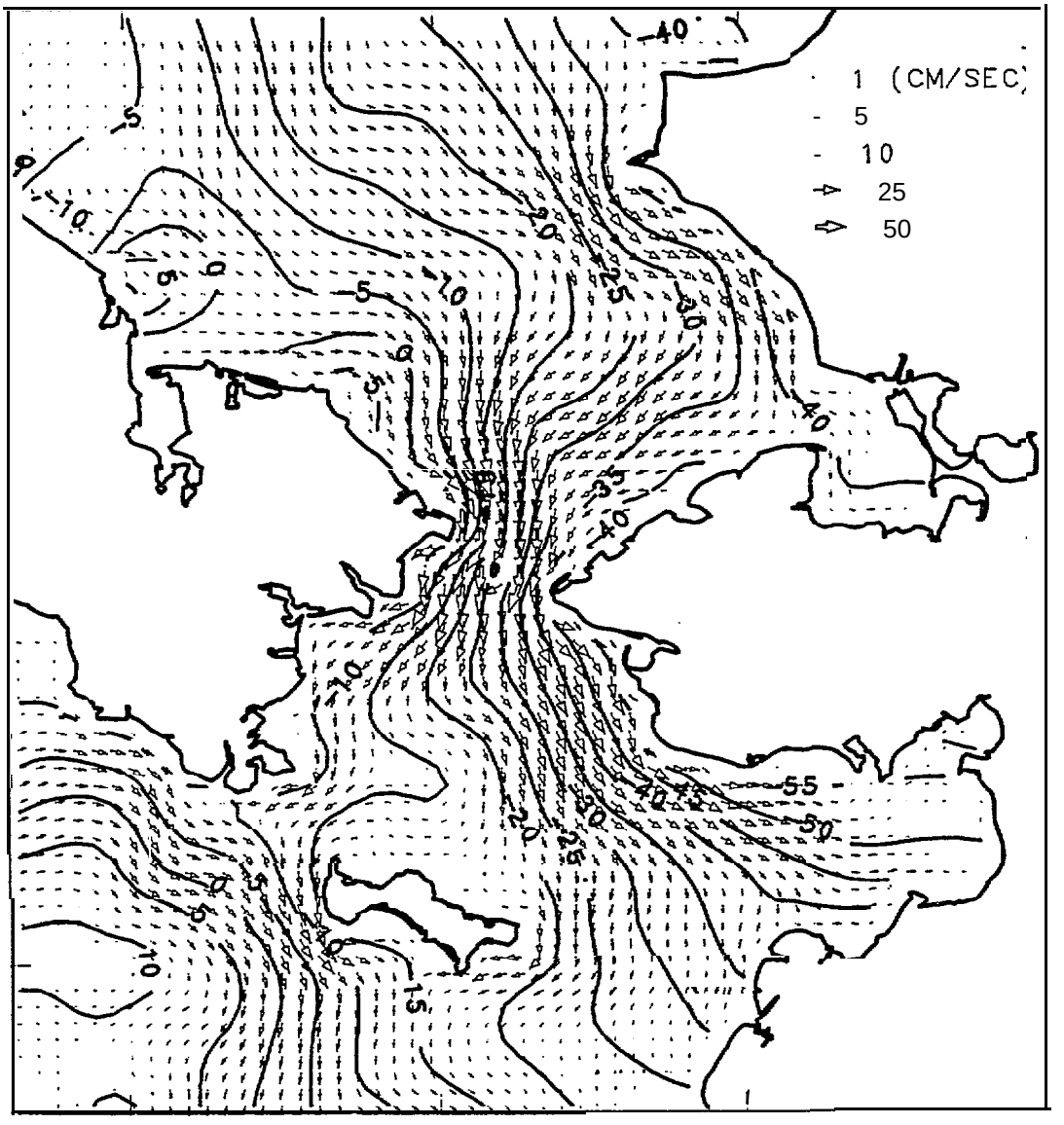

VERTICALLY AVERAGED VELOCITY &
SURFACE ELEVATION
FEBRUARY 19 ,1982 AT 0:00

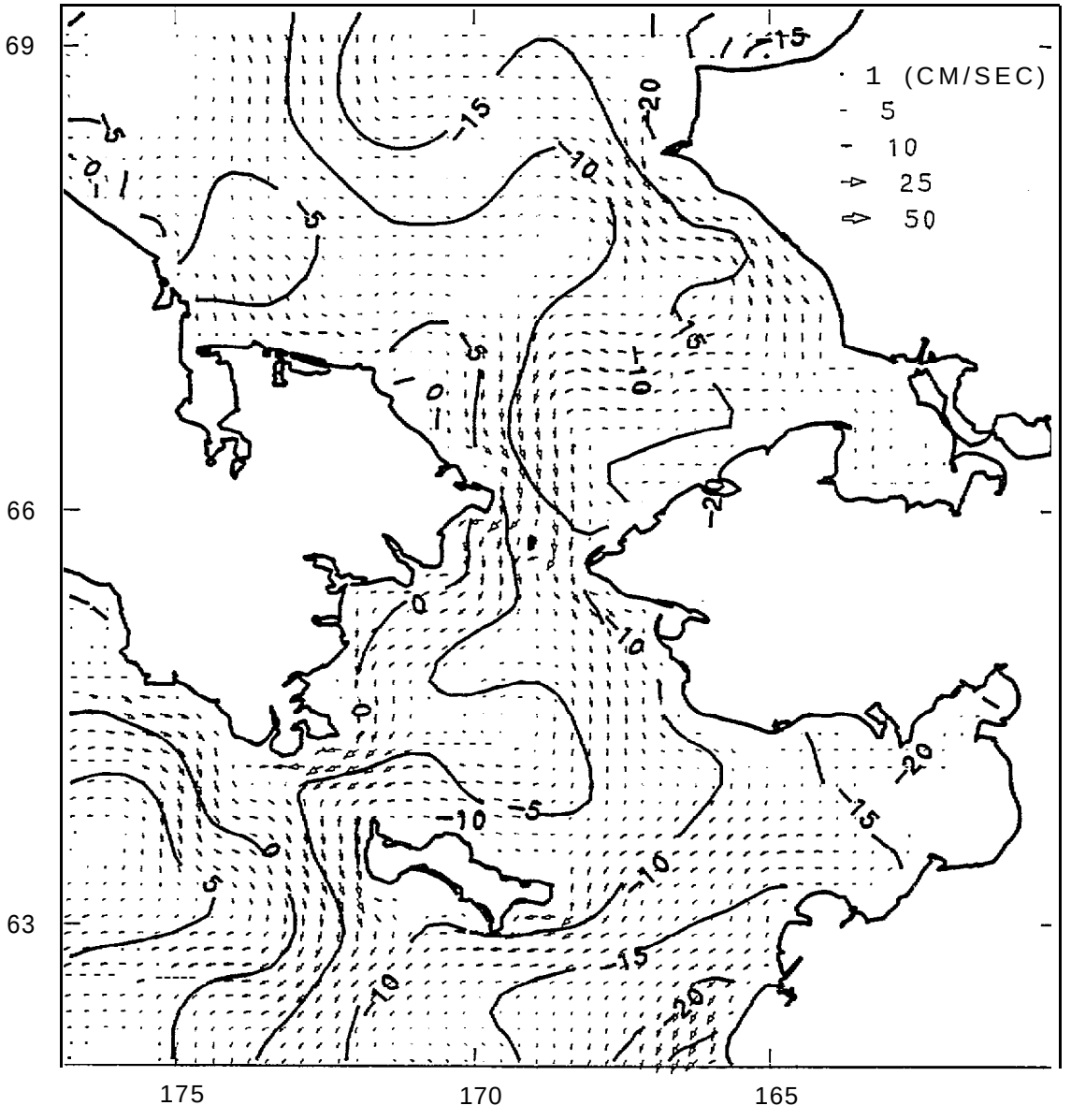

VERTICALLY AVERAGED VELOCITY &
SURFACE ELEVATION
FEBRUARY 20 ,1982 AT 0:00

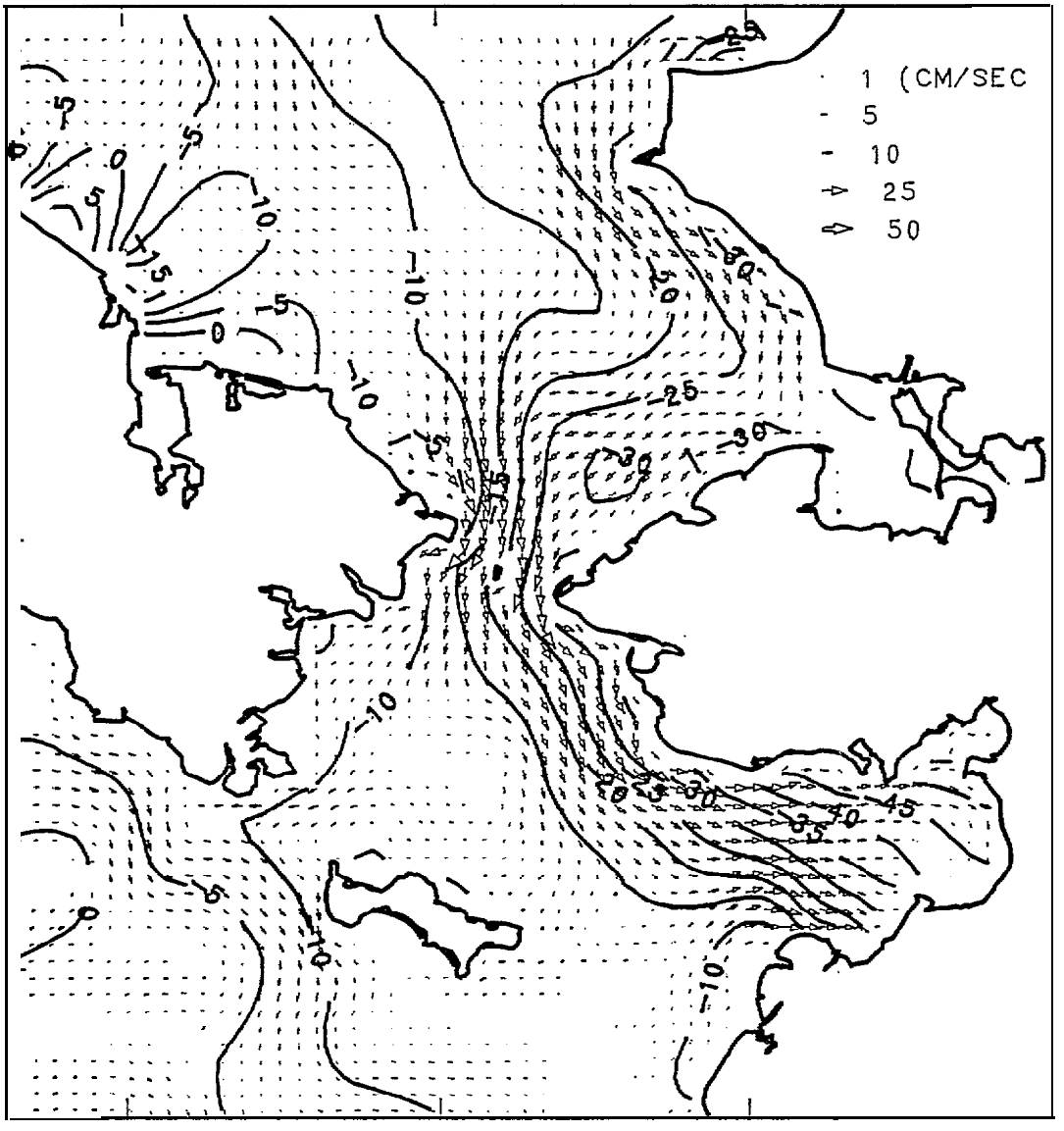

VERTICALLY AVERAGED VELOCITY &
SURFACE ELEVATION
FEBRUARY 21 ,1982 AT 0:00

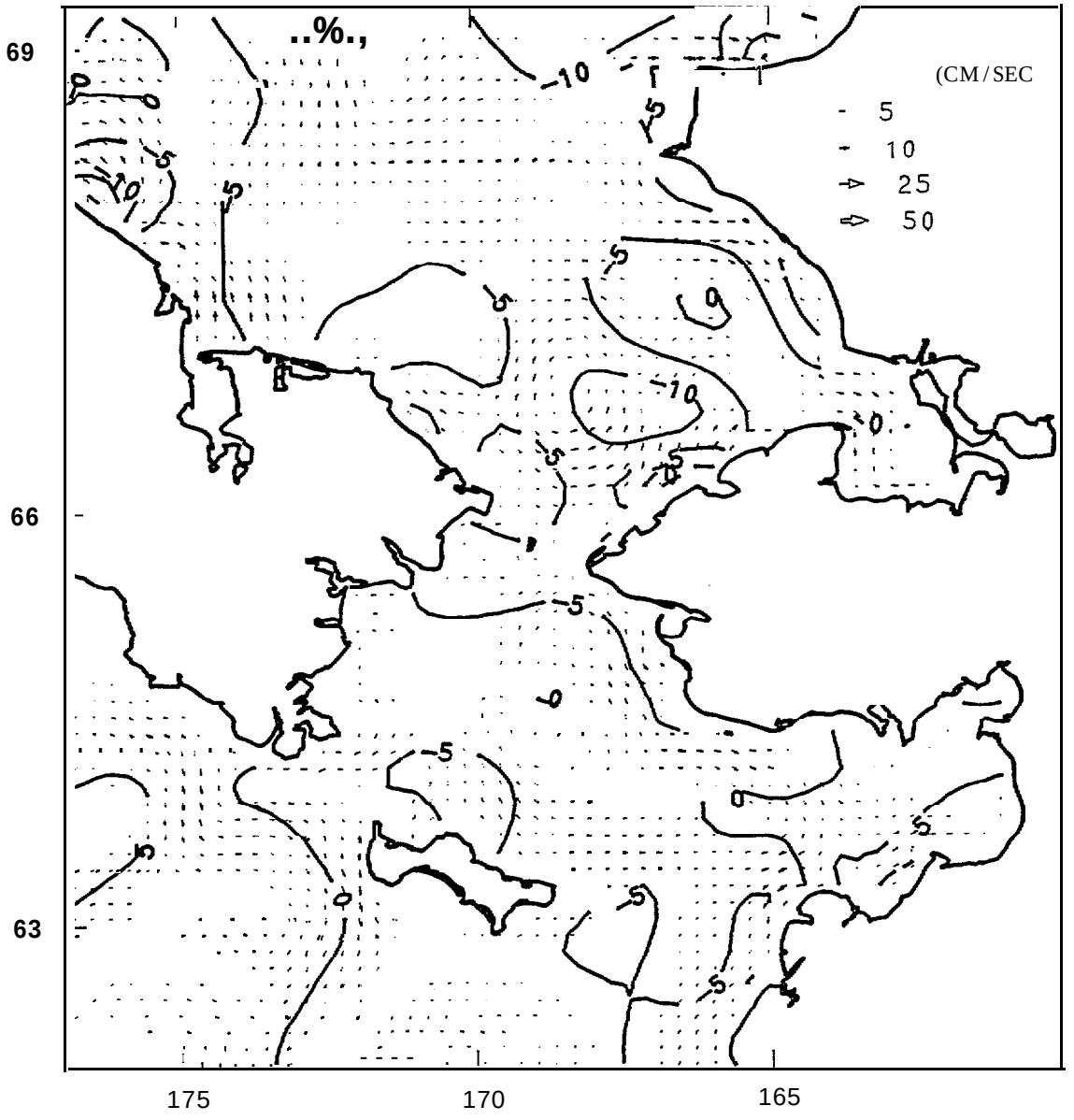

VERTICALLY AVERAGED VELOCITY &
SURFACE ELEVATION
FEBRUARY 22 ,1982 AT 0:00

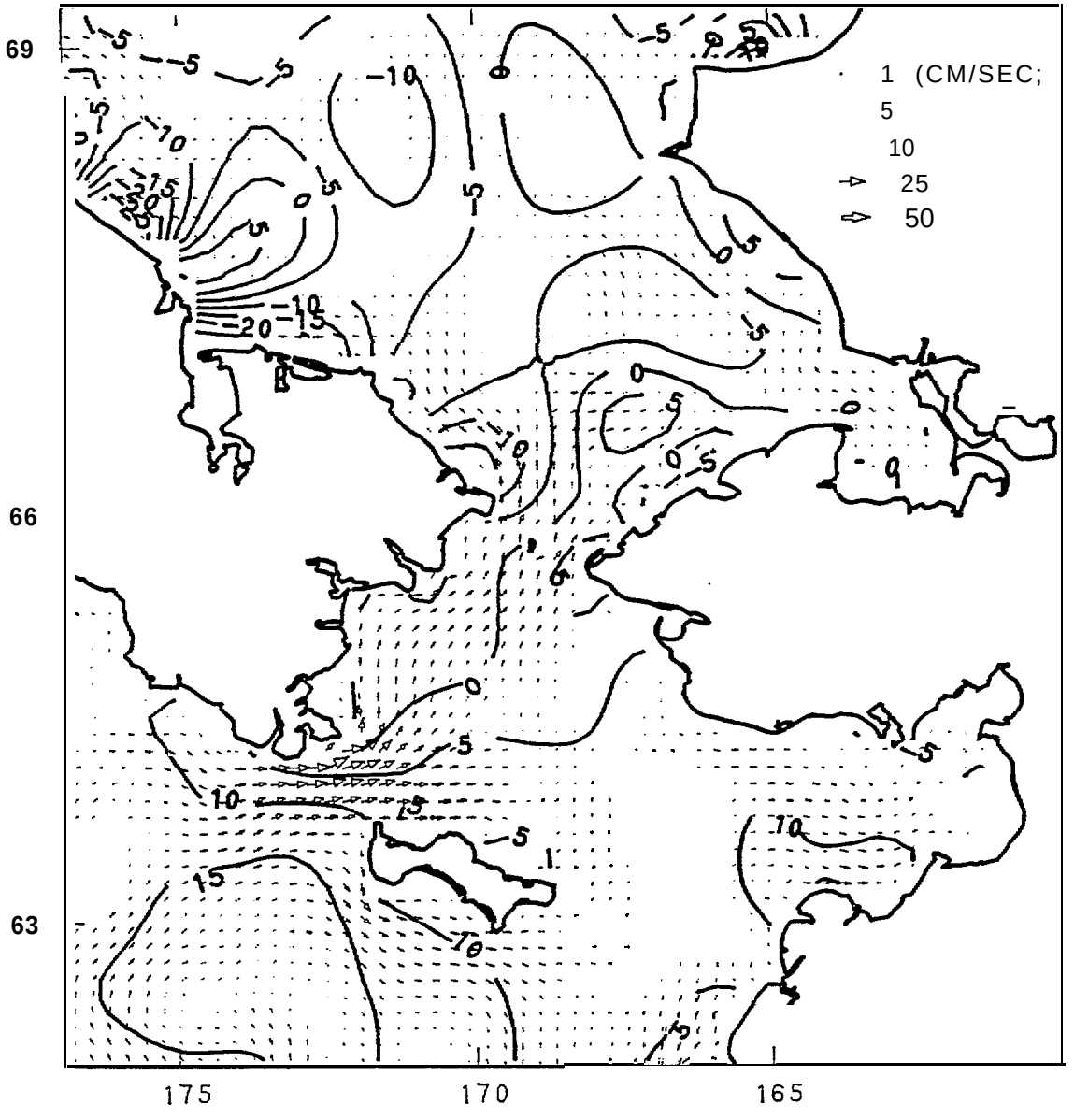

VERTICALLY AVERAGED VELOCITY &
SURFACE ELEVATION
FEBRUARY 23 , 1982 AT 0:00

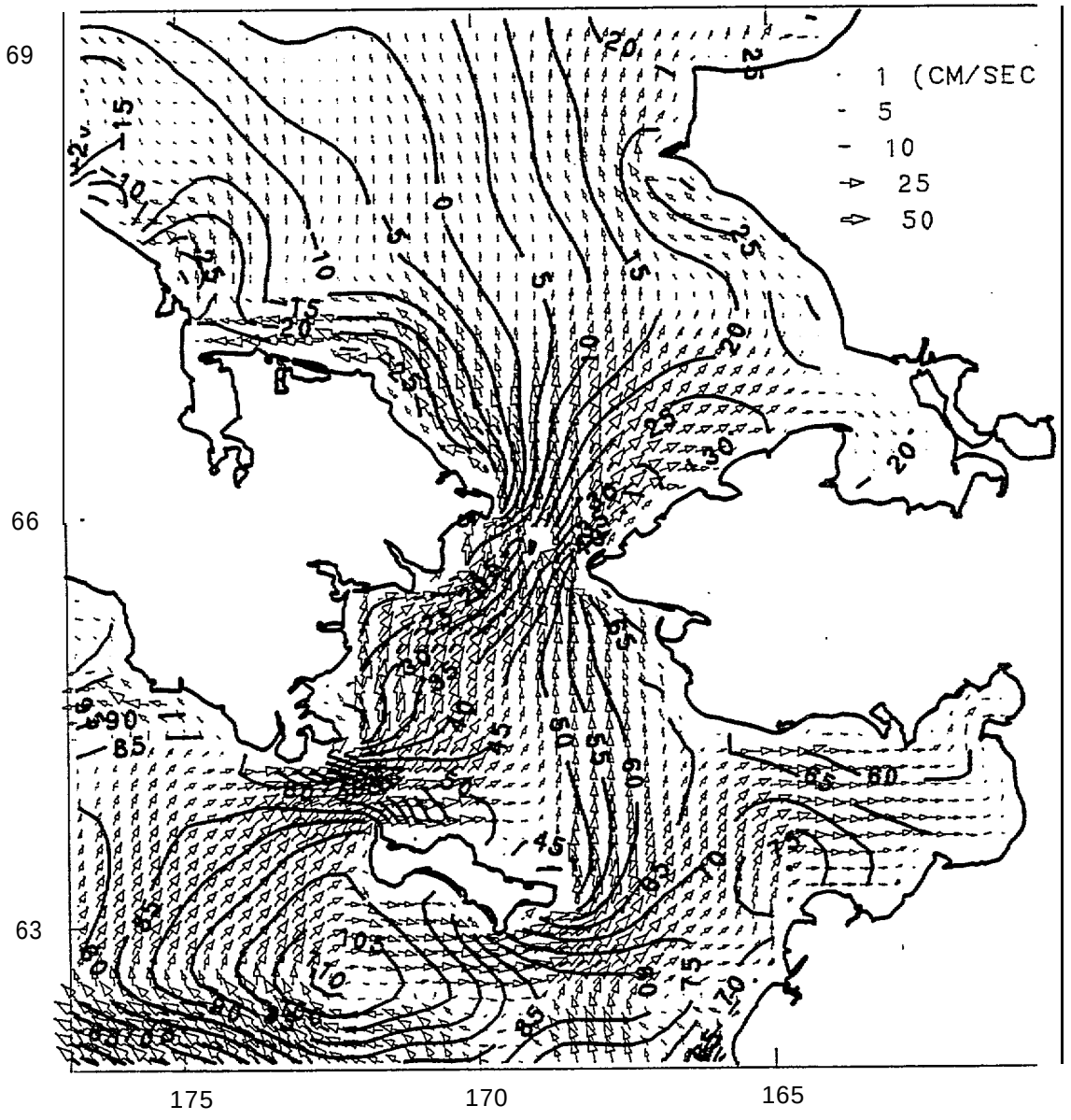

VERTICALLY AVERAGED VELOCITY &
SURFACE ELEVATION
FEBRUARY 24 ,1982 AT 0:00

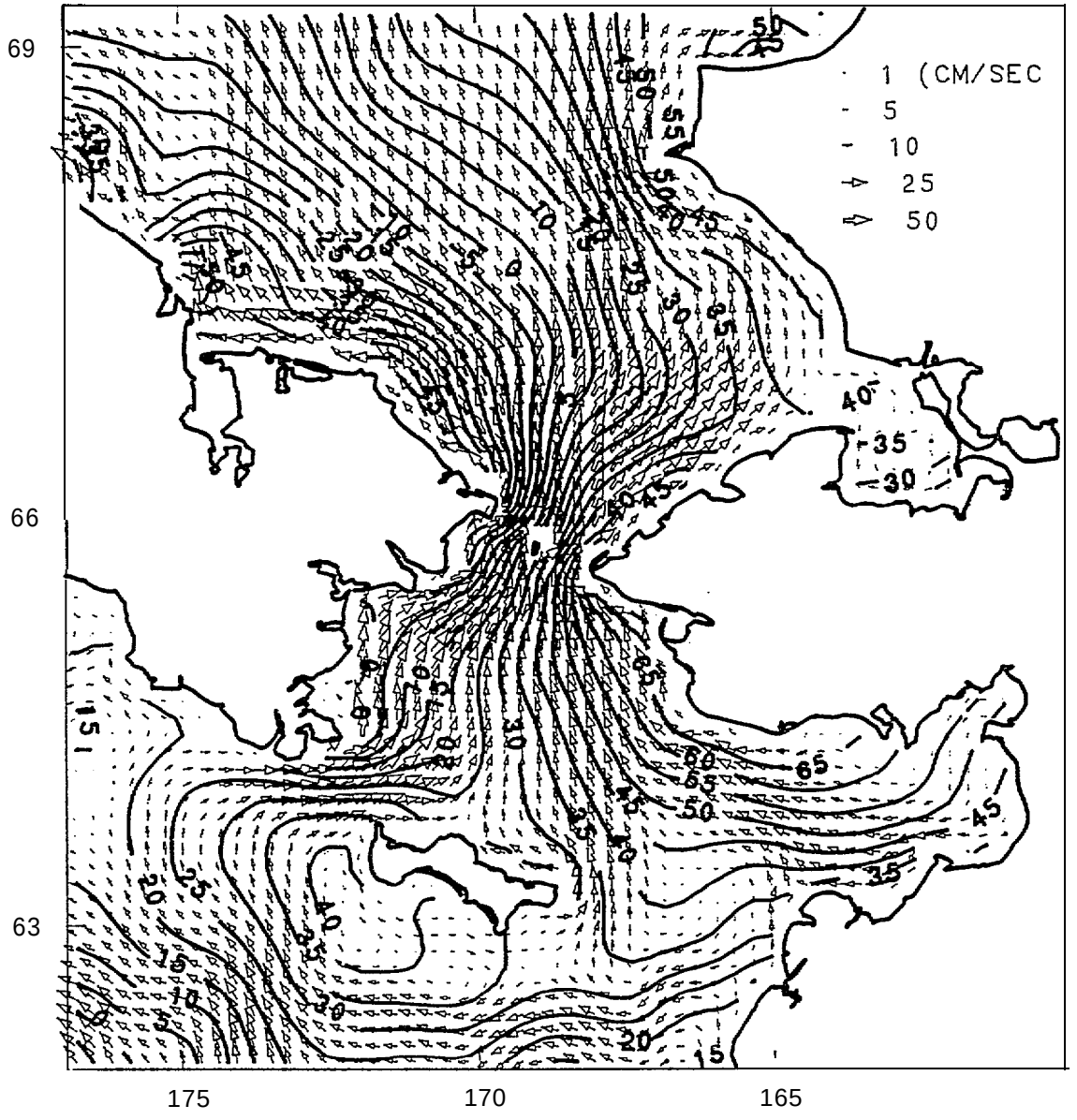

VERTICALLY AVERAGED VELOCITY &
SURFACE ELEVATION
FEBRUARY 25 , 1982 AT 0:00

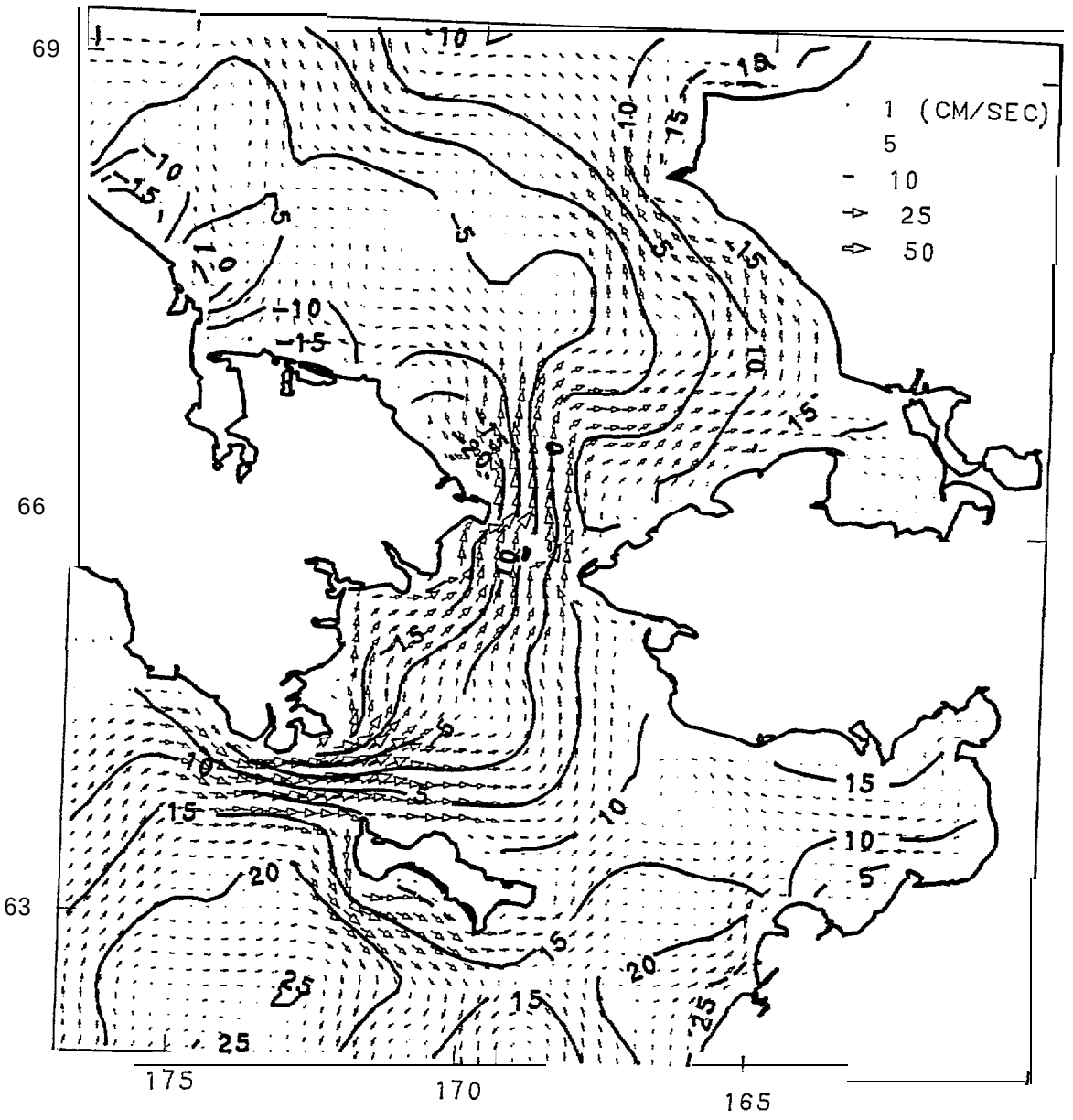

TRAIT_F1

VERTICALLY AVERAGED VELOCITY &
SURFACE ELEVATION
FEBRUARY 26 ,1982 AT 0:00

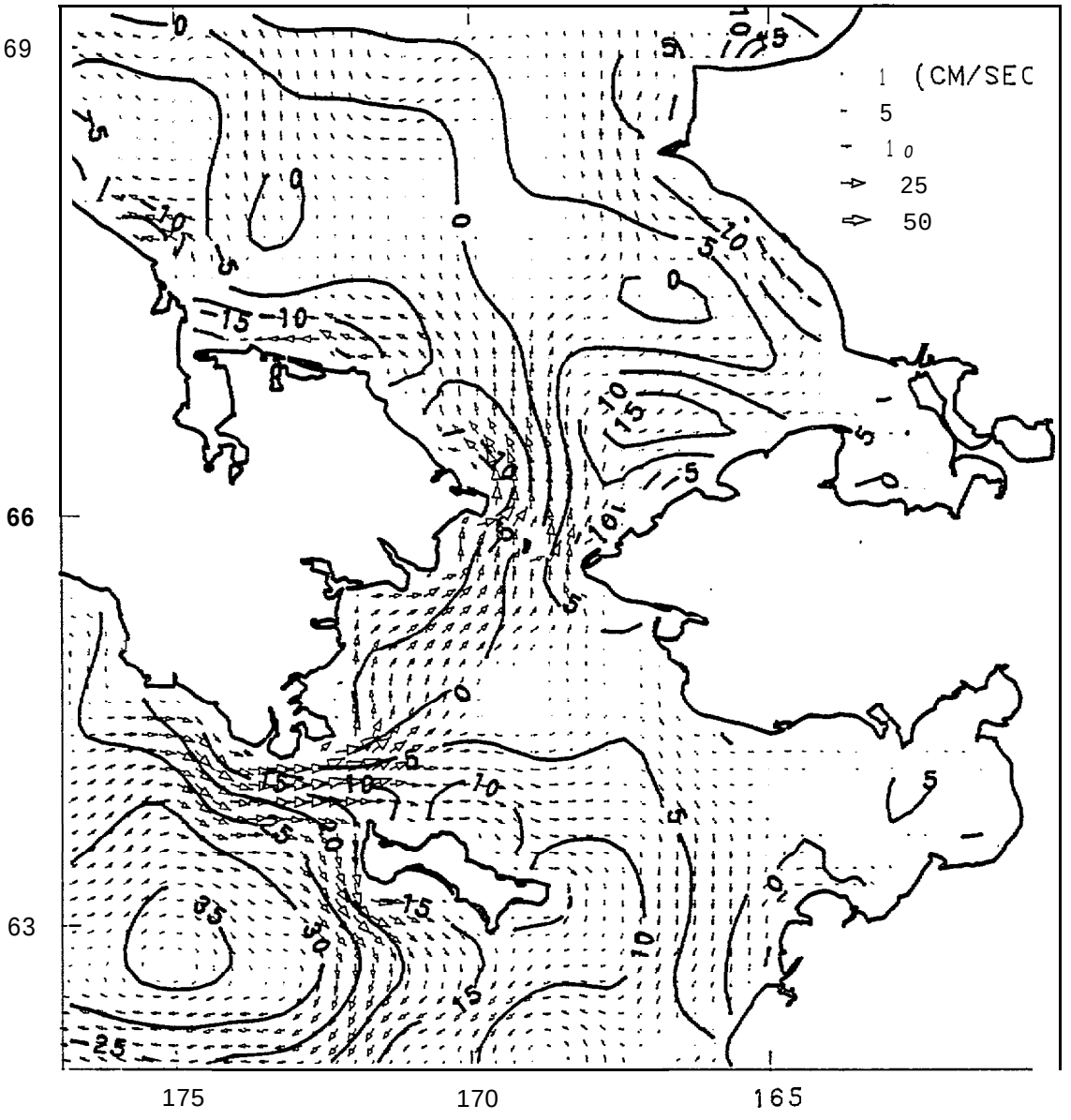

VERTICALLY AVERAGED VELOCITY &
SURFACE ELEVATION
FEBRUARY 27 ,1952 AT 0:00

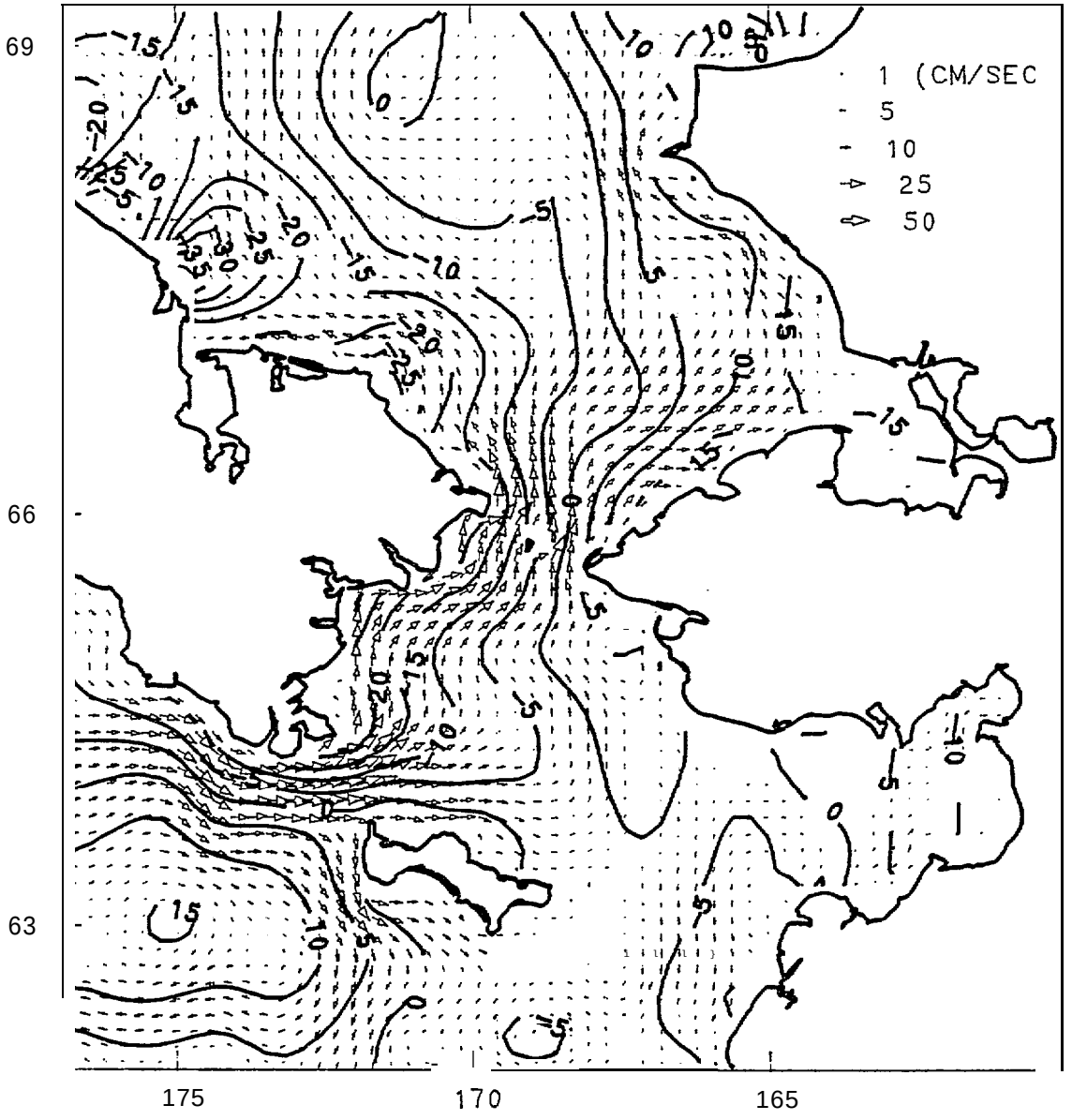

AIT_F1

VERTICALLY AVERAGED VELOCITY &
SURFACE ELEVATION
FEBRUARY 28 , 1982 AT 0:00